Tomas Bata University in Zlín
Faculty of Technology

Doctoral thesis

Investigation of polymer melt flow through different mixing elements and waving screw channels

Studium toku polymerních tavenin uvnitř různých typů míchacích elementů a vlnových šneků

Author: **Pavel Kubik**

Study programme: P2808 Chemistry and Material Technology

Study course: 2808V006 Technology of Macromolecular Substances

Supervisor: doc. RNDr. Jiri Vlcek, CSc.

Zlín, August 2014

Full version of the thesis is available in Library TBU in Zlín.

ACKNOWLEDGEMENT

THANK YOU VERY MUCH, INDEED.

I WILL ALWAYS REMEMBER!

ABSTRACT

One of the most important, yet problematic, issues in the extrusion process is achieving good mixing. A revelation of its principles inside of various types of mixing elements is always appreciated. So, an enormous effort was spent to study mixing principles not even by setting some experiments but also by 3D FEM simulation that allows to look at the mixing under the real processing conditions and its correlation with experimentally obtained data is acceptable.

At the beginning, the theoretical background focused on the extrusion process is presented. Specifications of all main zones in the single-screw extruder are shown. Basic mixing principles are also a part of the theoretical background. The biggest part of the theoretical background, however, is pointing to history of screw design and development of mixing elements. Some methods of mixing quantification are presented, as well.

Then, the performance of three different mixing elements on color dispersion in polymer stream during extrusion is studied. Two similarly designed Maddock mixers and a Stratablend II mixer are used as the last part of a general purpose single screw. Moreover, an in-line melt camera is used for quantification of mixing quality by visualization of grayscale of the color dispersion and thus mixing. The Stratablend II mixer produces the lowest and most uniform standard deviation. Comparison with 3D FEM simulations clearly indicate that the Stratablend II mixer has the best mixing abilities and that these are mainly given by its unique design with high average value of shear stress. The results also suggest that the key factor for achieving better mixing is the frequency by which a large fraction of the material passes through the high shear stress regions of the mixer. A new average stress criterion is developed for a purpose of its quantification.

The next step is studying of a mixing efficiency of two slightly different fluted mixing elements by RGB spectral analysis. This method is used for the quantification of the speed of mixing, but the overall mixing appears to be equal after sufficient mixing time. The fluted mixer without the wiping flight, however, creates a stagnation layer of material which rotates between the mixer and the barrel. This layer is characterized by a long residence time. The long residence time is again measured by RGB spectral analysis and also visualized in the video.

Finally, a detail 3D FEM study by using two different rheological models, of the mixing performance of the Fusion screw geometry is presented. Special criteria characterizing the mixing performance in dependence of the barrier undercut separating the waving channels are developed. A great mixing performance is achieved when a right balance in both dispersive and distributive part of the mixing process is found.

ABSTRAKT

Jednou z nejdůležitějších a nejproblematičtějších součástí procesu vytlačování je dosažení správného míchání, a tak odhalení jeho principů a zákonitostí uvnitř různých typů míchacích elementů je velmi žádoucí. Proto je studiu míchání věnováno velké úsilí. Není nutno využívat pouze experimentálních dat, ale velkou výhodou je také použití 3D FEM simulací, které umožňují výzkum míchání za v podstatě reálných procesních podmínek neboť korelace mezi predikovanými a experimentálními daty je velmi dobrá.

Teoretická část definuje základní pojmy extruzního procesu a popisuje jednotlivé zóny jednošnekového vytlačovacího stroje. Dále jsou představeny základní principy míchání s důrazem na představení historického vývoje designu šneků a míchacích elementů. V poslední sekci teoretické části jsou pak představeny vybrané metody, které jsou vhodné pro kvantifikaci míchání.

V experimentální části je nejprve prověřována míchací účinnost třech odlišných typů míchacích elementů na disperzi barvy v polymerní tavenině. Pro tento účel byly použity dva míchací elementy typu Maddock s podobným designem a jeden míchací element typu Stratablend II, které byly umístěny v poslední zóně standardního šneku. Vizualizace procesu míchání barvy v polymerní tavenině byla provedena pomocí speciální kamery instalované přímo na vytlačovací lince, a to na základě analýzy stupňů šedi dispergovaného barviva. Bylo zjištěno, že míchací element typu Stratablend II vykazoval nejlepší míchání. Tento závěr byl podpořen pomocí 3D FEM simulace, z které vyplynulo, že design míchacího elementu typu Stratablend II umožňuje jak výrazný zpětný tok, tak dlouhodobé generování vysoké hodnoty průměrného smykového napětí, což je klíčové pro dosažení vysokého míchacího účinku. Pro účely kvantifikace intenzity míchání bylo vyvinuto nové napěťové kritérium.

V další části práce byla studována míchací účinnost dvou velmi podobných míchacích elementů typu Maddock vizualizací toku a hodnocením rychlosti míchání pomocí RGB analýzy. Bylo zjištěno, že míchací element typu Maddock s podřezanou smykovou štěrbinou a stírací plochou, generoval vrstvičku polymerní taveniny rotující blízko stěny komory mající zdržnou dobu mnohonásobně delší, než průměrná zdržná doba. Celková míchací účinnost obou testovaných míchacích elementů však byla prakticky totožná.

V poslední části práce byla provedena detailní 3D FEM analýza pomocí dvou odlišných reologických modelů s cílem pochopit proces míchání uvnitř vlnového šneku. Pro účely kvantifikace míchání byly navrženy dvě kritéria v závislosti na podřezání bariéry oddělující dva vlnové kanály. Bylo prokázáno, že nejvyšší míchací účinnosti je možné dosáhnou vybalancováním disperzních a distributivních složek míchání specifickou změnou designu vlnového šneku.

LIST OF ARTICLES INCLUDED IN THESIS AND AUTHOR'S CONTRIBUTION

Method of analyzing and quantifying the performance of mixing sections

Pavel Kubik (83%), Jiri Vlcek, Costas Tzoganakis, Luke Miller

3D simulation of the fluted mixer element behavior

Pavel Kubik (78%), Jiri Vlcek, Jiri Svabik, Martin Zatloukal

Experimental and numerical analysis of the performance of two fluted mixer designs

Pavel Kubik (54%), Martin Zatloukal, Yutaro Asai, Ryuichi Haruna, Yoshihiko Iwasaki, Jiri Vlcek, Ilja Paseka

Three-dimensional finite element method simulation study of the fusion screw geometry

Pavel Kubik (71%), Martin Zatloukal, Jiri Vlcek, Tim Womer

CONTENT

INTRODUCTION

1. Extrusion

Plastics extrusion is a manufacturing process in which a raw material is conveyed, melted and pushed through an extruder die to form a continuous profile. This can be done in two common types of extruders: continuous or discontinuous. Continuous extruders are typical by using a rotating member for material transportation. Not only profiles but also tubes, sheets, coating and cable insulation can be produced [1].

1.1 Solids conveying zone

Typical single-screw extruder usually consists of three main parts. The first one is called solids conveying zone where polymer particles in form of powder or pellets are fed gravitationally into the hopper. Other additives like some colorants or UV inhibitor can be put to the base material into the hopper, as well. The solids conveying zone channel is relatively deep, but the depth should not be bigger than 0.2 times screw diameter. Particles are also conveyed and forced to move forward by the effect of friction. It is required to achieve a low friction coefficient in between the material and the screw but, on the other hand, a high friction coefficient in between the material and the barrel. It means that a surface of the screw should be as smooth as possible, usually polished, while a surface of the barrel should be rough. The more is the roughness of the barrel, the more is the material conveyed. Some tricks like cooling of the material under the hopper or making grooves into the barrel are very helpful to increase the friction coefficient. The high enough friction coefficient is also useful to generate much more pressure as shown in Figure 1. [2]
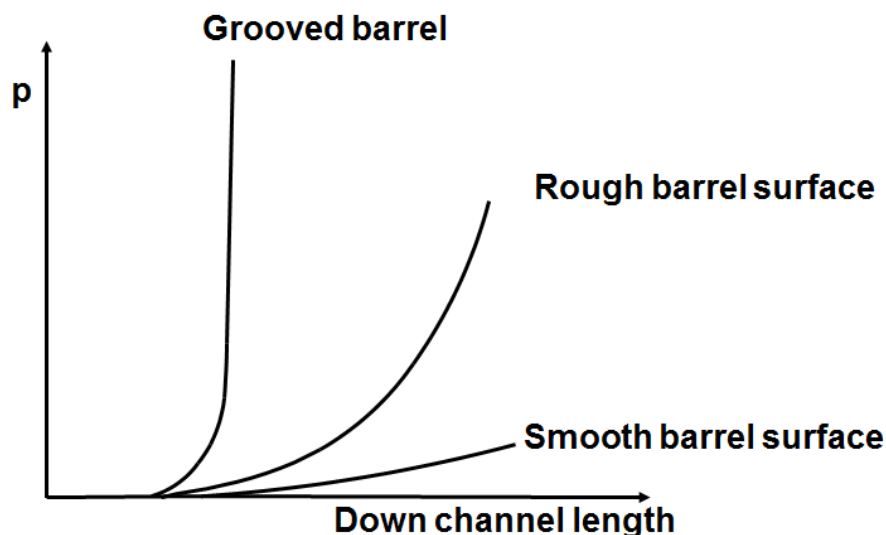

Fig. 1. Pressure generation in solids conveying zone

1.2 Melting zone

The second zone is a melting zone. There are two phases of the material coexisting together in the melting zone. It is the melt and the solid bed. The most complex part of particles journey throughout the extruder is certainly the melting. This process is too complicated. Therefore, an enormous effort needs to be done by using an experimental investigation to fully understand the melting. The first mathematical analysis of the melting process was presented by Tadmor [3] who analyzed samples obtained by Maddock [4]. The Tadmor's model assumes that the barrel is rotating and the screw is stationary. It also considers the solid bed as a rectangular shape and do not take into account heating of the screw. It means that the solid bed cannot be melted by the screw. Melting characteristics is given by solid bed ratio SBR (see equation 1.1)

$$SBR = \frac{L_{SB}}{L}$$
(1.1)

Where L_{SB} means the length of the solid bed and L stands for the length of the flight.

$SBR = 1 => L_{SB} = L$ … only solid bed exists

$SBR = 0 => L_{SB} = 0$ … only melt exists

Good melting is characterized by decreasing of the length of the solid bed and solid bed ratio. Bad melting is usually connected to some solid bed defects as a solid bed break up. The solid bed is wrapped by melt and it is not melted because the melt works as an insulator. SBR can be sometimes incorrectly considered as a degraded material. The most significant effect of the melting zone is that a core diameter of the screw is increasing along the length of this section. Increasing of the diameter lowers a space for a solid bed and generates pressure. The material is pushed to a narrower gap. Particles in direct contact to the barrel are intensively dragged and sheared. The drag, shearing and friction forces particles to melt and create a thin film layer close to the barrel surface. Nothing important happens until the layer is thicker than a flight clearance. Then, the melt is dragged and pushed towards the screw and accumulating at the pushing flight. Next, so called a melt pool is formed. A width of the melt pool is increasing, while the width of the solid bed is decreasing. Particles should be fully melted or plasticized before they reach the end of the melting zone. [2]

1.3 Metering zone

The last zone of the conventional extruder is metering zone in which only polymer melt occurs. Melt is only transported to end of the screw. The easiest way of melt transport is a drag flow. The drag flow can be visualized as the flow in between two plates where one of plates is stationary and the second one is

moving. A scheme of this situation is presented in Figure 2. A Movement of the upper plate also creates a velocity profile with a maximal velocity value close to the moving plate. Velocity on the stationary plate is equal to zero. This flow domain does not generate any pressure.

Moving wall
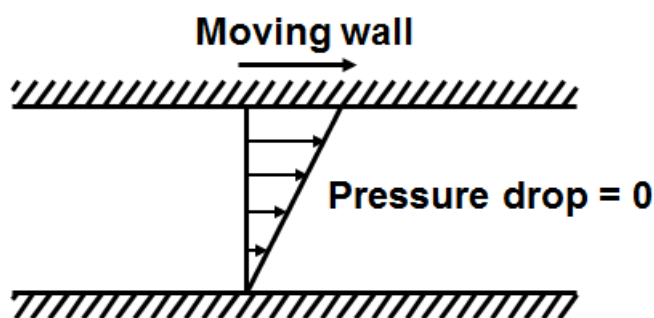
Pressure drop = 0

Fig. 2. Drag flow

The second way of polymer melt transportation is a pressure driven flow. The melt is transported by pressure in between two stationary plates in this flow domain. Velocity profile is parabolic and its maximal value is in the middle of the channel. The movement of the material stops when pressure is released. Pressure driven flow is visualized in Figure 3. [2]

Stationary wall
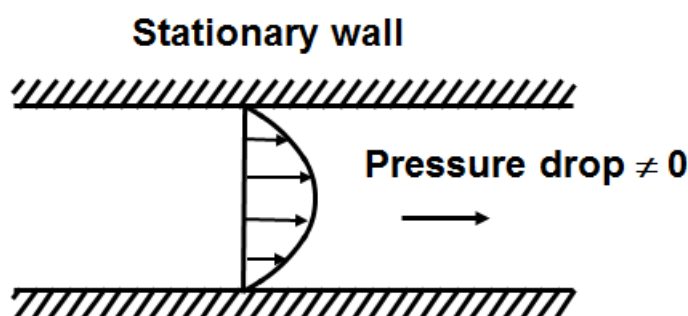
Pressure drop ≠ 0

Fig. 3. Pressure driven flow

Thus, combination of both flow principles is needed to push the melt throughout the extruder. The drag flow transports the material always in the moving wall direction. The pressure driven flow transports the material in the pressure drop direction. If there is a flow situation where a combination of both flows occurs, the material transport direction depends on the strength and orientation of each contribution. In case when the drag flow direction and the pressure drop have an opposite orientation (see Figure 4), the material close to the moving wall will obey the drag flow. The material close to the stagnant wall will more feel the pressure drop. The velocity shape and the transported amount depend on the strength of each component. When the drag flow direction and the pressure drop have the same orientation (see Figure 4), the pressure drop helps the drag flow to transport the material. In such a case, the transported amount would be higher than the amount transported with the drag flow only.
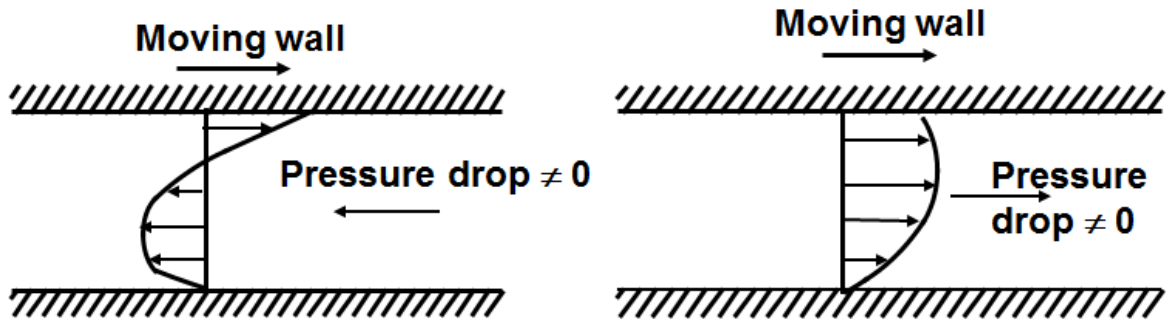
Fig. 4. Combined flows

A part of the material moving by the drag flow in a part with the moving wall can pass the second part where the walls do not move and they are closer. Therefore, the contribution of the drag flow is reduced by the generation the opposite pressure drop which lowers down the amount of the pumped material. Thus, a flow domain where the drag flow is in a combination with the closed end is able to pump the material and generates a pressure drop. Drag flow pump is visualized in Figure 5. The extruder principle is created when the drag flow pump is wrapped on a helix.
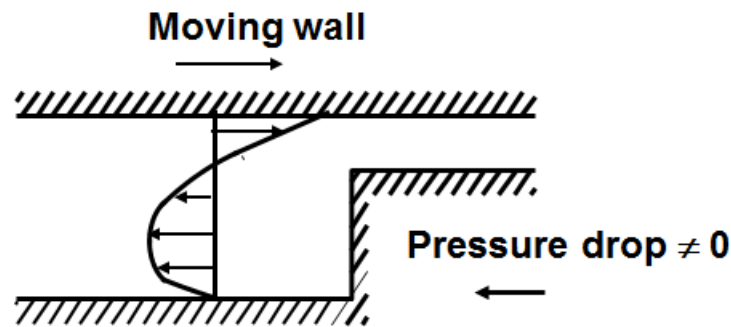
Fig. 5. Drag flow pump

2. Mixing principles

Mixing is an operation that reduces a nonuniformity of a mixture by physical motion of other ingrediences. A dominant factor responsible for mixing in polymer processing is convection. Thus, convection creates a movement of particles from one area to another. This can be done mainly by shear and elongational deformation or their combination of the mixture with a rise of the interfacial area separating the components. Rheological properties of all phases can also have a huge impact on the component deformation. Moreover, the mixing transformation assemble of repeated stretching and folding allow very effectively decrease the nonuniformity of the mixture to any appropriate level. This mechanism is used in some kind of static mixers like Kenics or Ross and produce mainly a laminar shear flow of particles, thus laminar mixing. Laminar mixing is occurred in polymer melt extrusion.

Nevertheless, there are in principle two basic mixing mechanisms. The first one, so called dispersive mixing, is based on lowering of the size of mixture components. The process has a cohesive complexion due to van der Walls forces between particles. However, the main reason to break particles is stress. Both shear and elongational stress has a big contribution in this kind of mixing process. The second one is distributive mixing which redistributes the particles in the volume. So, obstacles have to be created to change a trajectory of the material. Usually, some pins are the best and the easiest option to achieve this. A scheme shown dispersive and also distributive mixing development is presented in Figure 6. [2]
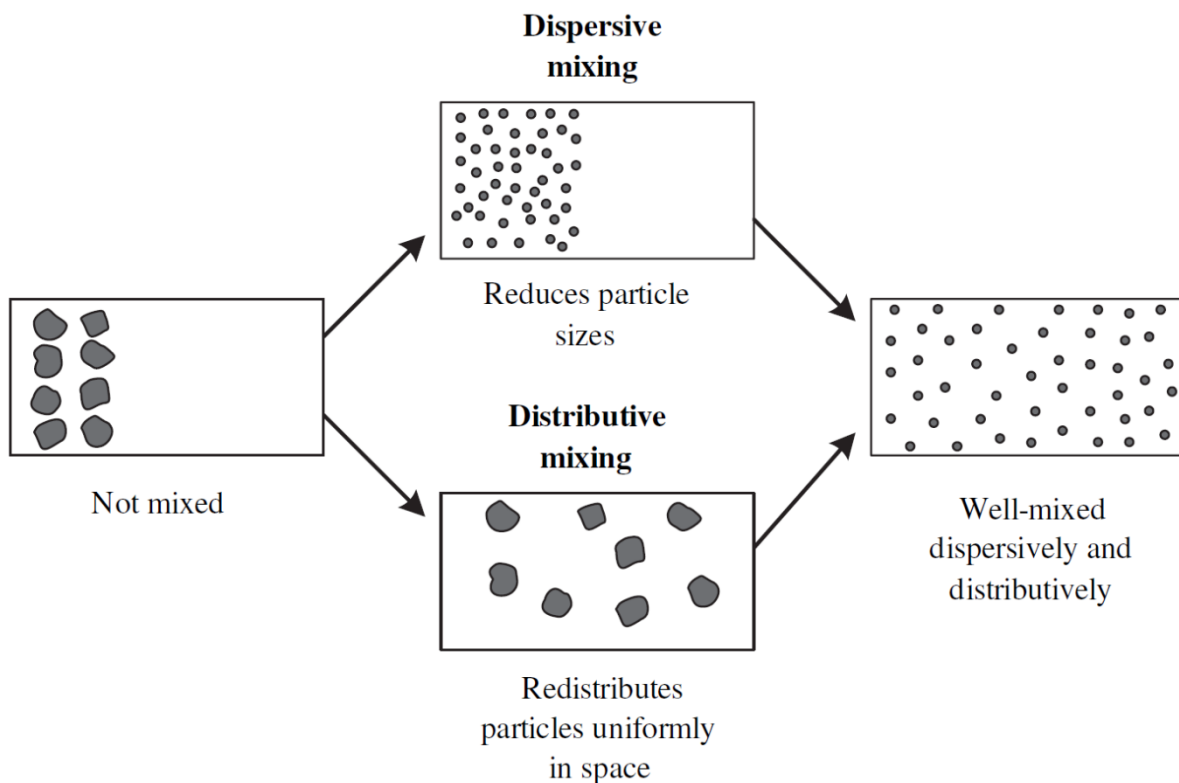
Fig. 6. Basic mixing mechanisms [2]

3. Historical development of screw design and mixing elements

A proper screw design is an important factor in achieving good mixing performance and homogenous melt temperature in extrusion process. Many useful inventions were made to improve extrusion process over the past 120 years. It all started in 1885 when the first commercial extruder was patented by Vernon and John Royle [5]. This simple early machine had already all main components that can be recognized in present extruders.

Sometimes in between years 1928 and 1932 new advantages were developed and the first screws with variable lead were presented. Their L/D ratios were about 4:1 or 8:1. They allowed a procession of new material like PVC or cellulose.

Later, in the second half of 1940's extruders with L/D ratio about 16:1 were commonly used. The most important inventions were patented by W.A. Magerkurth (1946) [6] and F.E. Dulmage [7] (1948). The first one brought the invention of torpedo screw design, while the second one came with a design of the first distributive mixer used mainly for processing styrene. Many variations of the famous Dulmage mixing section are still widely used nowadays. First of all, polymer is pushed through a huge amount of narrow channels. Then, a flow is combined together in a small metering zone. Finally, polymer is divided again by another round of narrow channels. The geometry concept based on the Dulmage mixer, patented later by Dow Chemical in July 1956 [8], is shown in Figure 7.
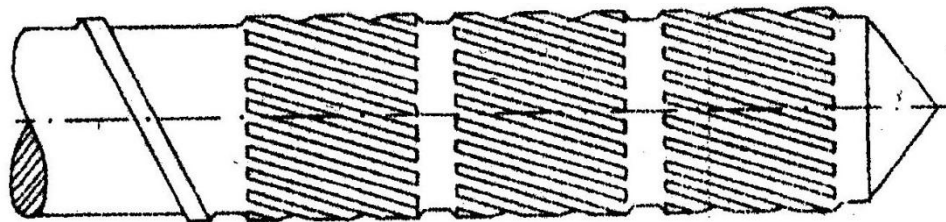
Fig. 7. Dulmage mixer [1]

New material like LDPE was also started to be produced and used for the first blown film LDPE lines with throughput about 40kg/hr.

A progress of single-screw extrusion was running fast also in 1950's. The most useful idea was a construction of screws with L/D ratio of 20:1. LDPE blown film line throughput was extended to almost 80kg/hr. Very important was also invention of the vented extrusion and a square pitch screw design developed by P. Squires. Acrylic material and Saran became a newly processed material. The first dispersive mixing elements based on blisters were created. Dispersive mixing is based on reducing size of particles. A material is usually squeezed through a narrow gap to achieve high shear stress level and thus good dispersive mixing. The blister ring is probably a simplest mixing element ever. Thus, it is a cylindrical part of an extruder with small shearing gap size. All the material is forced to flow over this shearing gap which causes a high reduction of pressure drop. The blister ring is therefore very often used especially in vented-screw extruders. Typical design of blister ring is provided in Figure 8.
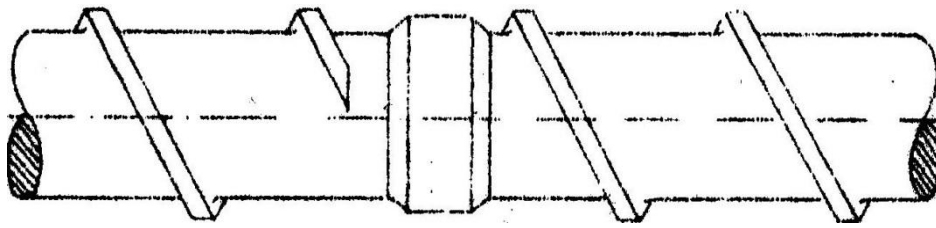
Fig. 8. Blister ring [1]

Maddock's solidification experiment came with the understanding of the single-screw extruder in 1959. The experiment revealed an existence of the solid bed and the melt pool in the screw channels. Moreover, the experiment showed mixing of the material during a melting process. Partial mixing occurred in the downstream section of the screw, as well. In general, the level of mixing was found to be poor for a simple single-screw extruder. However, the understanding of these phenomena started a new era of inventions to improve a mixing performance.

Requirements of the best possible polymer melt homogenization lay stress on mixing. The real boom of new inventions to support mixing process started in 1960's. In principle, almost the same mixing section as the Dulmage mixer was presented and also patented in 1961 by R. L. Saxton [9]. The only difference is the orientation of non-flighted screw sections separated the multi-flighted screw section. The design is presented in Figure 9.
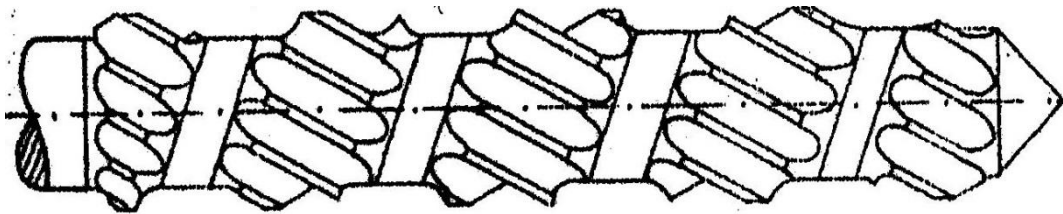
Fig. 9. Saxton mixer [1]

The first part of mixing process starts in the melting zone of the single-screw extruder. An invention of Maillefere's long barrier screw was then a true breakthrough in understanding of melt homogenization, thus mixing. C.E. Maillefer patented his barrier screw design in 1967 [10]. His screw design allowed a unique separation of solid particles and polymer melt inside of the screw channel. An increased clearance flight started in the downstream side of the primary flight and its lead was longer than a primary flight lead. As a result, the primary channel was intersected into two separated channels by the barrier flight and restrained the solids and melting process. R.B. Gregory also came in 1968 with a unique design of the first distributive mixer with reverse helix to create flow resistance and dynamically mixed material. His design was the first dispersive mixer using a barrier as a key parameter to achieve better mixing.

LDPE blown film line could produce a throughput of 160kg/hr and double venting extruders were used, too.

Gene Le Roy [11] patented in 1969 probably one of the most widely used mixing elements ever invented. The commercial meaning and modification of the mixer to single-screw extrusion was later (1973) presented by Bruce Maddock [12, 13]. The Maddock mixer had several pairs of fluted channels separated with a shearing gap in between. The shearing gap was undercut and provided intense dispersive mixing. Channels of the mixer were oriented in an axial direction of the screw and a construction of the mixer allowed the material only one pass over the shearing gap. The Maddock mixer was mainly situated in the metering zone of the extruder and strongly influenced the overall quality of the mixing process. However, a constant channel depth should lead in stagnation regions at the end of the channel. A tapered channel is hence more useful to avoid possible degradation problems. The design of the mixer also does not allow too much spreading of particles. There is usually pressure consumption in the mixer but pressure can be generated under specific processing conditions, as well. Fluted mixer design is shown in Figure 10.
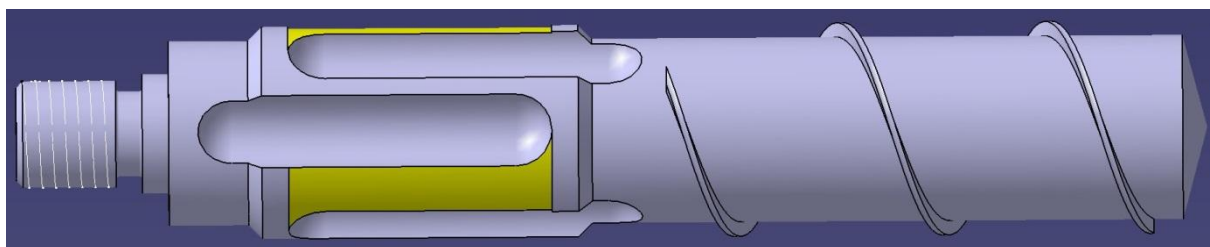
Fig. 10. Fluted mixer [14]

Another representative of fluted mixing sections is the Egan mixer. Its design is shown in Figure 11. The design was created and patented by R. B. Gregory and L. F. Street in November 1968 [15]. The biggest difference between the Egan and the fluted mixer is that channels are made in helical direction. This design improvement allows forward drag transportation in inlet and outlet channels. Besides, pressure consumption is lesser than in case of the fluted mixer with straight channels. Channels are also tapered to reduce a possibility of unwanted effects such as polymer melt degradation.
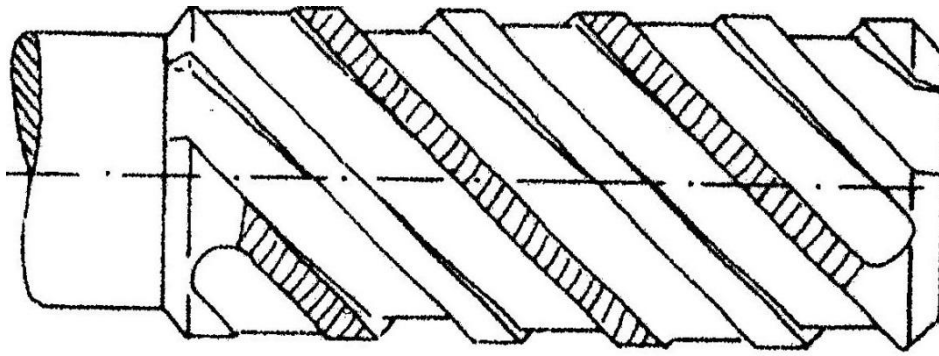
Fig. 11. Egan mixing section [1]

Similar design was presented by Dray [16] and Gregory [17] in January 1974. His design has an open outlet channel since the beginning of the mixer. It was the first mixer characterized with dispersive and also distributive mixing. Its design could utilize a bi-directional flow. However, there is a chance that not all material has to flow over the shearing gap. As a result, non-homogenous shear history can be obtained from the material. Dray mixing section can be seen in Figure 12.
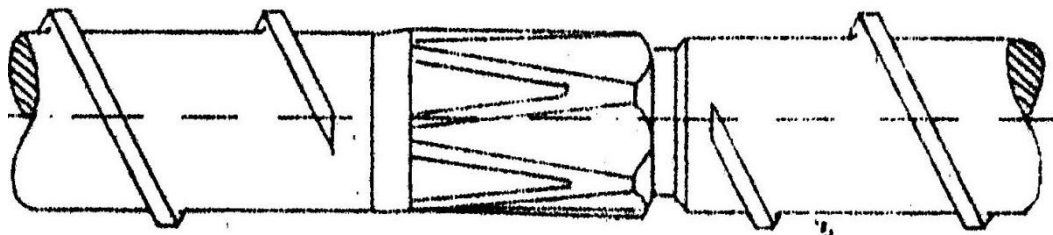
Fig. 12. Dray mixing section [1]

It is much easier to achieve a distributive mixing, because every change in flow direction causes a distributive mixing. Well-known Pin mixing element is probably one of the easiest distributive mixing element sections. Pins are placed in few patterns around a screw where creating a significant change in velocity profile. On the other hand, geometry of pins should have a certain shape to get the best mixing efficiency. Pin mixing section can be seen in Figure 13.
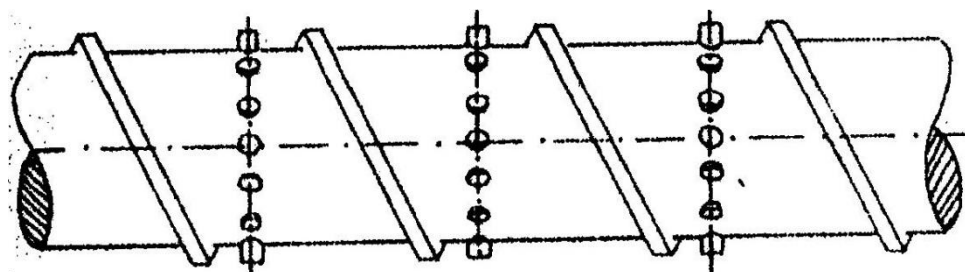
Fig. 13. Pin mixing element [1]

Pineapple mixing section, see Figure 14, can be used for achieving of distributive mixing, as well.

Fig. 14. Pineapple mixing section [18]

Another goal to get distributive mixing is to put grooves in the flight. This solution was patented by a Swedish company Axon in many European countries [1]. Axon screw is displayed in Figure 15.
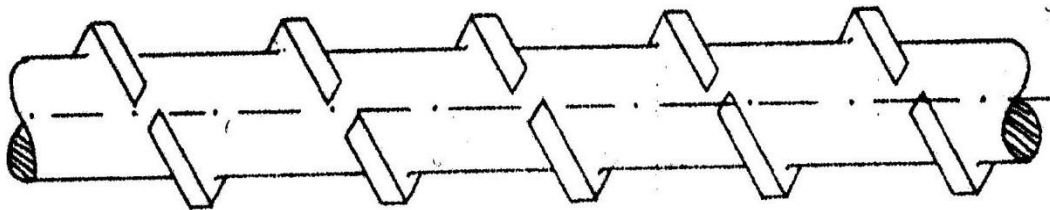
Fig. 15. Axon screw design [1]

New advances came with a patent of H. Schippers who patented in 1972 [19] new concept of barrier screw where primary channel shallows, while auxiliary channel deepens. Barrier flight clearance is about two times the screw to barrel clearance.

R.F. Dray patented so called efficient screw design in 1972 [20]. Unique part of this screw was changing lead at the end of the feeding section which was always longer than at the beginning. This lead together with an auxiliary channel created better continuity in melt film.

A significant invention of the wave screw [21] by George Kruder in 1975 solved a problem of overheating of the material caused by increasing of the screw speed. However, the Double Wave screw became the most common design [22]. The metering section of the conventional single-screw extruder was replaced with double flighted Double Wave section. The secondary flight was undercut to support dispersive mixing. The undercut allowed the material to

flow over the secondary dispersive flight from one channel to another one. Both screw channels alternately changed their depth every 90° or 180° that forced the material to flow over the secondary flight.

Barr and Chung [23] in 1983 improved the Double Wave concept where not only the secondary flight was undercut but the main flight was undercut, as well.

In 1984, R. F. Dray [24] patented a triangle mixer screw design. This distributive mixer diverted flow from the trailing side of the flight to a groove maintaining cross section area throughout the device. Later, in the second half of 1980's concept design and reverse flow mixer patented again by R. F. Dray [25] were presented. The first one established the melt film in the auxiliary channel independent on the primary channel, while the second one was designed to improve heat transfer by utilizing of the reverse flow.

Probably the latest screw concept extensions were provided by Tim Womer et. all [26-28]. Their concepts of the Double-Wave screw were based on coupling the Wave section with the upstream barrier section and the material reorientation section. The Fusion™ screw geometry [29] is available for injection molding, extrusion, pipes and profiles production etc.. Its geometry is illustrated in Figure 16.

Fig. 16. Fusion™ screw geometry [18]

As can be seen, the Fusion™ screw is a double-wave screw where two channels are separated by a barrier between them. A clearance of the barrier has a strong effect on an amount of a material which can flow over it from one channel to another one. Furthermore, both channels have a cyclic variation in a depth. Thus, the depth of the first channel goes up and reaches a maximum, while the depth of the second channel has to go down to get a minimum. The material is therefore not even only rotating inside of the channels but the huge amount is forced to flow over the gap clearance by an influence of drag flow. However, this effect occurs mostly because of channel depth variation. Finally, an overall shear stress level achieved by the Fusion™ screw geometry is very high. So, the Fusion™ screw provides chaotic mixing.

Probably the best mixer based on the fluted mixer concept is called the Stratablend. Few generations of this mixing section have been also created by Xaloy, Inc. The second evolution of this mixer is displayed in Figure 17.
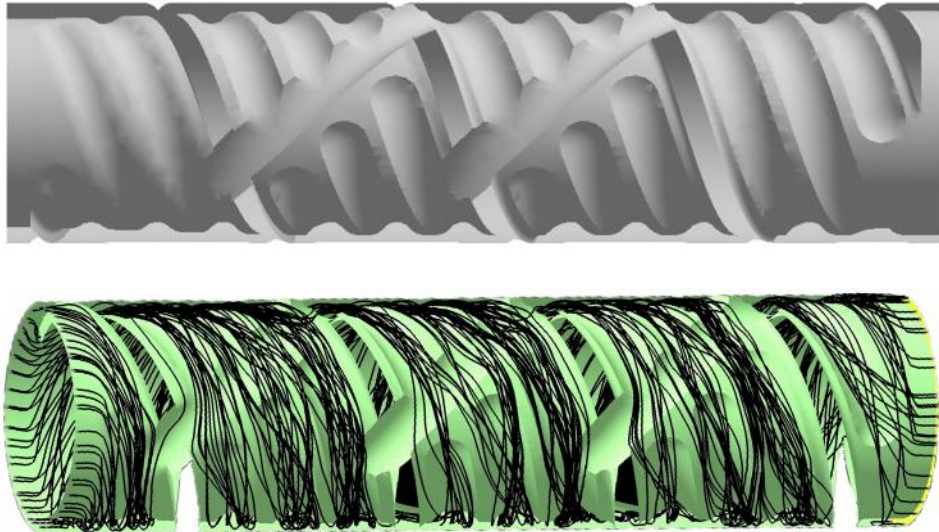
Fig. 17. Stratablend II [14]

The manufacturer claims "The unique, patented geometry of Stratablend II produces highly effective mixing. The Cut-through melt channels allow back flow for chaotic and distributive mixing effects with low shear and little or no temperature rise" [30]. The mixer was patented in 2007 [31]. Stratablend II has much more variability in the way of melt flow and shows more "spreading" of the initial group of particles. For example, only few pathlines, representing a way of particles, appear to exit in a similar location while some of them exit on the opposite side of the mixer (180 degrees away). Moreover, the particles cross into the higher shearing gap regions more often. Hence, overall mixing efficiency is much better than for other fluted mixing sections.

The most sophisticated mixing element ever was created by Gale at the RAPRA. It is called the Cavity Transfer mixing section and illustrated in Figure 18.
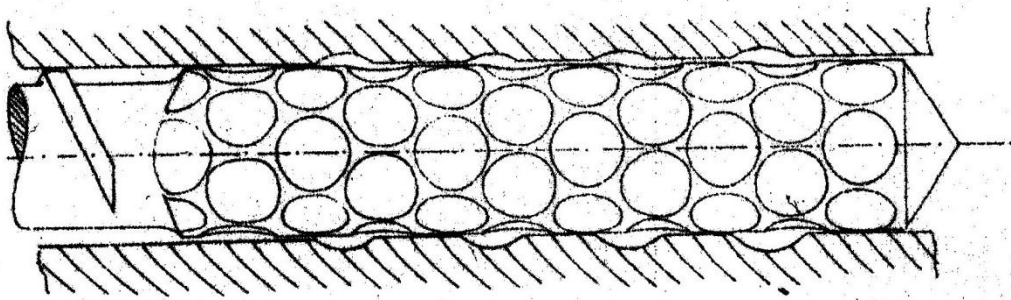
Fig. 18. Cavity Transfer mixing section [1]

As can be seen, the mixer has cavities on both the screw and the barrel. Hence, a combination of shearing and redistribution of particles is found. Thus, not even distributive but also dispersive mixing is reached and both mixing principles are combined together.

THE AIMS OF THE DOCTORAL RESEARCH WORK

The main goal of the doctoral thesis is to come up with a better understanding of the mixing process in single-screw extruder. A lot of different types of mixing elements can be used to obtain very well mixed material. Therefore, it should be good to:

- Develop some new criteria, which can be helpful to quantify the mixing process

- Work with different methods of mixing evaluation

- Use visualization experiments to clearly see the flow behavior inside of mixing elements

- Study, check and predict the flow behavior of mixing elements by using 3D FEM simulation

- Get better knowledge of the true nature of the mixing process in chosen mixing elements

SUMMARY OF PAPERS

In this thesis, new look into the mixing process in various types of mixing sections is presented. Some new methods of mixing quantification are successfully tested and compared with 3D FEM simulation to obtain the knowledge and better understanding of the mixing process. The influence of viscosity properties, different materials and stress into the final mixing quality is show, as well.

Paper I
Method of analyzing and quantifying the performance of mixing sections

In this article, the performance of three different mixing elements on color dispersion in high-density polyethylene and linear low-density polyethylene polymer stream during extrusion is studied. Two similarly designed Maddock mixers and a Stratablend II mixer are used as the last part of a general purpose single screw. Moreover, an inline melt camera is used for the quantification of mixing quality by visualization of grayscale of the color dispersion and thus mixing. The Stratablend II mixer produces the lowest and most uniform standard deviation. Both the Maddock mixers showed the same trend but higher values of standard deviation. All results are then compared with a full 3D finite element method simulation. Simulations clearly indicate that the Stratablend II mixer has the best mixing abilities and that these are mainly given by its unique design with high average value of shear stress. The role of elongational stress does not appear to have a high influence on mixing for these mixers. The results also suggest that the key factor for achieving better mixing is the frequency by which a large fiction of the material passes through the high shear stress regions of the mixer.

Paper II
3D simulation of the fluted mixer element behavior

One of the most important, yet problematic, issues in the extrusion process is achieving good mixing. Considerable prior efforts have been made to understand different types of mixing elements for single-screw and twin-screw extrusion. However, there is still a lack of good process values or criteria that can be used for design purposes. The focus of this work is to better quantify the mixing behavior, using 3D FEM analysis, to develop some design criteria. This study will focus on the fluted mixer, comparing common design variations and the effect of material viscosity and process conditions.

Paper III
Experimental and numerical analysis of the performance of two fluted mixer designs

In this paper, the effect of the Maddock mixer design on its performance in single screw extrusion of HDPE melt has been investigated experimentally on a special extrusion line equipped with a barrel having several glass windows as well as theoretically by using a three dimensional finite element method simulation. The red-green-blue spectral analysis has been used for experimental quantification of the mixing efficiency whereas generalized Newtonian model (with Carreau-Yasuda viscosity function) and viscoelastic modified White-Metzner model have been utilized in flow simulations. Based on the performed experimental work it has been found that the mixer with no undercut wiping flight ("Closed" mixer) has a faster mixing/purging but a similar final mixing performance as the mixer with undercut wiping flight ("Open" mixer). It has also been revealed that the "Open" mixer creates unwanted dead zone (in the form of the stagnation layer of material rotating between the mixer and the barrel) at which the polymer melt degradation may takes the place. It has been found that based on the stress, residence time and pathline calculation it is possible to predict the experimentally observed tendency of the "Closed" mixer for a faster mixing/purging in comparison with the "Open" mixer as well as the presence of stagnation layer in the "Open" mixer. The performed theoretical parametric study indicates that the gradual opening of the wiping gap causes that the pressure driven flow became more dominant than the drag flow in shearing as well as in the wiping gap independently of the utilized rheological model. On the other hand, the predicted particle trajectories inside the mixer were found to be shorter for the viscoelastic model, tending to occur mainly in the middle of the channel and thus leaving the mixer a little bit faster in comparison with the purely viscous calculations. Finally, it has been revealed that for the highest tested wiping flight opening, the viscoelastic modified White-Metzner model predicts back flow over the wiping flight whereas the purely viscous Carreau-Yasuda do not, which can be explained by the elongational viscosity, considered in the viscoelastic modified White-Metzner model. This suggests that modified White-Metzner model should be preferred more than purely viscous Carreau-Yasuda model in the mixing element die design optimization.

Paper IV
Three-dimensional finite element method simulation study of the fusion screw geometry

In this paper, a detail 3D FEM study of the mixing performance of the Fusion screw geometry by using two different rheological models is presented. Special criteria characterizing the mixing performance in dependence of the barrier undercut separating the waving channels are developed. A great mixing performance is achieved when a right balance in both dispersive and distributive part of the mixing process is found. An optimal undercut of the barrier was found to be about 2mm. Both rheological models were successfully used to validate data of the real experiment with an error less than 15%.

CONCLUSIONS

Mixing process is one of the most mysterious parts of the extrusion. A revelation of its principles inside of various types of mixing elements is always appreciated. So, an enormous effort was spent to study mixing principles not even by setting some experiments but also by 3D FEM simulation that allows to look at the mixing under the real processing conditions and its correlation with experimentally obtained data is acceptable.

Probably the only tool which allows mixing quantification directly in-line is the in-line melt camera. The measurements of the color dispersion in polymer melt made by the In-line Melt Camera clearly shows that Stratablend II has the best mixing performance, of three mixers studied, in all processing conditions. The mixer keeps much lower and more uniform standard deviation than Maddock mixers. These mixing results of Stratablend II appear to be a result of its unique design concept which creates high average shear stress values in a relatively short residence time period. It is interesting to note that the higher average shear stress values are achieved with a larger shearing gap. The number of passage through these high stress regions is believed to be the key variable for better mixing. Finally, a new average stress criterion has been developed to quantify a level of stress inside of the selected mixers.

The performed 3D FEM simulation study showed different behavior of the open and closed fluted mixers. The main reason of this difference is the existence of insulation layer for the open mixer. This layer is located at the barrel surface and it works as a barrier of heat transfer. On the other hand, since the layer is there, it occupies certain part of the gap over the undercuts and thus it makes the gap effectively smaller than for the closed mixer. It has been found that the shear stress in the insulation layer is lower than 20 kPa, which may lead to polymer melt degradation. The analysis clearly shows that the mixing efficiency defined by the λ parameter is independent of the material properties and the geometry variations of the fluted mixer.

RGB spectral analysis was used to experimentally quantify the speed of the mixing process for the "Open" and "Closed" fluted mixers. The "Closed" mixer showed a transition from the pure polymer melt to fully mixed that was about half a minute faster than the "Open" mixer. However, the overall, final mixing performance of both fluted mixer designs appears to be equal.

The "Open" mixer configuration of the fluted mixing element also creates a slow moving layer of the material which rotates in the shearing and wiping gaps, i.e. near the barrel surface. This layer is formed because of the absence of the wiping flight. An almost independent, slow moving flow field appears to form in this region. The mass flow rate of this layer (i.e. the mass flow rate over the wiping gap) was found through the 3D FEM calculation to be about 50% of the

24

mass flow rate entering the mixer. The layer is characterized by the long residence time and increases the residence time distribution of the mixer. RGB spectral analysis was used to calculate the time needed for the purging of the colorant out of the extruder. Purging time of the extruder equipped with the "Open" mixer is twice as long as that for the "Closed" fluted mixer. Recorded video of the experiment, on a glass window extruder showed the development of the slow moving layer in the "Open" mixer. The longer residence time of the layer with the "Open" mixer has also been confirmed by 3D FEM simulation. The long residence time of this layer can explain some extrusion problems such as polymer melt degradation. Thus, even if the "Open" fluted mixer is easier to manufacture, it is not recommended for processing thermally sensitive polymers.

Finally, the 3D FEM parametrical study of the Fusion™ screw geometry clearly shows that 2 mm undercut of the barrier separating screw channels appears to be the optimal parameter for the most efficient mixing performance. A solution where dispersive and distributive parts of the mixing process are even is considered to provide the most efficient mixing performance. The solution is achieved by two criteria developed just for the purpose of dispersive and distributive mixing quantification of the Fusion™ screw geometry. These two criteria give also a helpful tool in designing of the Fusion™ screw geometry. However, it is still necessary to spend an effort to find some general quantitative criteria judging the mixing process.

REFERENCES

1. RAUWENDAAL, Chris. *Polymer Extrusion*. Cincinnati: Hanser Gardner Publications, 2001. ISBN: 978-1-569-90321-6
2. TADMOR, Zehev and Costas G. GOGOS. *Principles of polymer processing - 2nd edition*, Hoboken: John Wiley & Sons, 2006. ISBN: 978-0-471-38770-1
3. TADMOR, Zehev. Fundamentals of Plasticating Extrusion. I. A. Theoretical Model for Melting. *Polymer Engineering and Science*, 6, 185–190 (1966).
4. MADDOCK, B. H. AVisual Analysis of Flow and Mixing in Extruder Screws. Tech. Papers, Vol. V, *15th Annu. Tech. Conf., Society of Plastics Engineers*, New York, January 1959
5. ROYLE, Vernon and Jonh Royle, Jr. U. S. Patent 325,363 (September 1st, 1885).
6. MAGERKURTH, W. A. U. S. Patent 2,407,503 (September 10th, 1946)
7. DULMAGE, F. E. U. S. Patent 2,453,008 (November 2nd, 1948)
8. DULMAGE, F. E. U. S. Patent 2,753,595 (July 10th, 1956)
9. SAXTON, R. L., U. S. Patent 3,006,029 (1st October, 1968)
10. MAILLEFER, C. E. U. S. Patent 3,358,327 (19th December 1967)
11. LE ROY, G. U. S. Patent 3,486,192
12. MADDOCK, B. H. U. S. Patent 3,730,492 (1st May 1973)
13. MADDOCK, B. H. U. S. Patent 3,756,574 (4th September 1973)
14. KUBIK, P., J. Vlcek, C. Tzoganakis, L. Miller. Method of analyzing and quantifying the performance of mixing sections, *Polymer Engineering and Science*, 52 (6), pp. 1232-1240. (2012)
15. GREGORY, R. B. and L. F. STREET. U. S. patent 3,411,179 (19th November 1968)
16. DRAY, R. G. U. S. patent 3,788,612 (31st December 1975)
17. GREGORY, R. B. U. S. patent 3,788,614 (1974)
18. *Compuplast International, Inc.* [online]. ©2014 [viewed 2014-02-08]. Available from: http://www.compuplast.com/
19. SCHIPPERS, H. U. S. Patent 3,751,512 (13th October 1972)
20. DRAY, R. F. U. S. patent 3,650,652 (21st March 1972)
21. KRUDER, G. A. U. S. patent 3,870,284 (March 11, 1975)
22. KRUDER, G. A. U. S. patent 4,173,417 (1979)
23. CHUNG, C. I. and R. A. Barr. U. S. patent 4,405,239 (1983)
24. DRAY, R. G. U. S. patent 4,444,507 (24th April 1984)
25. DRAY, R. G. U. S. patent 4,896,969 (30th January 1990)

26. WOMER, T. W., E. J. Buck and B. J. Hudac Jr. U. S. patent 6,672,753 (6th January 2004)
27. WOMER, T. W., E. J. Buck and B. J. Hudac Jr. U. S. patent 7,014,353 (21st March 2006)
28. WOMER, T. W. and W. Smith. U. S. patent 7,156,550 (2nd January 2007)
29. *Nordson Xaloy, Inc.* [online]. ©2012 [viewed 2014-02-08]. Available from: http://www.xaloy.com/Product-Fusion-TM-DEsign-Barrier-Screws
30. *Nordson XALOY* [online]. © 2012 [viewed 2014 – 06 – 05]. Available from: http://www.xaloy.com/Product-Stratablend-Mixer
31. WOMER, T. W. and Brian L. Lepore. U. S. patent 6,488,399 (3rd December 2007)

Method of Analyzing and Quantifying the Performance of Mixing Sections

Pavel Kubik,[1] **Jiri Vlcek,**[2] **Costas Tzoganakis,**[3] **Luke Miller**[4]
[1] *Tomas Bata University in Zlín, Faculty of Technology, Department of Polymer Engineering, Namesti T.G. Masaryka 275, 762 72 Zlín, Czech Republic*

[2] *Compuplast International Inc., Suat Cecha 293, 760 01, Zlín, Czech Republic*

[3] *Department of Chemical Engineering, University of Waterloo, Waterloo, Ontario, Canada*

[4] *Xaloy Corporation, New Castle, Pennsylvania*

In this article, the performance of three different mixing elements on color dispersion in high-density polyethylene and linear low-density polyethylene polymer stream during extrusion is studied. Two similarly designed Maddock mixers and a Stratablend II mixer are used as the last part of a general purpose single screw. Moreover, an inline melt camera is used for the quantification of mixing quality by visualization of gray-scale of the color dispersion and thus mixing. The Stratablend II mixer produces the lowest and most uniform standard deviation. Both the Maddock mixers showed the same trend but higher values of standard deviation. All results are then compared with a full 3D finite element method simulation. Simulations clearly indicate that the Stratablend II mixer has the best mixing abilities and that these are mainly given by its unique design with high average value of shear stress. The role of elongational stress does not appear to have a high influence on mixing for these mixers. The results also suggest that the key factor for achieving better mixing is the frequency by which a large fraction of the material passes through the high shear stress regions of the mixer. POLYM. ENG. SCI., 52:1232–1240, 2012. © 2012 Society of Plastics Engineers

INTRODUCTION

Mixing is very important in many plastics processing industries. Therefore, it is not surprising that considerable effort is spent to study mixing and different types of mixing elements. In principle, there are at least two basic mixing mechanisms. The first one, so-called dispersive mixing, is based on lowering of the size of mixture components. The process has a cohesive complexion due to van der Waals forces between particles. Finally, the second one is distributive mixing, which redistributes the particles through the volume [1]. Benkreira at al. [2] focused on mixing characteristics of single screw plasticating extruder where the most mixing was found due to melting. Later, Benkreira and Britton [3] again discussed about mixing quality. Good masterbatch with a lower melting point and less viscosity than a base polymer was important to achieve a uniform mixture in this case, but they never used a single screw with a mixing section to compare their results. Somers et al. [4] showed results from two similarly designed screws where one of them was equipped with a mixing section with a Stratablend mixer. They clearly confirmed that better mixing can be achieved by using a mixing section on single screw extruder. An inline melt camera (IMC) available at the Xaloy Laboratory in New Castle, Pennsylvania, has been used in the past to provide information about the overall uniformity of polymer mixtures and thus mixing. Womer et al. have tried to investigate mixing quality in extrusion [5], but they have concentrated more on injection molding applications [6, 7].

In this article, a quantitative comparison on mixing quality is presented for an extrusion operation using the IMC. The study is focused on color dispersion in a general purpose screw having a mixing section at the end where two slightly different Maddock mixers and a Stratablend II mixer are used. High-viscosity high-density polyethylene (HDPE) and low-viscosity linear low-density polyethylene (LLDPE) are used to study the effect of the material rheological properties on mixing. Then, all experimental data are compared with numerical simulation
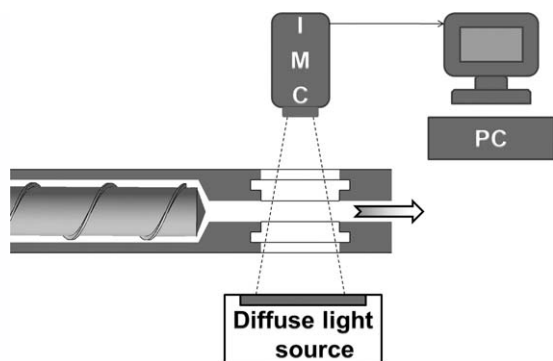
FIG. 1. Inline melt camera system.

results from a full 3D finite element method study, and an effort is made to elucidate the effect of dispersive mixing of shear and elongational stress on the mixing performance of these mixers.

METHODS

The IMC system used in these experiments is shown in Fig. 1.

All measured data are projected on a monitor screen, which is directly connected to a computer with the Mix Quality Analysis software. The main part of the system is the IMC. The camera subsystem consists of a 2048 × 1 pixel scan camera and a high-resolution Schneider Macro Lens in a protective enclosure with configurations for mechanical alignment, focus, and exposure. A light-emitting diode linear light source is also used to illuminate the melt stream. The light goes through two high temperature Pyrex windows, each 2-inch diameter, within a special flat extrusion die. Moreover, the light source and camera are fixed to the same structure to aid alignment so that the light shines straight into to the lens.

The camera scans a grayscale image of the melt stream between the Pyrex windows in the die. A grayscale is a range of shades of gray without apparent color. The darkest possible shade is black with minimum value of 0, which is the total absence of transmitted or reflected light. The lightest possible shade is white with maximum value of 255. This means the total transmission or reflection of light at all visible wavelengths.
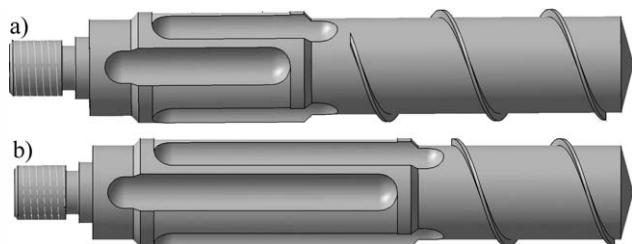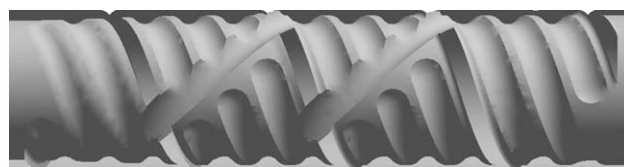

FIG. 2. Maddock mixers.

FIG. 3. Stratablend II mixer C.

GEOMETRY OF MIXING ELEMENTS

Two similar Maddock mixers (Mixers A and B) and a Stratablend II mixer (Mixer C) were used for measurements. The internal diameter of the barrel was 50.8 mm. All mixers were located at the last section of a general purpose screw with a thread at the end to facilitate changing of the mixers. Maddock mixers have been widely used in the plastics industry for a long time while the Stratablend II mixer represents a relatively newer design. The design of the Maddock mixers is displayed in Fig. 2.

As can be seen, the only difference between the mixers A and B was the length of the mixer section. The first mixer has a length of 101.6 mm (2D) and the second mixer has the length 152.4 mm (3D). Both mixers have three pairs of channels with both shearing and wiping flights. The wiping flight cleans the barrel surface. In this case, the material enters the gap over the shearing flight only through the inlet channel. Mixer C is shown in Fig. 3.

The manufacturer claims "The unique, patented geometry of Stratablend II produces highly effective mixing. The Cut-through melt channels allow back flow for chaotic and distributive mixing effects with low shear and little or no temperature rise" [8]. As this mixer is proprietary, the complete design cannot be disclosed. However, we have been allowed to include the key dimensions.

Table 1 contains the key dimensions on the mixers. Both mixers A and B have channels with 8.76 mm radii and shearing gaps of 0.38 mm. Mixer C has channels with a radius of 6.35 mm and shearing gaps of 1.72 mm.

All mixers were tested under processing conditions specified in Table 2.

MATERIALS

The main aim of the chosen materials was to see the effect of material viscosity on mixing. Therefore, a low-viscosity LLDPE and a high-viscosity HDPE were used in the measurements. Material viscosity descriptions are based on the Carreau-Yasuda model in the following form:

TABLE 1. Key mixer dimensions.

Mixer	A	B	C
Channel radius (mm)	8.76	8.76	6.35
Shearing gap (mm)	0.38	0.38	1.72

32

TABLE 2.   Processing conditions.

Heat zones temperature (°C)			
Zone 1	Zone 2	Zone 3	Zone 4
193	205	215	221
Screw speed (RPM)	Mixer A	Mixer B	Mixer C
HDPE—mass flow rate (kg/hr)			
90	37.7	40.4	36.0
75	31.5	33.4	31.2
60	25.4	27.2	24.7
45	19.3	19.7	18.8
30	11.8	13.0	11.5
LLDPE—mass flow rate (kg/hr)			
90	44.7	46.2	44.0
75	37.8	38.9	37.2
60	30.4	32.2	30.0
45	22.1	23.5	22.6
30	14.9	16.5	16.4

$$\eta(\dot{\gamma}, T) = \frac{A f(T)}{\left[1 + (r\dot{\gamma}f(T))^a\right]^{\frac{1-n}{a}}} \qquad (1)$$

where A is the zero shear viscosity, a, n, r are constants, T is temperature, and $\dot{\gamma}$ stands for the shear rate. The material temperature dependence $f(T)$ is exponential and is given by Eq. 2:

$$f(T) = e^{-b(T-T_r)} \qquad (2)$$

The parameter b represents the temperature sensitivity and T_r is the reference temperature. Viscosity curves of both materials at different temperatures are shown in Figs. 4 and 5. Model variables are presented in Tables 3 and 4.

The last material used for the study was a red colorant Profax 6523PP and its melt flow index was 4. The colorant was always added as 1% of the total weight of the base material in form of pellets.

EXPERIMENTAL PROCEDURE

First of all, the extruder was heated up to stabilize temperature in all heat zones. The stabilization of temper-
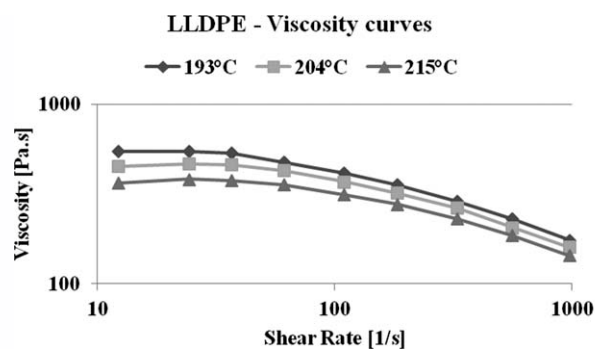

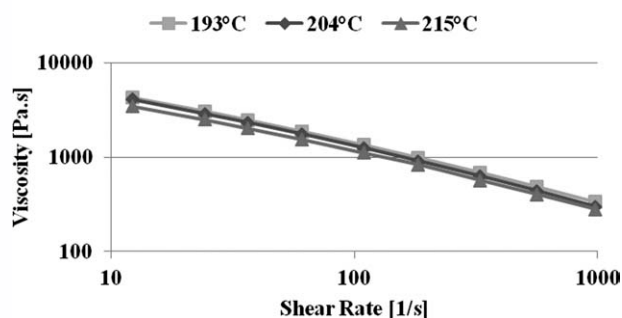FIG. 4.   Viscosity curves for LLDPE.

FIG. 5.   Viscosity curves for HDPE.

ature took at least 1 hr before the start of the measurements. Next, a purging material mixture was extruded to clean the screw and the barrel surface after previous experiments. The cleaning period lasted for 20 min and was repeated again after each new mixer or material change. The camera calibration was done during the cleaning period, too. Thus, a lens aperture, shutter speed and light level were checked to be set correctly. The lighting calibration was especially important because of the uniform lighting background. Moreover, the calibration helped avoid a possibility of fluctuations in grayscale made by nonuniform responses. Then, the colorant was mixed with a polymer as 1% of the total weight of the base material. The amount of the colorant was very important because a wrong amount could strongly change the transparency of the material and thus its proper analysis of the grayscale. Finally, the mixture was poured into a hopper and ran through the extruder. The Mixing Quality Analysis software was used to record all data during the extrusion process. The software recorded data at 500 lines per frame and the sampling time was set at 0.3 sec. The software saved minimum, maximum, average, bandwidth, and standard deviation gray values. Poor mixing therefore corresponded to high standard deviation of gray values, which could be caused by areas with high or low level of color pigment dispersion. On the other hand, good mixing was characterized by uniformly dispersed color areas across the melt stream. Nevertheless, the uniformity was also connected with corresponding low stand-

TABLE 3.   LLDPE model variables.

LLDPE—model variables	
Rheology	
A (Pa s)	539.49
n (-)	0.1
r (s)	0.0022
a (-)	0.7027
T_r (°C)	204
b (1/°C)	0.0172
Thermal properties	
ρ (kg/m^3)	760
C_p (J/(kg C))	2300
λ (W/(m K))	0.24

33

TABLE 4. HDPE model variables.

HDPE—model variables	
Rheology	
A (Pa s)	48,684
n (-)	0.1
r (s)	0.1171
a (-)	0.2542
T_r (°C)	204
b (1/°C)	0.0191
Thermal properties	
ρ (kg/m^3)	770
C_p (J/(kg C))	2250
λ (W/(m K))	0.25

ard deviation and gray values. Melt temperature was measured directly by a hand held melt probe during each test.

All experimental data were later compared with a full 3D finite element method simulation. The simulations were performed with the Virtual Extrusion Laboratory (VEL^{TM}) [9] software created by Compuplast International, Inc.

RESULTS

The data from this study show mainly the effect of different type of the mixer on color dispersion and mixing of the polymer melt. Pictures of color dispersion taken by an 8 mega pixels digital Panasonic camera at the die exit for HDPE at 30 RPM can be seen in Fig. 6.

As shown in the figure, the mixer A had the worst mixing performance, because there were unmixed, dark regions of the colorant in the melt sample visible to the eye. Mixer B was a little bit better, but there were still some unmixed regions in the melt sample. The photo of the sample from Mixer C showed an almost perfectly homogenous mixture. This indicated that Mixer C had the best mixing performance, in this case.

The results of color dispersion from the IMC for LLDPE are given in Table 5.

Table 5 also shows average values from more than 600 points of 10 min measuring period for each RPM. The most important variable from the presented values was the standard deviation. Thus, the high standard deviation or grayscale values were connected to poor mixing, because of regions with a high and low concentration of the color pigment. On the other hand, good mixing referred to uniformly dispersed color in the melt stream and therefore appropriate level of grayscale with the low standard deviation. Moreover, its value could characterize the spread of data points much better than minimum, maximum, or average values, which showed only the location along of 0–255 grayscale.

For a better visualization, values of standard deviation for LLDPE are displayed in Fig. 7.

As can be seen, the measured data also indicate that Mixer C had the best performance. Its standard deviation values were much lower with a small difference between minimum and maximum value of 0.52, than for Mixers A and B, which were close to each other but the long mixer "B" had a little bit better performance and lower standard deviation than the short mixer "A". This was also in agreement with the visual observations of pictures from the digital camera. A trend of decreasing standard deviation increasing value of RPM for all mixers was observed.

Values measured by the IMC for HDPE are summarized in Table 6.

As shown in this table, all values were very similar to LLDPE. Mixer C, once again, had the lowest and the most uniform standard deviation which minimum and maximum value difference was exactly 0.5. The visualization of decreasing standard deviation trend for HDPE is shown in Fig. 8.

The measurements of the color dispersion made by IMC clearly showed that Mixer C had the best mixing performance for both materials in all processing conditions.

A full 3D finite element method simulation was used to simulate the experiment. The simulation of the Maddock mixer was presented in a previous article [10] and
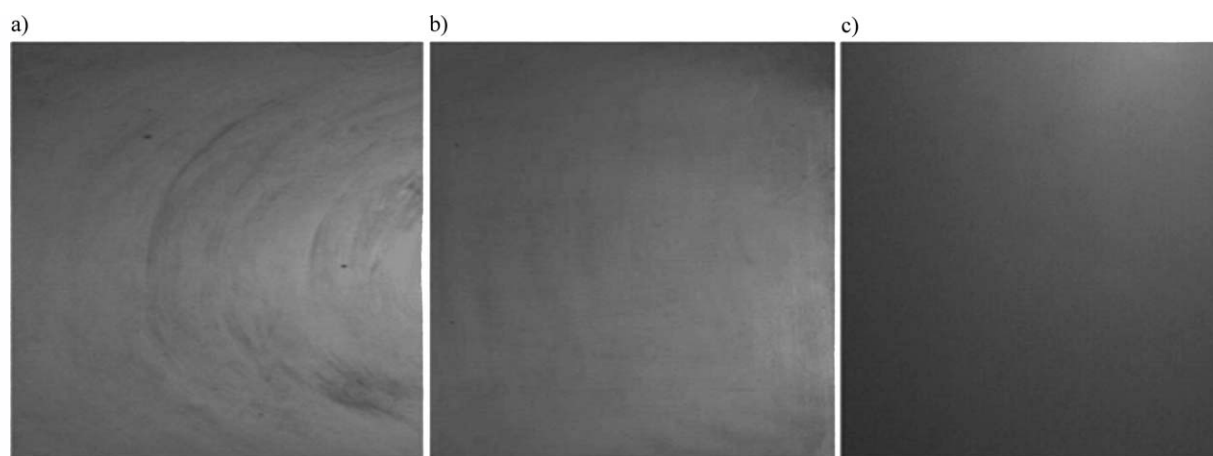

FIG. 6. Melt samples pictures from digital camera: mixer A (left), mixer B (middle), mixer C (right).

34

TABLE 5.   IMC data for LLDPE.

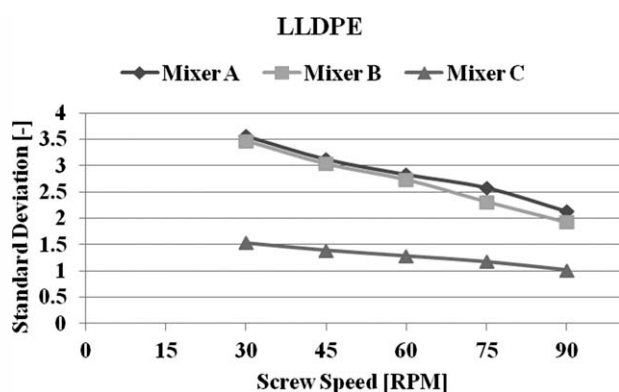| Screw speed (RPM)	30	45	60	75	90
Mixer A—LLDPE—IMC results					
Minimum	8.35	10.29	9.57	9.12	8.50
Average	9.93	11.93	10.68	10.52	10.08
Maximum	11.01	13.36	11.89	12.25	11.47
Band width	2.66	3.07	2.32	3.13	2.97
St. Dev.	3.56	3.12	2.83	2.58	2.13
Mixer B—LLDPE—IMC results					
Minimum	10.35	12.53	11.18	12.56	10.89
Average	12.22	13.62	12.43	14.51	12.35
Maximum	13.92	14.86	13.23	16.39	13.37
Band width	3.57	2.33	2.05	4.34	2.48
St. Dev.	3.47	3.03	2.73	2.31	1.92
Mixer C—LLDPE—IMC results					
Minimum	6.80	9.47	10.41	6.40	6.44
Average	8.03	11.36	13.35	9.67	11.15
Maximum	8.87	12.55	14.93	10.92	12.90
Band width	2.07	3.08	4.52	4.53	6.46
St. Dev.	1.53	1.39	1.28	1.17	1.01

FIG. 7.   Standard deviation for LLDPE.

the same procedure was used here. Grid parameters for mixer A, B, and C are shown in Tables 7 and 8. Typical 3D FEM grid examples are presented in Figs. 9 and 10.

TABLE 6.   IMC data for HDPE.

Screw speed (RPM)	30	45	60	75	90
Mixer A—HDPE—IMC results					
Minimum	8.12	10.07	9.34	8.99	8.27
Average	9.47	11.67	10.48	10.56	9.76
Maximum	10.86	13.17	11.64	11.96	11.21
Band width	2.74	3.63	2.30	2.97	2.94
St. Dev.	3.46	3.01	2.75	2.46	2.03
Mixer B—HDPE—IMC results					
Minimum	10.14	12.32	10.89	12.27	10.46
Average	12.02	13.39	11.91	14.12	11.81
Maximum	13.76	14.49	13.08	15.82	13.19
Band width	3.62	2.17	2.19	3.55	2.59
St. Dev.	3.39	2.94	2.66	2.25	1.88
Mixer C—HDPE—IMC results					
Minimum	4.31	5.12	4.98	5.12	5.03
Average	5.35	6.65	5.80	6.47	5.89
Maximum	6.62	8.89	7.46	8.66	7.64
Band width	2.30	3.37	2.47	3.54	2.61
St. Dev.	1.48	1.33	1.25	1.16	0.98
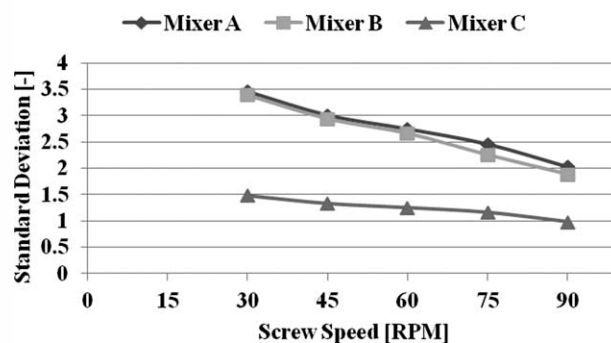
FIG. 8.   Standard deviation for HDPE.

TABLE 7.   Grid parameters of mixer A and B.

Element type—Hexahedral			
Mixer A		Mixer B	
NOF. Points	15,588	NOF. Points	21,220
NOF. Elements	13,888	NOF. Elements	19,040

There are many interesting variables that can be investigated with the simulation. Figure 11 shows some pathlines, as calculated by the simulation, for Mixers B and C. The starting location of all the pathlines (or particles) is similar.

It can be seen, from Fig. 11, that pathlines inside mixer B (or mixer A) had similar patterns. The design of mixers A and B generally resulted in particles mostly rotating slowly in the mixer channels and having only a single pass through the shearing gap. On the other hand, mixer C had much more variability in the pathlines and showing more "spreading" of the initial group of particles. For example, all of the pathlines in Mixer B exit, on the right, in the same general region. In mixer 3, only two pathlines appear to exit in a similar location while the third pathline exits on the opposite side of the mixer (180° away). Furthermore, the pathlines cross into the higher shear gap regions more often.

Thus, it was believed that the average stress criterion would be the most reasonable parameter for quantification of mixing performance. The maximum level of shear stress experienced by the melt has been used frequently in the literature to quantify the mixing performance. However, the polymer melt experiences a distribution of stresses and only a fraction of it passes through the high stress region. Therefore, an average stress is calculated as shown in *Eq. 3* using several pathlines:

TABLE 8.   Grid parameters of mixer C.

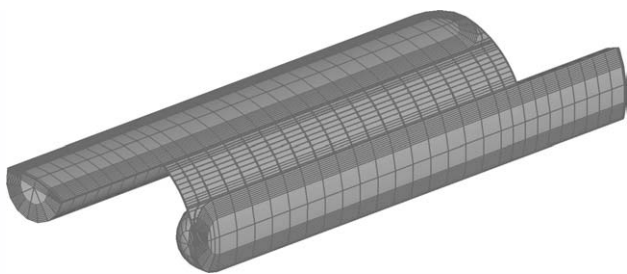| Element type—Tetrahedral	
Mixer C	
NOF. Points	42,617
NOF. Elements	163,656

35

FIG. 9.   Three-dimensional FEM grid example for mixer A or B.
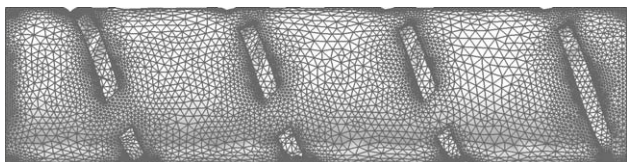
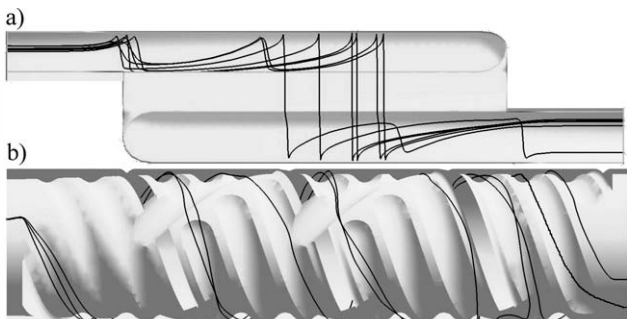
FIG. 10.   Three-dimensional FEM grid example for mixer C.

FIG. 11.   Typical particle pathlines inside mixers.

FIG. 12.   Pathlines used for average stress calculation – mixer A.
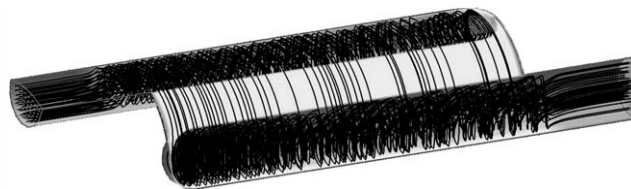

FIG. 13.   Pathlines used for average stress calculation – mixer B.
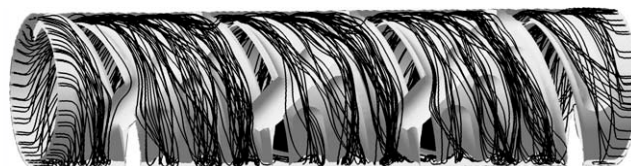

FIG. 14.   Pathlines used for average stress calculation – mixer C.

$$\overline{\tau} = \frac{1}{t_{max}} \int\limits_{0}^{t_{max}} |\tau(t)| dt \qquad (3)$$

where t_{max} is the residence time of particles and $t(t)$ represents stress (shear or elongational) along the chosen pathline. Average stress criterion values counted on more than 50 pathlines (see Figs. 12–14) for all mixers on 60 RPM are shown in Tables 9–11. As can be seen, values of shear stress were much higher than values of elongational stress. Mixer A had the lowest average shear stress for both materials, while mixer C had always the highest value. Elongational stress was at least three times smaller than shear stress. Hence, shear stress was the most important variable responsible for mixing performance of those mixers.

All results were then compared with the results of average stress on a typical pathline. The typical pathline, which traveled through the center of the shearing gap and also the center of the mixer A or B, was chosen for average stress calculations. This pathline had always a similar pattern for each RPM. On the other hand, the most representative pathline for mixer C was the pathline which showed the back flow experience. A comparison of average stress values on typical pathlines given by *Eq. 3* are presented in Table 12.

Interestingly, average stress values taken from the typical pathline were in a good correspondence with results from more than 50 pathlines. The only exception was the elonational stress of mixer C for HDPE, but the value was close enough to not have any strong effect on evaluating the mixing performance of the mixer. Therefore, other values of average stress criterion were counted only for the typical pathline. The results are given in Table 13.

As indicated in this table, elongational stress was very low for all cases. Thus, the shear stress really was the

TABLE 9.   Mixer A average stress values.

Mixer A—60 RPM			
HDPE		LLDPE	
Shear stress (kPa)	Elongational stress (kPa)	Shear stress (kPa)	Elongational stress (kPa)
35.5 ± 2.2	10.5 ± 1.1	7.4 ± 0.7	2.7 ± 0.2
Number of Pathlines		Number of Pathlines	
50		50	

TABLE 10. Mixer B average stress values.

MIXER B—60 RPM			
HDPE		LLDPE	
Shear Stress (kPa)	Elongational Stress (kPa)	Shear Stress (kPa)	Elongational Stress (kPa)
37.1 ± 2.8	11.4 ± 0.9	8.7 ± 1.1	2.9 ± 0.2
	Number of Pathlines		Number of Pathlines
	50		50

TABLE 11. Mixer C average stress values.

MIXER C—60 RPM			
HDPE		LLDPE	
Shear Stress (kPa)	Elongational Stress (kPa)	Shear Stress (kPa)	Elongational Stress (kPa)
62.4 ± 2.2	7.1 ± 0.6	14.6 ± 1.4	1.8 ± 0.3
	Number of Pathlines		Number of Pathlines
	69		64

most important variable responsible for mixing. The trend of calculated values corresponded well with data from the IMC. Mixer C had the highest average values of shear stress for both HDPE and LLDPE.

Typical patterns of both shear and elongational stress along typical pathlines are shown in Figs. 15–18.

Figures 15 and 17 show similar periodic elongation stresses in all mixers with the HDPE experiencing higher elongation stress than the LLDPE. Figures 16 and 18 show that shear stress patterns and levels are relatively similar in both mixers A and B. Mixer B has somewhat higher values, which explains the better mixing performance that was observed over mixer A. However, it is difficult to make a judgment from the results of single pathline, so the average stress criterion, described above, is recommended.

The last part of the comparison of IMC measured values and 3D FEM simulation was focused on the melt temperature. The melt temperature was measured with a hand-held probe directly in the melt stream at the die exit. All temperature values can be seen in Table 14.

TABLE 12. Comparison of average stress results.

60 RPM	Mixer A	Mixer B	Mixer C
HDPE—average shear stress (kPa)			
Several pathlines	35.5 ± 2.2	37.1 ± 2.8	62.4 ± 2.2
Typical pathline	36.5	39.8	62.2
HDPE—average elongational stress (kPa)			
Several pathlines	10.5 ± 1.1	11.4 ± 0.9	7.1 ± 0.6
Typical pathline	10.1	10.6	10.0
LLDPE—average shear stress criterion (kPa)			
Typical pathline	7.4 ± 0.7	8.7 ± 1.1	14.6 ± 1.4
Several pathlines	7.7	9.0	13.9
LLDPE—average elongational stress criterion (kPa)			
Several pathlines	2.7 ± 0.2	2.9 ± 0.2	1.8 ± 0.3
Typical pathline	2.9	2.9	2.1

The results showed a nice correspondence for all processing conditions. The general trend was predicted correctly and the difference between simulations and measurements was not greater than 2.5°C, which is less than 1%.

CONCLUSIONS

The measurements of the color dispersion in polymer melt made by the IMC clearly shows that mixer C has

TABLE 13. Average stress data for HDPE and LLDPE.

Screw speed (RPM)	Mixer A	Mixer B	Mixer C
HDPE—average shear stress criterion (kPa)			
90	43.1	47.8	64.7
75	40.4	44.0	65.3
60	36.5	39.8	62.2
45	31.9	34.8	49.7
30	27.1	29.2	40.6
HDPE—average elongational stress criterion (kPa)			
90	12.2	12.7	7.2
75	11.2	11.6	9.4
60	10.1	10.6	10.0
45	8.8	9.1	6.9
30	7.4	7.6	4.8
LLDPE—average shear stress criterion (kPa)			
90	10.8	11.7	22.6
75	9.3	10.8	17.0
60	7.7	9.0	13.9
45	6.0	7.2	10.5
30	4.2	5.1	6.5
LLDPE—average elongational stress criterion (kPa)			
90	3.8	2.2	2.5
75	3.5	3.5	2.4
60	2.9	2.9	2.1
45	2.2	2.4	1.7
30	1.6	1.7	1.1

37

HDPE - ELONGATIONAL STRESS - 60RPM

— Mixer A — Mixer B — Mixer C
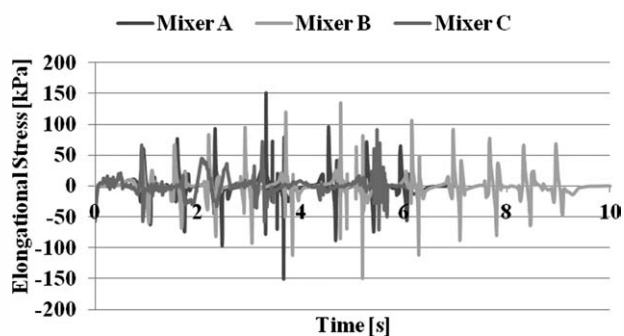
FIG. 15.   Elongational Stress for HDPE at 60 RPM.

LLDPE - ELONGATIONAL STRESS - 60RPM

— Mixer A — Mixer B — Mixer C
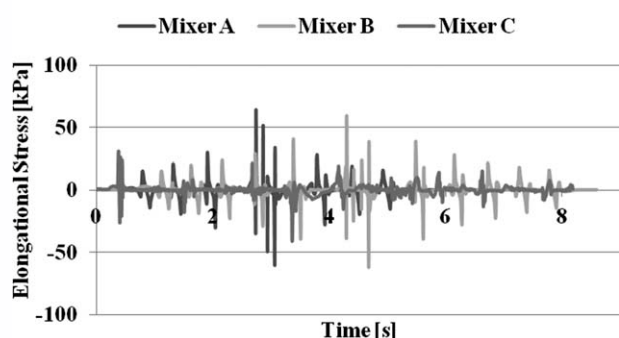
FIG. 16.   Elongational stress for LLDPE at 60 RPM.

HDPE - SHEAR STRESS - 60RPM

— Mixer A — Mixer B — Mixer C
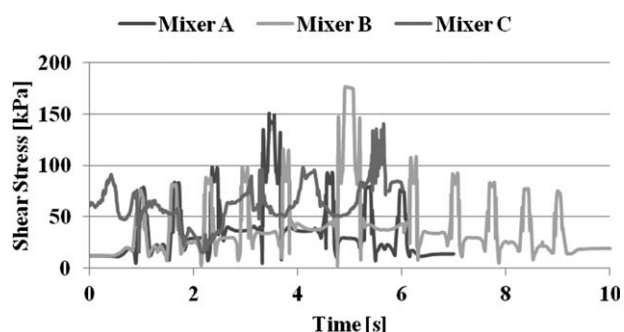
FIG. 17.   Shear stress for HDPE at 60 RPM.

LLDPE - SHEAR STRESS - 60RPM

— Mixer A — Mixer B — Mixer C

FIG. 18.   Shear stress for LLDPE at 60 RPM.

TABLE 14.   Comparison of melt temperature.

Screw speed (RPM)	Mixer A	Mixer B	Mixer C
HDPE—Melt Temperature (°C)—Measurements			
90	225.8	226.5	227.2
75	224.2	225.9	226.9
60	224.9	225.8	226.9
45	223.8	224.3	225.1
30	223.4	224.3	225.8
HDPE—melt temperature (°C)—simulations			
90	224.6	225.3	224.7
75	224.1	224.7	225.4
60	223.6	224.2	225.3
45	223.1	223.5	223.5
30	222.5	222.8	224.2
LLDPE—melt temperature (°C)—measurements			
90	223.4	224.7	225.1
75	222.9	223.4	224.7
60	223.1	224.0	224.5
45	222.6	223.3	224.2
30	222.3	222.6	223.1
LLDPE—melt temperature (°C)—simulations			
90	222.3	223.5	222.7
75	222.1	222.1	222.2
60	221.9	221.9	221.8
45	221.7	221.7	221.8
30	221.5	221.5	221.5

the best mixing performance, of three mixers studied, for both materials in all processing conditions. The mixer keeps much lower and more uniform standard deviation than either of mixers A or B. These mixing results of mixer C appear to be a result of its unique design concept which creates high average shear stress values in a relatively short residence time period. It is interesting to note that the higher average shear stress values are achieved with a larger shearing gap. The number of passage through these high stress regions is believed to be the key variable for better mixing, which is supported by 3D FEM simulations. Moreover, simulations also indicate that the influence of elongation stress appears less important for mixing performance in these mixers. Finally, the melt temperature is in a good correspondence, too. The IMC is therefore a very useful tool, which provides a quantitative analysis of the mixing behavior of different types of mixing elements.

38

REFERENCES

1. Z. Tadmor and C.G. Gogos, *Principles of Polymer Processing*, Wiley, Hoboken, New Jersey (2006).

2. H. Benkreira, R.W. Shales, and M.F. Edwards, *Int. Process.*, **7**, 126 (1992).

3. H. Benkreira and R.N. Britton, *Int. Process.*, **9**, 205 (1994).

4. S.A. Somers, M.A. Spalding, K.R. Hughes, and J.D. Frankland, *SPE-ANTEC Tech. Papers*, **4**, 272 (1998).

5. G. Harrah and T. Womer, *SPE-ANTEC Tech. Papers*, **1**, 267 (1998).

6. R. Sickles, L. Miller, W. Smith, and T. Womer, *SPE-ANTEC Tech. Papers*, **2**, 708 (2007).

7. L. Miller, W. Smith, and T. Womer, *SPE-ANTEC Tech. Papers*, **5**, 2473 (2009).

8. Xaloy Corporation, U.S. Patent 6,488,399 (2002).

9. Courtesy of Compuplast International, Inc., Zlín, Czech Republic.

10. P. Kubik, J. Vlcek, J. Svabik, and M. Zatloukal, *SPE-ANTEC Tech. Papers*, **1**, 773 (2010).

3D SIMULATION OF THE FLUTED MIXER ELEMENT BEHAVIOR

Pavel Kubik, Department of Polymer Engineering, Faculty of Technology, Tomas Bata University in Zlín, Zlín, Czech Republic.

Jiri Vlcek and Jiri Svabik, Compuplast International, Inc., Zlín, Czech Republic

Martin Zatloukal, Polymer Centre, Faculty of Technology, Tomas Bata University in Zlín, Zlín, Czech Republic

Abstract

One of the most important, yet problematic, issues in the extrusion process is achieving good mixing. Considerable prior efforts have been made to understand different types of mixing elements for single-screw and twin-screw extrusion. However, there is still a lack of good process values or criteria that can be used for design purposes. The focus of this work is to better quantify the mixing behavior, using 3D FEM analysis, to develop some design criteria. This study will focus on the fluted mixer, comparing common design variations and the effect of material viscosity and process conditions.

Introduction

Mixing elements can be viewed as unknown and mysterious parts of plastics industry. Therefore, it is not surprising that considerable effort is done to study different types of mixing elements in single-screw [1-3] and twin-screw [4-11] extrusion. Even if many useful conclusions can be extracted from the open literature, full understanding of mixing elements behavior is still not available.

Another aspect, very important in study of mixing elements, is practical knowledge of experienced workers but reality can be different.

In this paper, a deep attention is focused on a fluted mixing element widely used in the plastics industry. Two slightly different designs are studied. One type is much easier to manufacture and many people believe that this geometry change has very little impact on its performance.

For this purpose, a full 3D Finite Element Method simulation will be utilized to understand the effect of the fluted mixer element in extrusion process.

Methods

Two types of fluted mixing elements can be seen in Figure 1. The first one, so called a closed mixer, had an undercut on one flight between the channels. The second flight of this mixer does not have an undercut. This flight wipes the surface of the barrel. In this case, the material entered the gap over the undercut only through the inlet channel. The second one, so called an open mixer, had undercuts from both sides of the channels and there was no wiping of the material from the barrel surface. Because of this, the melt did not enter the channel only from the inlet, but also from the side.
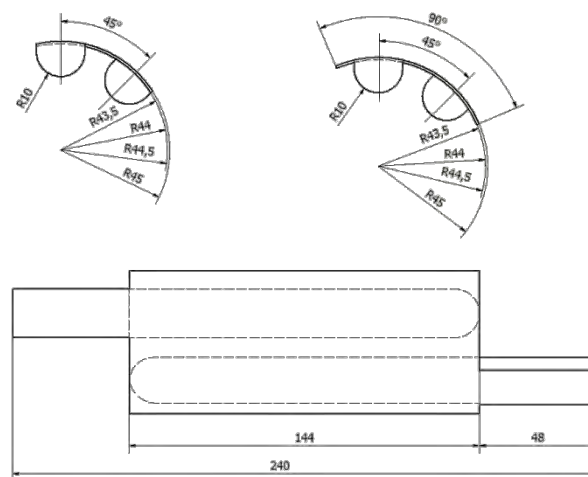

Figure 1. Design of the investigated fluted mixers in closed and open configurations

A basic 3D FEM grid was generated by a fluted mixer template, which is a special part of the VEL™ software [12]. Now, the grid was refined especially in the corners and along the length to minimize the computational errors and to increase the numerical stability. The diameter of the mixer analyzed was 90mm

and three different undercut gaps, 0.5 - 1.0 - 1.5 mm, were used for the numerical analysis. Both fluted mixers were tested under the same process conditions specified in Table 1.

Table 1. Process conditions

Screw Rotations [rpm]	30	60	90
Mass Flow Rate [kg/h]	75	150	225

Materials

The main material used for the study was low viscosity LDPE, which was completely predefined in the VEL™ software material database. The material description is based on the Carreau-Yasuda model, in which the viscosity dependence is decribed by the following equation:

$$\eta(\dot{\gamma},T) = \frac{A f(T)}{\left[1 + \left(r \dot{\gamma} f(T)\right)^a\right]^{\frac{1-n}{a}}} \tag{1}$$

Where A is the zero shear viscosity, a, n, r are the constants, the T is temperature and $\dot{\gamma}$ is the shear rate. The material temperature dependence $f(T)$ is exponential and is given by the following equation:

$$f(T) = e^{-b(T-T_r)} \tag{2}$$

The parameter b represents the temperature sensitivity and T_r is the reference temperature. The equation parameters and the material properties are summarized in Table 2.

Table 2. Material properties - LDPE

Rheology		Thermal Properties	
A [Pa.s]	8000	ρ [kg/m³]	750
n [-]	0.17		
r [s]	0.97	Cp [J/(kg.C)]	2300
a [-]	0.50		
T_r [°C]	200	λ [W/(m.K)]	0.24
b [1/°C]	0.02		

The material had a very low shear viscosity (its MFI is about 4). It was chosen to eliminate the dissipation during the flow through the element and thus to see the effect of mixing.

The second material used for comparison at the 1.0mm gap was a high viscosity HDPE. Its viscosity is described by the Power-law model. The viscosity equation is:

$$\eta(\dot{\gamma},T) = Af(T)\dot{\gamma}^{n-1} \tag{3}$$

Where A is the zero shear viscosity, $\dot{\gamma}$ is the shear rate, n is the Power-law constant. The temperature dependence $f(T)$ is the same as for the LDPE material (eq. 2). Values of the Power-law parameters and melt properties can be seen in Table 3.

Table 3. Material properties - HDPE

Rheology		Thermal Properties	
A [Pa.s]	27409	ρ [kg/m³]	790
n [-]	0.37		
T_r [°C]	190	Cp [J/(kg.C)]	2500
b [1/°C]	0.02	λ [W/(m.K)]	0.18

This material was much more viscous (its MFI is about .3). When such a material flows through the mixing element there was a coupling of two effects. The first one was mixing as in the previous case and the second one was the dissipation.

Modeling

The inlet temperature was set as a temperature field in the range of 220°C to 200°C. The temperature contours are shown in Figure 2. As can be seen, the hottest melt was in the center of the inlet channel and the walls were set as the coolest place with constant temperature 200 °C. The aim of this was to see the changes in the temperature field. This can helped understand the behavior of the fluted mixing element. There were two expected effects. One was the cooling/heating of the material while going through the mixing element. The second one was the homogenization of the temperature field. The temperature homogenization was given partially by the conductivity but mainly by mixing. Such a mixing corresponded to a pure blending and it was based on particle displacement only. It was not say anything about breaking particles inside the element etc. If it was found that the mixer homogenized temperature well it means that it would also mix compatible materials with similar viscosities.

The temperature change in the average temperature showed how much the material generated heat and how much heat was conducted through the wall, mainly the barrel.

For the LDPE material with its low viscosity we could expect that the dissipation will be low and thus the temperature changes were given mainly by the heat transfer. For the HDPE material we have a combination of both effects.
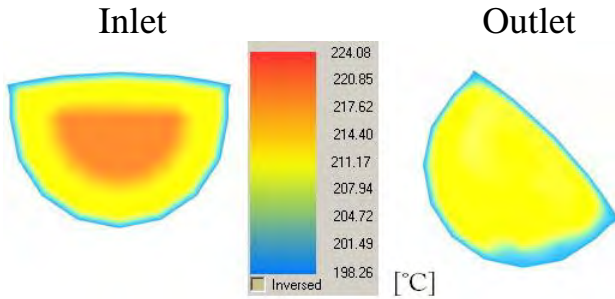
Inlet   Outlet

Figure 2. Inlet and outlet temperature profile

Results

The difference in the average inlet and outlet temperatures, ΔT, as a function of the screw rotation and the fluted mixer gap are given in Tables 4-7. Tables 4-5 contain the results for the LDPE material, while Tables 6-7 provide the results for a comparison with the HDPE material for the undercut gap 1.0mm. As can be seen from the calculated data summarized in Tables 4-7, the value ΔT differs significantly between the open and closed fluted mixers even if the corresponding processing conditions are identical.

Table 4. Temperature Difference – Open Mixer

Mixer Gap [mm]	ΔT [°C]		
	n = 30rpm	n = 60rpm	n = 90rpm
0.5	- 12.5	- 8.9	- 6.6
1.0	- 8.9	- 5.7	- 4.0
1.5	- 7.4	- 4.5	- 3.1

Table 5. Temperature Difference – Closed Mixer

Mixer Gap [mm]	ΔT [°C]		
	n = 30rpm	n = 60rpm	n = 90rpm
0.5	- 13.9	- 11.1	- 9.4
1.0	- 12.5	- 9.5	- 7.8
1.5	- 12.0	- 9.1	- 7.5

Table 6. Temperature Difference Comparison – Open Mixer

Mixer Gap 1.0mm	ΔT [°C]	
	HDPE	LDPE
n = 30rpm	- 2.3	- 8.9
n = 60rpm	2.9	- 5.7
n = 90rpm	5.7	- 4.0

Table 7. Temperature Difference Comparison – Closed Mixer

Mixer Gap 1.0mm	ΔT [°C]	
	HDPE	LDPE
n = 30rpm	- 6.8	- 12.5
n = 60rpm	- 2.3	- 9.5
n = 90rpm	0.4	- 7.8

The highest temperature drops of LDPE occurred for the lowest screw rotations because the melt had the longest residence time allowing a more effective heat flux through the walls.

A comparison of temperature changes for both materials indicated that temperature decreased for all screw rotations for LDPE, while for HDPE the sign of the temperature change depended on screw rotations. Temperature decreased for slow rotations and increased for the highest one. This means that the dissipation was higher than the cooling. A comparison of values for LDPE and HDPE also showed that HDPE temperature drop is much higher than for LDPE. This was because of the dissipation in the HDPE material. If we subtracted the temperature difference for the LDPE material from the value for the HDPE one this gave the temperature rise because of the dissipation. It can be seen that the difference is in all cases about 7 °C.

Interestingly, the open fluted mixer had always lower temperature drops ΔT than the closed one. This can be explained by a presence of a layer, which was rotating very close to the barrel and it was not wiped by the flight. The polymer melt has a low thermal conductivity and the layer functioned as an insulation layer. Thus, the layer restricted heat flux through the walls. A flow path of a particle from the insulation (not wiped) layer is shown in Figure 3.
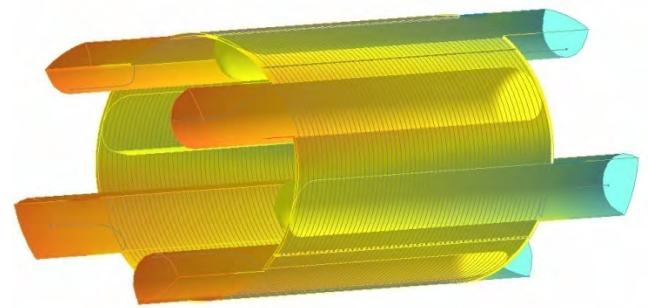

Figure 3. Visualization of a flow path of a particle from the insulation layer for the open fluted mixer

It should be also mentioned that the residence time of the particles in the insulation layer was six times longer than residence time of other particles and the shear stress in this layer was found to be less than 20 kPa. A low shear stress may lead to polymer melt degradation [13]. The shear stress profile along the flow path of the particle in the insulation layer is shown in Figure 4.
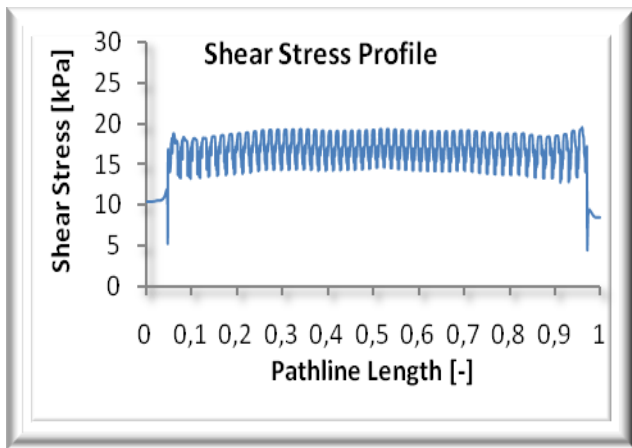
45

Figure 4. Shear stress profile for a particle from the insulation layer

Figure 5. Pressure profile through the open fluted mixer

A comparison of the behavior of a mixing element with and without the wiping flight showed that there was a difference in the mixing element behavior and that the mixing element without the wiping flight had a lower cooling efficiency and much higher residence time, which means it could easier initiate the material degradation.

The second studied effect was the pressure drop on the mixing element. All pressure values were counted from the same path line, which was going through the center of the gap and mixing element. The pressure drop and the barrier pressure drop on the open mixer are shown in Table 8 and Table 9. As can be seen, the pressure drop of the most closed gap was almost three times bigger than on the open gap. The path line position was chosen in a way that the shear stress was not dominant and therefore the influence of the drag flow was the controlling factor. The pressure drop went down with the increase of screw rotations and also with opening the gap. The barrier pressure drop shown in Figure 5 in a highlighted rectangle shows what part of the overall pressure drop was consumed during the flow over the undercut. There were local maxima when the material was comes close to the barrel and minima when the material was at the bottom of the channel. The highest drop was over the barrier.

Table 8. Pressure Drop – Open Mixer

Mixer Gap [mm]	Pressure Drop [MPa]		
	n = 30rpm	n = 60rpm	n = 90rpm
0.5	1.66	1.51	1.13
1.0	0.56	0.68	0.75
1.5	0.45	0.55	0.62

Table 9. Barrier Pressure Drop – Open Mixer

Mixer Gap [mm]	Barrier Pressure Drop [MPa]		
	n = 30rpm	n = 60rpm	n = 90rpm
0.5	1.04	1.04	0.95
1.0	0.20	0.23	0.23
1.5	0.14	0.15	0.16

The pressure drop on the closed mixer is shown in Tables 10 and 11. It can be seen that the situation was completely different from results for the open mixer. The barrier pressure drop became sometime negative. Therefore, pressure was generated while the material flowed through the gap on the closed mixer. It is demonstrated in figure 6. As displayed in Figure 6, pressure decreased again until the undercut area, which is represented by a yellow rectangle, where the pressure rose. The local minima and maxima were again close to the screw or the barrel surface. The pressure drop also increased more for higher screw rotation and the gap size. Pressure was consumed for the smallest gap.

Table 10. Pressure Drop – Closed Mixer

Mixer Gap [mm]	Pressure Drop [MPa]		
	n = 30rpm	n = 60rpm	n = 90rpm
0.5	0.53	0.64	0.72
1.0	0.14	0.20	0.25
1.5	0.08	0.14	0.20

Table 11. Barrier Pressure Drop – Closed Mixer

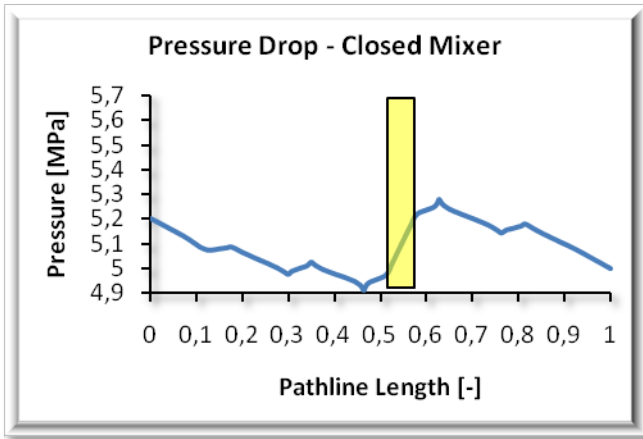| Mixer Gap [mm]	Barrier Pressure Drop [MPa]		
	n = 30rpm	n = 60rpm	n = 90rpm
0.5	0.13	0.17	0.18
1.0	- 0.15	- 0.18	- 0.18
1.5	- 0.21	- 0.23	- 0.26

46

Figure 6. Pressure profile through the closed fluted mixer

Table 12. Pressure Drop Comparison

Mixer Gap 1.0mm	Pressure Drop [MPa]			
	HDPE		LDPE	
	Open	Closed	Open	Closed
n = 30rpm	3.91	- 0.39	0.56	0.14
n = 60rpm	4.86	- 0.53	0.68	0.20
n = 90rpm	5.51	- 0.61	0.75	0.25

Table 13. Barrirer Pressure Drop Comparison

Mixer Gap 1.0mm	Barrier Pressure Drop[MPa]			
	HDPE		LDPE	
	Open	Closed	Open	Closed
n = 30rpm	1.81	- 1.91	0.20	- 0.15
n = 60rpm	2.37	- 2.43	0.23	- 0.18
n = 90rpm	2.55	- 2.75	0.23	- 0.18

A comparison of the pressure drops for a 1 mm gap on both types of mixers is shown in Tables 12 and 13. It can be seen that the pressure drop on the closed mixer was always higher than on the open mixer. As has been demonstrated by previous tables for LDPE, the open and closed mixers behave differently. The pressure behavior of the more viscous HDPE in the open and closed configuration was similar to LDPE. Pressure drop and barrier pressure drop profiles had a similar trend like for LDPE but the values were higher because of the material viscosity.

In the final stage of the research, the mixing efficiency of the closed and open fluted mixers was investigated by a λ parameter, which is defined as:

$$\lambda = \frac{|\omega| + |D|}{|D|} \qquad (4)$$

Where D is the deformation rate tensor and ω is the vorticity tensor. The mixing coefficient λ was calculated along the same path line as the pressure and is depicted in Figure 7.
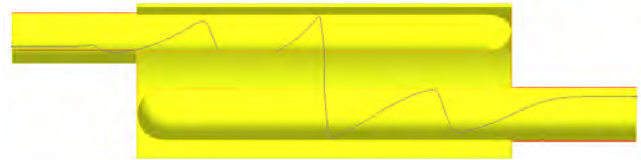

Figure 7. Path line for pressure and mixing efficiency calculation
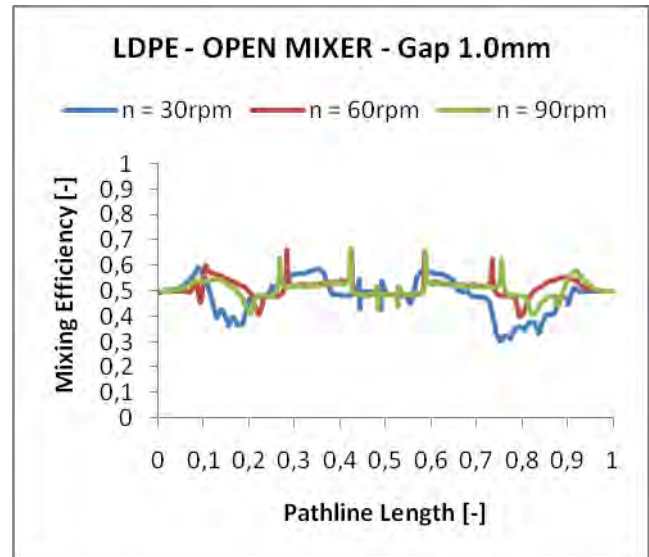

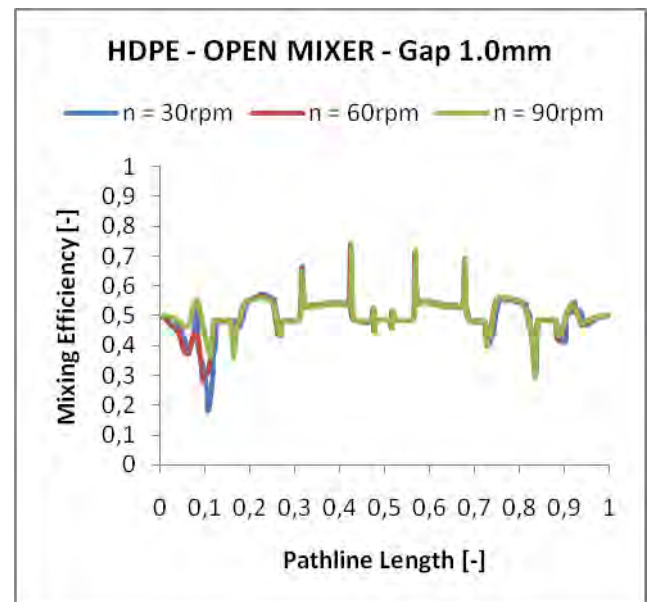Figure 8. LDPE Mixing efficiency of the open fluted mixing element

Figure 9. HDPE Mixing efficiency of the open fluted mixing element

Figures 8 - 11 show the calculated mixing efficiency parameter λ for 1.0mm gap on the open and closed fluted mixer elements. Interestingly, the mixing efficiency is almost the same in all cases. Thus, the geometry changes

47

and material properties did not have any impact to mixing efficiency parameter.

It can be seen that the parameter λ was in most cases around a value.5, which means the shearing. This confirmed that the majority on both cases of the mixers was the shear mixing.
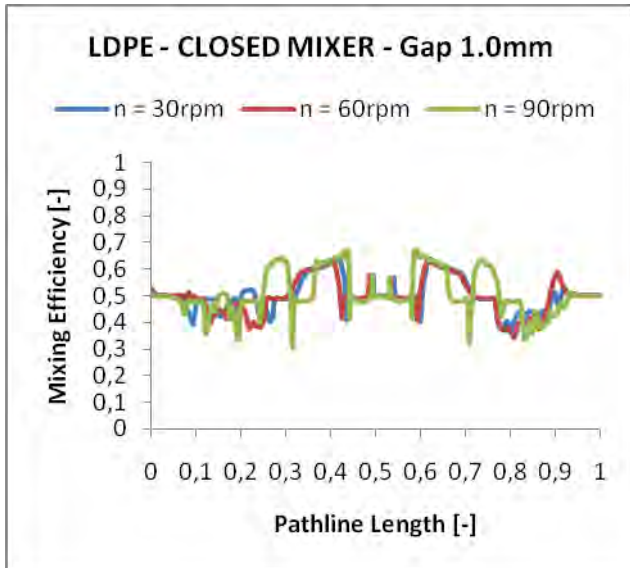

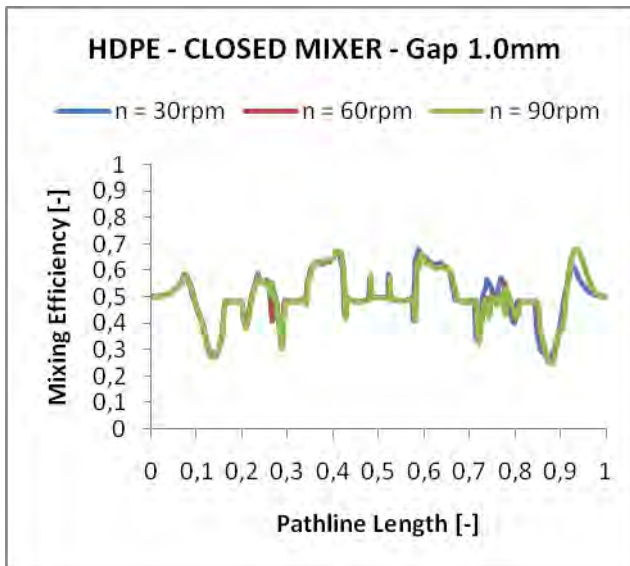Figure 10. LDPE Mixing efficiency of the closed fluted mixing element

Figure 11. HDPE Mixing efficiency of the closed fluted mixing element

Resume

The simulations performed show different behavior of the open and closed fluted mixers. The main reason of this difference is the existence of insulation layer for the open mixer. This layer is located at the barrel surface and it works as a barrier of the heat transfer. On the other side, since the layer is there it occupies certain part of the gap over the undercuts and thus it makes the gap effectively smaller than for the closed mixer. This layer is wiped out in the closed mixer. It has been found that the shear stress in the insulation layer is lower than 20 kPa, which may lead to polymer melt degradation. Pressure profiles and pressure drops depend also on the material type, gap size and the speed of rotation. The analysis clearly shows that the mixing efficiency defined by the λ parameter is independent on the material properties and the geometry variations of the fluted mixer.

References

1. A. L. Kelly, E. C. Brown and P. D. Coates, *Polymer Engineering and Science* **46**, 1706-1714 (2006).
2. M. E. Ghir, C. G. Gogos, D. W. YU, D. B. Todd and B. David, *Advances in Polymer Technology 17,* 1-17 (1998).
3. D. Strutt, C. Tzoganakis and T. A. Duever, *Polymer Engineering and Science* **40**, 992-1003 (2000).
4. G. Shearer and C. Tzoganakis, *Advances in Polymer Technology* **20**, 169–190 (2001).
5. D. Strutt, C. Tzoganakis and T. A. Duever, *Advances in Polymer Technology* **19**, 22–33 (2000).
6. M. A. Huneault, M. F. Champagne and A. Luciani, *Polymer Engineering and Science* **36**, 1694-1706 (1996).
7. V. L. Bravo and A. N. Hrymak, *Polymer Engineering and Science*, **40**, 525-541 (2000).
8. V. L. Bravo, A. N. Hrymak and J. D. Wright, *Polymer Engineering and Science* **44**, 779-793 (2004).
9. R. Valette, T. Coupez, C. David and B. Vergnes, *International Polymer Processing* **24**, 141-147 (2009).
10. T. Ishikawa, et al., *International Polymer Processing* **21**, 354-360 (2006).
11. Ch. Rauwendall, *Polymer Extrusion*, Munich: Carl Hanser Verlag, 1990.
12. http://www.compuplastvel.com
13. M. Zatloukal, J. Vlcek, A. Slanik, A. Lengalova and J. Simonik, *Applied Rheology* **12**, 126-132 (2002).

Key Words: Fluted Mixer, Insulation Layer, 3D Finite Element Method Simulation

EXPERIMENTAL AND NUMERICAL ANALYSIS OF THE PERFORMANCE OF TWO FLUTED MIXER DESIGNS

Pavel Kubik,
Tomas Bata University in Zlín, Faculty of Technology, Department of Polymer Engineering, Namesti T.G. Masaryka 275, 762 72 Zlín, Czech Republic

Martin Zatloukal,
Polymer Centre, Faculty of Technology, Tomas Bata University in Zlin, TGM 275, 762 72 Zlin, Czech Republic and Centre of Polymer Systems, University Institute, Tomas Bata University in Zlin, Nad Ovcirnou 3685, 760 01 Zlin, Czech Republic

Yutaro Asai,
I.T.S. Japan Corporation 7-22-7, Misaki, Funabashi-shi, Chiba, 274-0812 Japan

Jiri Vlcek, Compuplast International Inc., Svat Cecha 293, 760 01, Zlín, Czech Republic

Ilja Paseka,
Compuplast Software spol. s r. o., Svat Cecha 293, 760 01, Zlín, Czech Republic

Ryuichi Haruna and Yoshihiko Iwasaki,
PLA GIKEN CO., LTD 39-6, Toyotsu-cho, Suita-city, Osaka, 564-0051 Japan

ABSTRACT

In this paper, the effect of the Maddock mixer design on its performance in single screw extrusion of HDPE melt has been investigated experimentally on a special extrusion line equipped with a barrel having several glass windows as well as theoretically by using a three dimensional finite element method simulation. The red-green-blue spectral analysis has been used for experimental quantification of the mixing efficiency whereas generalized Newtonian model (with Carreau-Yasuda viscosity function) and viscoelastic modified White-Metzner model have been utilized in flow simulations. Based on the performed experimental work it has been found that the mixer with no undercut wiping flight ("Closed" mixer) has a faster mixing/purging but a similar final mixing performance as the mixer with undercut wiping flight ("Open" mixer). It has also been revealed that the "Open" mixer creates unwanted dead zone (in the form of the stagnation layer of material rotating between the mixer and the barrel) at which the polymer melt degradation may takes the place. It has been found that based on the stress, residence time and pathline calculation it is possible to predict the experimentally observed tendency of the "Closed" mixer for a faster mixing/purging in comparison with the "Open" mixer as well as the presence of stagnation layer in the "Open" mixer. The performed theoretical parametric study indicates that the gradual opening of the wiping gap causes that the pressure driven flow became more dominant than the drag flow in shearing as well as in the wiping gap independently of the utilized rheological model. On the other hand, the predicted particle trajectories inside the mixer were found to be shorter for the viscoelastic model, tending to occur mainly in the middle of the channel and thus leaving the mixer a little bit faster in comparison with the purely viscous calculations. Finally, it has been revealed that for the highest tested wiping flight opening, the viscoelastic modified White-Metzner model predicts back flow over the wiping flight whereas the purely viscous Carreau-Yasuda do not, which can be explained by the elongational viscosity, considered in the viscoelastic modified White-Metzner model. This suggests that modified White-Metzner model should be preferred more than purely viscous Carreau-Yasuda model in the mixing element die design optimization.

INTRODUCTION

Mixing is a very important process in single-screw extrusion. Achieving good mixing performance, under specified processing conditions, is a key requirement to obtain a uniform and homogenous mixture. So, it is not surprising that considerable effort is spent on analyzing different types of "mixing elements", "mixing heads" or "mixing sections" in single-screw [1-6] and also twin-screw [7-13] extrusion. In principle, there are two basic mixing mechanisms. Dispersive mixing is based mainly on reducing the size of mixture components by shear or elongational stress. The second one is distributive mixing that redistributes particles throughout the volume [14].

A fluted mixing element, also known as the Maddock mixer [15], is one of the most often examined dispersive mixing sections in extrusion. Almost forty years ago, Tadmor and Klein [16], studied certain designs of fluted mixing sections and proposed a model for calculation of pressure development through the fluted mixing section. Tadmor et al. [17] later improved the model by using the Flow Analysis Network method. Esseghir et al. [18] carried out a detailed comparative study of three different single-screw mixing elements including the Maddock mixer section.

Han and Lee [19] experimentally and also numerically investigated the flow in the Maddock mixer. Their work focused mainly on pressure drop and pressure rise through the mixer. Their results clearly concluded that pressure was generated, under specific processing conditions, and therefore drag flow was predominated over pressure-driven flow. In their work, only 2D analysis was used to compute simulation results and the mixing performance of the Maddock mixer section was not evaluated.

In this work, the evaluation of the mixing performance of the fluted mixer type depicted in Figure 1 using the Red-Green-Blue (RGB) spectral analysis method is presented. The study is focused on color dispersion of the material extruded by two general purpose screws having slightly different fluted mixing sections. The "Closed" design has alternating "shearing" and "wiping" dams (or flights) while the "Open" design is completely undercut so that there are no "wiping" dams. It can be seen that the "Open" design is easier to manufacture and many people assume that this geometry change has little, or negligible, impact on its overall mixing performance. To investigate this assumption, experiments, comparing these two fluted mixer designs, have been performed. A three dimensional Finite Element Method (3D FEM) simulation is also used to help analyze and better understand the fluted mixing element flow field.

METHODS

Two general purpose screw designs were prepared for this experiment. The basic screw dimensions are summarized in Table 1.

The only variation between these two screw designs was the mixing section where two slightly different fluted mixing elements were used. Both mixers had three pairs of channels. The shearing gap width was 9.0 mm, its depth was 0.4 mm and a radius of each channel was 7.2 mm. The length of the shearing gap was 80 mm.

The "Closed" mixer depicted in Figure 2 had separated pairs of inlet and outlet channels with a shearing gap in between. The wiping flight prevented material flow and cleaned the barrel surface.

The "Open" mixer depicted in Figure 3 was undercut from both sides of each channel. Thus, the material was not wiped from the barrel surface. Therefore, part of the melt could continuously flow in the gap between the mixer and the barrel.

Experiments were done on a special extrusion line with a barrel having several glass windows which are alternately placed on both sides of the barrel as shown in Figure 4. This allowed observation of the polymer melt along the extrusion line from the solids conveying zone to the metering zone. Dimensions of each window were 90x10 mm and the internal diameter of the barrel was 40 mm.

The mixer was positioned to be visible through the glass window (black window in Figure 4).

The extruder was part of a small sheet line that includes a flat die, chill roll stack and collection system. All experiments were continuously recorded by a video camera which was set on a tripod. Experimental processing conditions are given in Table 2.

MATERIAL

The main material used for the experiment and later simulation study was Hi-Zex 6300M HDPE. Rheological properties were measured on a laboratory grade twin-bore capillary rheometer (Imatek R6000 [20]) with ϕ1x16mm long die and ϕ1×0.25mm short die. For a purpose of 3D FEM simulations, rheological data was fitted by two different models.

The first one was the well known Carreau-Yasuda model, in which the viscosity dependence is decribed by the following equation:

$$\eta(II_D, T) = \frac{\eta_0 f(T)}{\left[1 + \left(\lambda \sqrt{II_D} f(T)\right)^a\right]^{\frac{1-n}{a}}} \tag{1}$$

Where η_0 is the zero shear viscosity, a, n, λ are constants, T is temperature and II_D stands for the second invariant of the deformation rate tensor. The material temperature dependence $f(T)$ is exponential and is given by an equation:

$$f(T) = e^{-b(T-T_r)}$$

(2)

The parameter b represents the temperature sensitivity and T_r is the reference temperature. For a purpose of more detailed understanding of the Fluted mixer, elongational viscosity data was added to the calculation model, as well. Uniaxial elongational viscosity was determined on a laboratory grade twin-bore capillary rheometer Imatek R6000 using the method presented by Cogswell [21]. In order to take steady shear as well as steady uniaxial elongational viscosity into account, the following modified White-Metzner model proposed by [22] was utilized:

$$\tau_{i,j} + \lambda(II_D)\frac{\delta\tau_{i.j}}{\delta t} = 2\eta(II_D)D_{i,j}$$

(3)

Where $\tau_{i,j}$ is the stress tensor, $\lambda(II_D)$ stands for the relaxation time, $\eta(II_D)$ means the viscosity defined by Eq. 1, $\delta\tau_{i.j}/\delta t$ is the upper-convected time derivative of the stress tensor, $D_{i,j}$ is the deformation rate tensor and II_D represents its second invariant. The relaxation time has a form:

$$\lambda(II_D) = \frac{L_0 f(T)}{1 + K_0 f(T) II_D}$$

(4)

Where L_0 and K_0 are constants. Rheological model parameters are presented in Table 3 and fitted viscosity curves of both models are shown in Figure 5.

A LLDPE based, green masterbatch was used for visualization and mixing performance analysis.

EXPERIMENTAL

The experiment was focused primarily on the mixing performance of the fluted mixing elements. To avoid blending errors, clear HDPE was pushed through the extrusion line until the hopper was almost empty. Next, a certain amount of the

colorant (about 60g) was added to the hopper to a 2 cm layer. This layer of colorant was followed by a new layer of clear HDPE of the same volume. By this method, five distinct layers in order colorant – HDPE – colorant – HDPE – colorant were prepared. Each new layer was always added after the previous layer had completely left the hopper. A screw speed at 21 RPM was used to run this experimental procedure.

The moment when the first colored particles appeared at the end of the extrusion line was the starting point of the measurement. Then, samples of the flat film were cut to see interactions between the clear and colored regions of the polymer. Thus, this experimental part provides some indication about the speed of the mixing process. All experimental parameters were identical for both mixing sections. These samples were later analyzed in a professional Canon scanner. The scanner light was strong enough to reveal the mixing patterns of the samples. Hi-resolution tiff format pictures were prepared for further analysis. All samples were 3x8 cm. Color pictures of scanned samples were studied in special program routine that performed a statistical analysis of the pixels. Some examples of the scanned flat film samples for the "Open" and "Closed" mixer are presented in Figure 6 and 7, respectively.

Then, an average value of RGB spectra was calculated and its deviation was obtained for each pixel. The average value of RGB spectra μ is described by the following equation:

$$\mu = \frac{1}{MN} \sum_{i=0}^{N} \sum_{j=0}^{M} d_{ij}$$ (5)

where M, N represents the number of pixels of the sample and d_{ij} stands for the RGB value of the relevant pixel and ij are indexes of the calculated matrix. d_{ij} was taken in each pixel as an average of three RGB values:

$$d_{ij} = \frac{R_{ij} + G_{ij} + B_{ij}}{3}$$ (6)

RGB color components of a pixel range values from 0 ({0,0,0} black) to 255 ({255,255,255} white). Thus, the material without any additives, pure polymer melt, has a high mean value of RGB. On the other hand, the dark material with added colorant had to have a low mean value of RGB. The degree of brightness, in between the low and high mean value, represents the degree of mixing. The value

of the unmixed regions is the deviation of average RGB color. The deviation of the average RGB spectra was calculated by the equation:

$$\sigma^2 = \frac{1}{MN} \sum_{i=0}^{N} \sum_{j=0}^{M} d_{ij}^{2} - \mu^2 \qquad (7)$$

Where M, N represents the number of pixels of the sample and d_{ij} stands for the RGB value of the relevant pixel and μ is the mean value of RGB color. The average RGB value reduces as the colorant is added into the process until the mean value of RGB reaches a steady state. The transition from the pure polymer to its colored form is detected by an increase of the deviation of RGB.

The results of RGB spectral analysis equations of the mixing performance can be seen in Figure 8.

As shown in Figure 8, both curves of the average RBG spectra started above 200, which meant that they both were close to the white color with a minimum amount of the green colorant. The decrease of both curves had a similar slope, but the mean value of RGB curves of the "Closed" mixer (μ_1) reduced sooner than the "Open" mixer (μ_2). The difference of RGB curves between the "Open" and "Closed" mixer was about 0.4 minutes. Furthermore, the final, steady state RGB value for each mixer is very close. This means that both mixers can provide similar mixing levels, given sufficient time.

The absence of the wiping flight allowed the formation of a layer of the slowly moving material which was rotating close to the barrel surface. The second experimental method was then focused on the behavior of this layer. Probably the most significant variable to characterize the behavior of this layer was the residence time. Thus, one layer of colorant followed by the pure polymer was again added into the almost empty hopper.

A low screw speed of 7RPM was intentionally used to clearly see the layer behavior. Samples of the flat film were again collected, in ten minute intervals, to calculate the mean value of RGB of the polymer. The transition from pure polymer to maximum color and back to the pure polymer also gave a residence time of the flow field. Samples were again evaluated with the RGB spectral analysis.

The RGB curves of the residence time of the "Closed" (μ_1) and "Open" mixer (μ_2) are displayed in Figure 9.

As can be seen, in Figure 9, the RGB curve started from a value of pure HDPE at time zero and after ten minutes, the minimum RGB value green color was obtained. The first ten minutes was sufficient time for both mixers to achieve the same level of mixing. Then, the amount of green colorant gradually reduced with each new

sample taken from the system. These results show that the "Closed" mixer resulted in faster purging than the "Open" mixer and returned close to its initial RGB value after forty minutes versus seventy minutes with the "Open" mixer. The longer purging time, of the "Open" mixer, was due to the presence of the slow moving layer rotating in the gap region. This layer was difficult to purge out because of the absence of the wiping flight. The layer was still clearly visible after ninety minutes but its effect on the product color was negligible by this time. The experiment was video recorded to help visualize the rotation of the material in this layer. The long residence time layer could potentially influence the final quality of a product due to polymer melt degradation. Furthermore, this layer would also affect the heat transfer from the melt to the barrel surface.

Screen captures from the video, comparing the color change in between the "Open" and "Closed" mixers are shown in Figure 10.

SIMULATION RESULTS

In this part, all experiments performed under the processing conditions summarized in Table 2 are followed theoretically by 3D FEM simulation in order to understand the flow field in both tested Maddock mixers. The stress, residence time and pathline calculation is performed to see if it is possible to predict, firstly, the experimentally observed tendency of the "Closed" mixer for a faster mixing/purging in comparison with the „Open" mixer, and secondly, the experimentally observed presence of the dead zone, i.e. the stagnation layer of material rotating between the „Open" mixer and the barrel. At the end of this section, theoretical parametric study is performed in order to understand the effect of wiping gap size on flow filed in Maddock mixer for the given processing conditions.

Description of the simulation methodology

A 3D FEM grid, of the mixer geometry, was generated with the fluted mixer template in the Virtual Extrusion Laboratory™ (VEL™) software [23]. To help ensure high accuracy, quadratic, 27 node, brick elements were used. The grid was constructed from 16,512 elements for the "Closed" mixer flow domain and 17,792 elements for the "Open" mixer. The periodic nature of the geometry allowed for the analysis of only 1 pair of channels. The closed 3D FEM grid is displayed in Figure 11.

All simulations were run on a personal computer (PC) equipped by 64-bit Windows Vista™ Business edition operating system with Service Pack 2. PC was powered by FPS Group Blue Storm II 400W power source. Intel(R) Core(TM)2 Quad Q9300 @2.5GHz CPU with a passive cooler was used as a processor. Display adapter was ATI Radeon HD 4800 series and four Transcend 2GB DDR2

800DIMM memories were also installed. One calculation by using this PC configuration took about two and half hour to reach a chosen maximum of 150 iterations with an overall tolerance set to 10^{-6}. Temperature was calculated once per iteration and a value of upwinding was set to 0.5. Solver settings for the main variables are given in Table 4.

A 3D FEM solver calculates convection-diffusion Navier-Stokes equations, mass and energy balance equations together with the particular constitutive equation. In more detail, the system is solved in a segregated manner, where node velocities are calculated first. Then, the node pressures are calculated. Next, the node velocities are corrected to satisfy the continuity equation. Finally, the node temperature is determined by solving the segregated energy balance equation using the latest stress data.

The solution of the system (Ax=b) is considered to be converged when some error or residual is below required threshold. The error is usually defined as some ratio between two subsequent iteration results:

$$Error = \frac{\sum \frac{\left| v^n - v^o \right|}{\max(v^n, v^o)}}{n}$$

(8)

The error is easy to be found after the each iteration. However, the error (or difference) might be close to zero, even though, the solution has not reached the correct results.

Another method of measuring the convergence is the residual. The residual is some suitable norm of |Ax-b|. The Galerkin FEM is based on minimizing the residuals. Once residuals are close to a set overall tolerance the solution is finished. Residual curves of the convergence are presented in Figure 12 for a typical analysis. As can be seen, the convergence was reasonably good. The continuity equation was well satisfied after less than thirty iterations. The Error reached a steady value below 0.01 after 50 iterations. However, the momentum residuum continued to decrease until about 140 iterations so the solution was stopped at one hundred and fifty iterations. This behavior was typical for all performed calculations.

Mixing efficiency evaluation through stress calculation

Probably the most significant variables to characterize the mixing behavior of the selected mixers were the shear and elongational stress. The polymer melt experiences a stress history and only a fraction of the melt passes through the high

stress region. Therefore, the maximum level of shear stress reached by the polymer melt cannot be used as a main parameter to quantify the mixing performance. On the other hand, an average stress value, defined according to Eq. 9, can be used to characterize the mixing performance [24]

$$\overline{\tau} = \frac{1}{t_{\max}} \int_0^{t_{\max}} |\tau(t)| dt \tag{9}$$

The average stress value and flow behavior were analyzed with several particle pathlines. The "seed" location of each pathline was placed in the center of the shearing gap, in the middle of the mixer and in a different position along the z axis of the mixer. The same "seed" points were used for both the "Open" and "Closed" mixer. This position of seeds was intentionally chosen to obtain reasonably similar pathlines for a comparison of flow behavior of both mixers. Calculated average shear and elongational stress values, by using these pathlines, are displayed in Table 5 for the same processing conditions as used in the experimental part of this work.

As presented in the table, the values of shear stress were very similar at all RPMs for both mixers. Both rheological models gave shear stress values of the "Closed" mixer a little bit higher than for the "Open"mixer. The Fluted mixer is considered to be a dispersive mixing element. A proper stress analysis is then really important and brings a better look at the overall mixing performance. Thus, if the average stress value should be taken as a determining variable of the mixing performance, the "Closed" mixer had a slightly better mixing performance than the "Open" mixer. This result is in good agreement with results of RGB analysis where the "Closed" mixer showed a faster mixing process but a similar final mixing performance as the "Open" mixer. Elongational stress was found to be much more different when the elongational viscosity was considered through the modified White-Metzner model but, once again, the "Closed" mixer showed a little bit higher values in comparison with the "Open" mixer.

Dead zones evaluation through residence time and pathlines calculation
In this part, the possible presence of dead zones (locations with long residence time where degradation of the polymer melt is highly probable) for the both Maddock mixers was investigated for the same processing conditions as used in the experimental part of this work. It was revealed that overall flow behavior, mainly the residence time of the particles, inside the mixer is strongly affected by the

elongational stress. The material rather stayed in the middle of the channel and did not want to flow to the corners of the mixer, where the biggest elongational stress was found. A reluctance of filling the corners of the geometry by using the White-Metzner model meant a shorter trajectory for particles inside the mixer. So, particles mainly stayed in the middle of the channel and left the mixer a little bit faster. The difference in residence time of particles was a few seconds. White-Metzner model, nevertheless, always showed shorter residence time than the Carreau-Yasuda model. Average residence times for all RPMs and both rheological models are displayed in Table 6.

Some typical pathlines, which are representatives of the flow behavior in the "Open" and "Closed" mixer, are depicted in Figures 13 and 14.

It can be seen, from Figure 13, that the "Closed" mixer resulted in the pathline making only one pass through the shearing gap while Figure 14 show a pathline making many rotations in the gap region. This represents a high residence time layer near the barrel surface. This layer is created because of the absence of the wiping flight. The residence time of this layer, estimated by the 3D FEM simulation, was also much longer than the overall residence time of all other pathlines. The residence time of some typical pathline in the layer was found to be at least ten times longer than the average residence time of the mixers. Calculated average, layer residence times, at three different screw speeds utilized in the experimental work are shown in Table 7.

Effect of wiping gap size on flow filed in Maddock mixer – parametric study

In order to investigate the stagnation layer origin as well as the velocity field in Maddock mixer through the flow modeling, the effect of the wiping gap (H_1 in Figure 15) was opened in four steps. The first step of this opening was made as one quarter of the shearing gap size (H_1=0.4mm in Figure 15). Next, the gap was opened to a half and then to three-quarters of the shearing gap size. Finally, the wiping gap was made the same size as the undercut of the shearing gap resulting in the „Open" mixer geometry. The theoretical parametric study was performed for experimental processing conditions, which are summarized in Table 2.

Surprisingly, it was revealed that the rotating layer was created immediately when the wiping gap was opened, but the rotating layer also fully filled the whole wiping gap channel. Then, the layer was squeezed above the deep channel of the mixer and remained near the barrel through the shearing gap and the other deep channel before it reached the opposite undercut.

The squeezing of the layer is due to the rotation of the material flowing from the inlet channel. Interestingly, the mass flow rate of this layer was found to be constant throughout the gap region essentially forming two almost separate, independent flows inside of the "Open" mixer. The mass flow rate over the wiping

gap, $\dot{m}_{2nd}$, was found to be about 50% of the overall mass flow rate, $\dot{m}_{in}$, coming from the inlet channel. The results of both rheological models are given in Table 8.

Tables 7 and 8 indicate that about 50% of the material flowing in the "Open" mixer has a much larger residence time. This effectively results in the "Open" mixer having a longer average residence time but also a much broader residence time distribution; both of which, may result in degradation problems for some polymers.

Finally, the gradual opening of the wiping gap caused a significant change in the gap velocity profiles of both mixers. This is shown in Figures 16 and 17 for the Carreau-Yasuda and White-Metzner models, respectively. In this case, the screw speed equal to 14 RPM was chosen, i.e. the same value as in the performed experiment. The solid black line in Figures 16 and 17 represents the angular velocity profile of the "Closed" mixer (across the gap). As can be seen, the velocity profile is almost a straight line. This means that a pure drag flow condition was presented in the shearing gap region. However, the flow situation through the shearing gap completely changed when the partial wiping gap was created. Pressure was consumed over the shearing gap and the pressure driven flow became more dominant than the drag flow. The effect of the wiping gap depth is shown by the 4 dashed curves in Figures 16 and 17. Curves above the solid black line display velocity profiles over the shearing gap at each opening of the wiping gap, while curves below the solid black line represent velocity profiles over the wiping gap. Only the smallest opening of the wiping gap showed a pure drag flow condition. The other openings showed the velocity profile over the wiping gap, where drag flow is combined with more dominant pressure driven flow. A similar trend was observed for both rheological models only if H_1 was adjusted between 0.1-0.3mm. For the wiping gap H_1=0.4mm, both utilized models starts to behave differently as shown in Figure 18. In this case, the viscoelastic White-Metzner model predicts back flow over the wiping flight within 0.6-1 relative gap size (i.e. the velocity is negative in this area) whereas the purely viscous Carreau-Yasuda do not. This can be explained by the elongational viscosity, considered in the viscoelastic modified White-Metzner model, which starts to restrict the flow from the deep inlet channel over the wide shearing channel so much that resistance against the flow over the narrow wiping channel becomes smaller i.e. more preferable at particular location. This suggests that modified White-Metzner model should be preferred more than purely viscous Carreau-Yasuda model in the mixing element die design optimization because it can take the resistance against the elongational flow field more precisely into account.

CONCLUSIONS

In this work, the effect of the Maddock mixer design on its performance in single screw extrusion of HDPE melt has been investigated experimentally on a special extrusion line with a barrel having several glass windows as well as theoretically by using a three dimensional finite element method simulation. RGB spectral analysis was used to experimentally quantify the speed of the mixing process for the "Open" and "Closed" fluted mixers. The "Closed" mixer showed a transition from the pure polymer melt to fully mixed that was about half a minute faster than the "Open" mixer. However, the overall, final mixing performance of both fluted mixer designs appears to be equal.

The "Open" mixer configuration of the fluted mixing element also creates a slow moving layer of the material which rotates in the shearing and wiping gaps, i.e. near the barrel surface. This layer is formed because of the absence of the wiping flight. An almost independent, slow moving flow field appears to form in this region. The mass flow rate of this layer (i.e. the mass flow rate over the wiping gap) was found through the 3D FEM calculation to be about 50% of the mass flow rate entering the mixer. The layer is characterized by the long residence time and increases the residence time distribution of the mixer. RGB spectral analysis was used to calculate the time needed for the purging of the colorant out of the extruder. Purging time of the extruder equipped with the "Open" mixer is twice as long as that for the "Closed" fluted mixer. Recorded video of the experiment, on a glass window extruder showed the development of the slow moving layer in the "Open" mixer. The longer residence time of the layer with the "Open" mixer has also been confirmed by 3D FEM simulation. The long residence time of this layer can explain some extrusion problems such as polymer melt degradation. Thus, even if the "Open" fluted mixer is easier to manufacture, it is not recommended for processing thermally sensitive polymers.

The performed theoretical parametric study indicates that the gradual opening of the wiping gap causes that the pressure driven flow became more dominant than the drag flow in shearing as well as in the wiping gap independently of the utilized rheological model. Interestingly, only the smallest opening (0.1mm in this case) of the wiping gap showed a drag flow condition in this channel. It has been found that utilization of the viscoelastic modified White-Metzner model leads to shorter residence times in comparison with the generalized Newtonian model due to reluctance of the viscoelastic polymer melt to fill the corners of the mixing element geometry, i.e. the particle trajectories inside the mixer were found to be shorter for the viscoelastic model, tending to occur mainly in the middle of the channel and thus leaving the mixer a little bit faster in comparison with the purely viscous model. Finally, it has been revealed that for the highest tested wiping flight opening (H_1=0.4mm) the viscoelastic modified White-Metzner model predicts back flow

over the wiping flight within 0.6-1 relative gap size (i.e. the velocity is negative in this area) whereas the purely viscous Carreau-Yasuda do not, which can be explained by the elongational viscosity, considered in the viscoelastic modified White-Metzner model. This suggests that modified White-Metzner model should be preferred more than purely viscous Carreau-Yasuda model in the mixing element die design optimization.

ACKNOWLEDGEMENT

REFERENCES

1. A. L. Kelly, E. C. Brown and P. D. Coates, *Polymer Engineering and Science* **46**, 1706-1714 (2006).

2. D. Strutt, C. Tzoganakis and T. A. Duever, *Polymer Engineering and Science* **40**, 992-1003 (2000).

3. B. Elbirli, J. T. Lindt, S. R. Gottgetreu, and S. M. Baba, *SPE-ANTEC Tech. Papers* **29,** 104 (1983).

4. A. Kiani, R. Rakos, and D. H. Sebastian, *SPE-ANTEC Tech. Papers* **35,** 62 (1989).

5. G. M. Gale, *SPE-ANTEC Tech. Papers* **29,** 109 (1983).

6. D. Herridge and D. Krueger, *SPE-ANTEC Tech. Papers* **48,** 633 (1991).

7. G. Shearer and C. Tzoganakis, *Advances in Polymer Technology* **20**, 169–190 (2001).

8. D. Strutt, C. Tzoganakis and T. A. Duever, *Advances in Polymer Technology* **19**, 22–33 (2000).

9. M. A. Huneault, M. F. Champagne and A. Luciani, *Polymer Engineering and Science* **36**, 1694-1706 (1996).

10. V. L. Bravo and A. N. Hrymak, *Polymer Engineering and Science*, **40**, 525-541 (2000).

11. V. L. Bravo, A. N. Hrymak and J. D. Wright, *Polymer Engineering and Science* **44**, 779-793 (2004).

12. R. Valette, T. Coupez, C. David and B. Vergnes*, International Polymer Processing* **24**, 141-147 (2009).

13. T. Ishikawa, et al., *International Polymer Processing* **21**, 354-360 (2006).

14. C. Rauwendall, *Polymer Extrusion*, Munich: Carl Hanser Verlag, 1990.

15. B. H. Maddock, *SPE Journal,* **23**, 23 (1967)

16. Z. Tadmor and I. Klein, *Polymer Engineering and Science* **13**, 382-389 (1973).

17. *Z* . Tadmor, E. Broyer, and C. Guttfinger, *Polymer Engineering and Science* **14**, 660-665 (1974).

18. M. E. Ghir, C. G. Gogos, D. W. YU, D. B. Todd and B. David, *Advances in Polymer Technology* *17,* 1-17 (1998).

19. C. D. Han, K. Y. Lee, and N.Wheeler, *Polymer Engineering and Science* **31,** 818-830 (1991).

20. http://www.imatek.co.uk/product-r6000.php

21. F.N. Cogswell, Polym. Eng. Sci., 12 (1972), pp. 64p

22. H.A. Barnes, G.P. Roberts, J. Non-Newtonial Fluid Mech., 44 1992), p. 113-126

23. Kubik, P., Vlcek, J., Tzoganakis, C., Miller, L., Polymer Engineering and Science, 52 (6), pp. 1232-1240 (2012)

24. http://www.compuplastvel.com

TABLE 1. Basic screw dimensions

	Total length	28D	Channel depth [mm]	
			Beginning	End
Solids conveying zone	4D		6	6
Melting zone	13D		6	2
Metering zone	2D		2	2
Mixing section	2D		Fluted mixer	
Metering zone	7D		2	2

TABLE 2. Processing conditions

Extrusion Line Heat Zones Temperature [°C]				
Zone 1	**Zone 2**	**Zone 3**	**Zone 4**	**Die**
110	230	250	250	250
Mass Flow Rate [kg/hr]				
Screw speed [RPM]	**7**	**14**	**21**	
"Closed" mixer	1.24	2.43	3.6	
"Open" mixer	1.23	2.37	3.5	

TABLE 3. Rheological model parameters

HDPE – Rheological model parameters			
Rheology		**Thermal Properties**	
η_0 **[Pa.s]**	48684	ρ **[kg/m^3]**	768
n [-]	0.1		
λ **[s]**	0.1171	**Cp [J/(kg.^{o}C)]**	2250
a [-]	0.2542		
T$_r$ [°C]	204	**k [W/(m.K)]**	0.25
b [1/°C]	0.0191		
L$_0$ [s]	0.3829	**H$_0$ [J/kg]**	180000
K$_0$ [s]	0.3050		

TABLE 4. Solver settings

Variable	Relaxation Residuum [min to max]	Relaxation [min to max]
Velocity	0.01 ÷ 0.3	0.1 ÷ 0.5
Pressure	0.001 ÷ 0.5	0.15 ÷ 0.8
Temperature	0.1 ÷ 0.4	0.000001 ÷ 0.1

TABLE 5. Average stress values

Mixer Type	RPM	Carreau-Yasuda		White-Metzner	
		Shear Stress [kPa]	Elongational Stress [kPa]	Shear Stress [kPa]	Elongational Stress [kPa]
OPEN	7	19.5 ± 1.3	5.6 ± 0.6	21.1 ± 0.3	8.7 ± 0.2
	14	24.8 ± 1.7	7.1 ± 0.8	26.3 ± 0.8	12.3 ± 0.3
	21	28.6 ± 2.4	8.1 ± 0.9	29.4 ± 0.8	13.4 ± 0.4
CLOSED	7	20.9 ± 0.9	5.7 ± 0.5	22.9 ± 0.3	9.4 ± 0.2
	14	26.8 ± 1.1	6.9 ± 0.6	28.0 ± 0.5	13.2 ± 0.3
	21	30.7 ± 1.3	8.1 ± 0.6	32.4 ± 0.7	14.1 ± 0.4

TABLE 6. Average residence time

RPM	Average RT [min]			
	Carreau-Yasuda		White-Metzner	
	"Closed"	"Open"	"Closed"	"Open"
7	1.06	1.09	1.00	1.02
14	0.56	0.58	0.48	0.52
21	0.37	0.40	0.32	0.36

TABLE 7. Calculated layer residence times

| RPM | Carreau-Yasuda | | White-Metzner | |
	"Closed"	"Open"	"Closed"	"Open"
7	-	13.33	-	12.69
14	-	6.01	-	4.73
21	-	5.58	-	2.75

TABLE 8. Calculated mass flow rate over the wiping gap, $\dot{m}_{2nd}$, for the given overall mass flow rate coming from the inlet channel, $\dot{m}_{in}$, in the "Open" mixing element

RPM	Mass Flow Rate [kg/hr]		
	$\dot{m}_{2nd}$	$\dot{m}_{in}$	$\dot{m}_{2nd}/\dot{m}_{in}$
C-Y			
7	0.18	0.42	0.44
14	0.40	0.80	0.51
21	0.60	1.20	0.50
W-M			
7	0.17	0.42	0.40
14	0.35	0.80	0.43
21	0.52	1.20	0.43

LIST OF FIGURE CAPTIONS

FIGURE 1. Visualization of the shearing and wiping flights in Maddock mixer (dimensions are in mm)
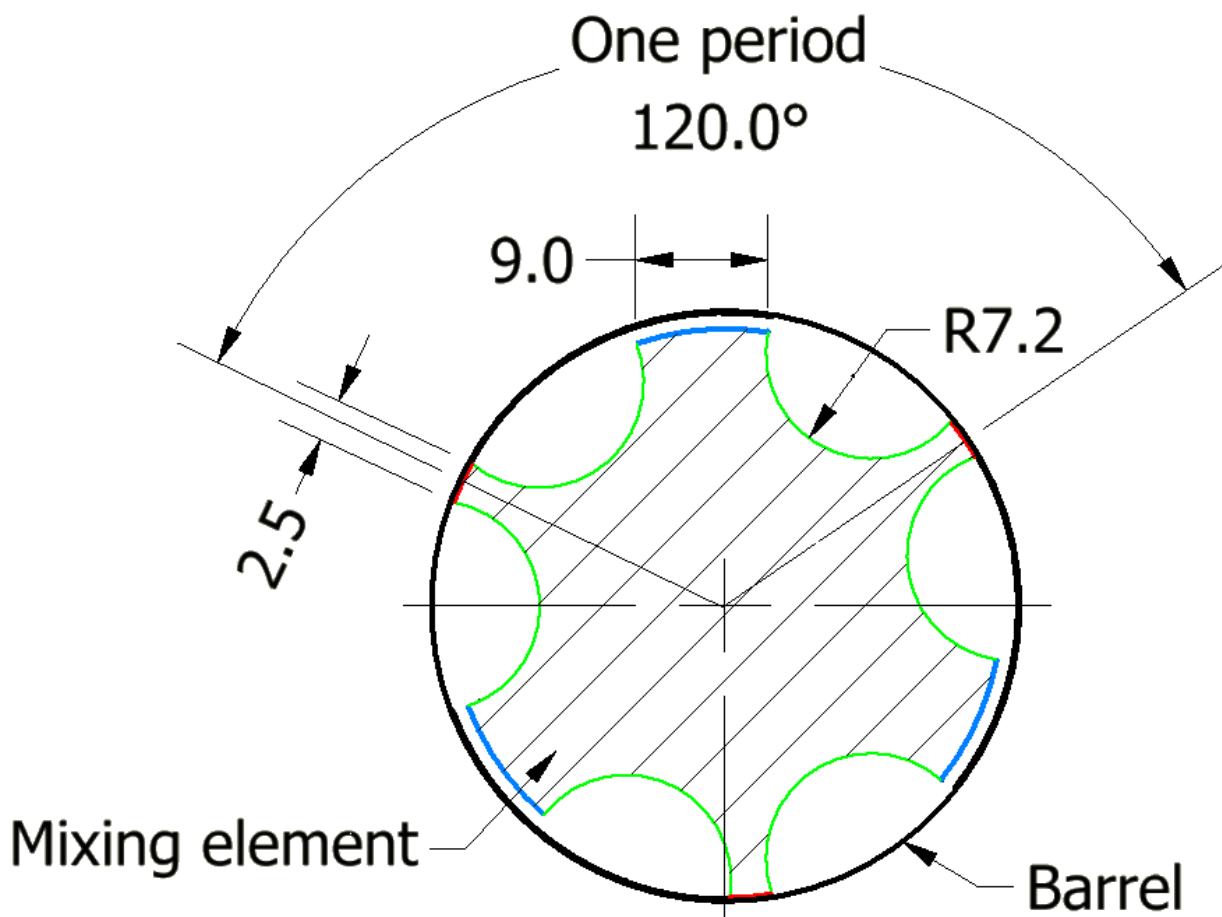
FIGURE 2. Cross section view of "Closed" Maddock mixer (dimensions are in mm) where the gap between the barrel and the wiping flight (section with 2.5mm width) is 0 mm
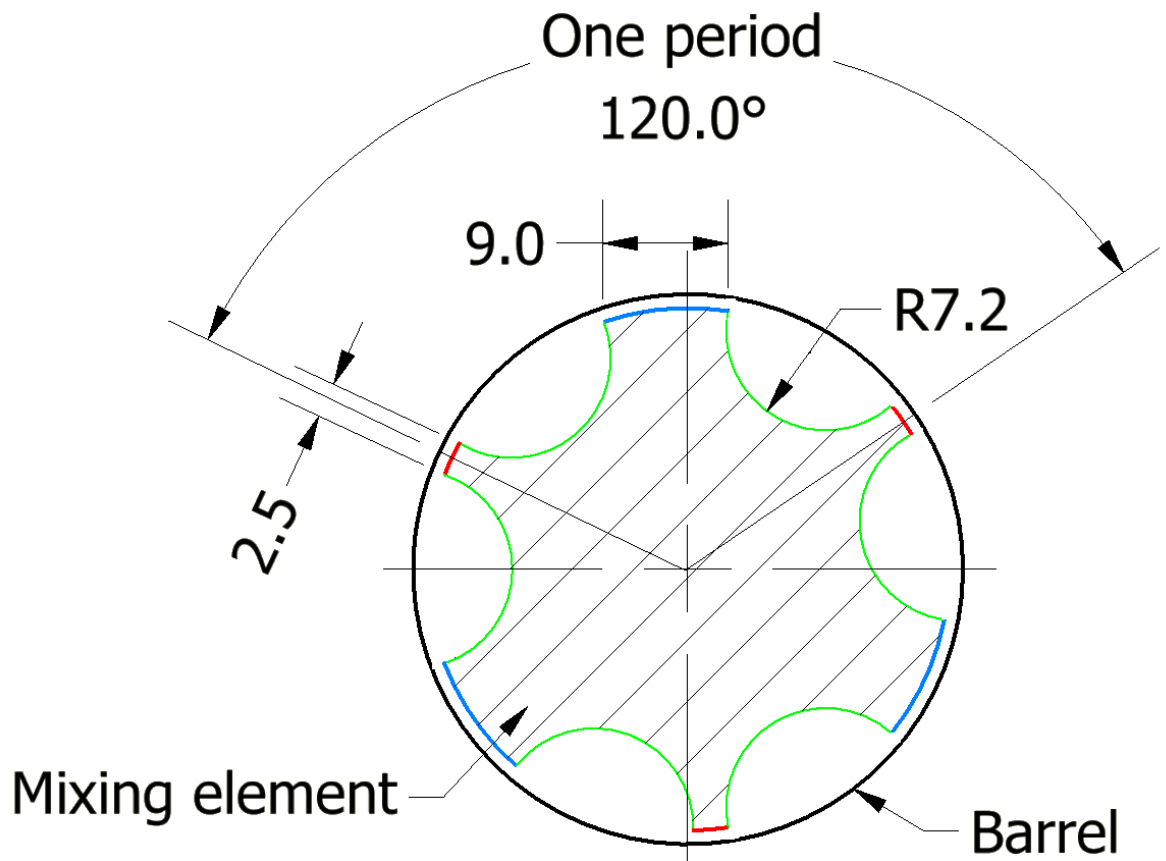
FIGURE 3. Cross section view of "Open" Maddock mixer (dimensions are in mm) where the gap between the barrel and the wiping flight (section with 2.5mm width) is 0.4 mm
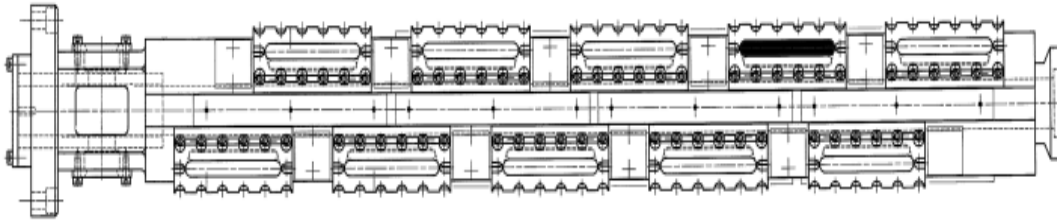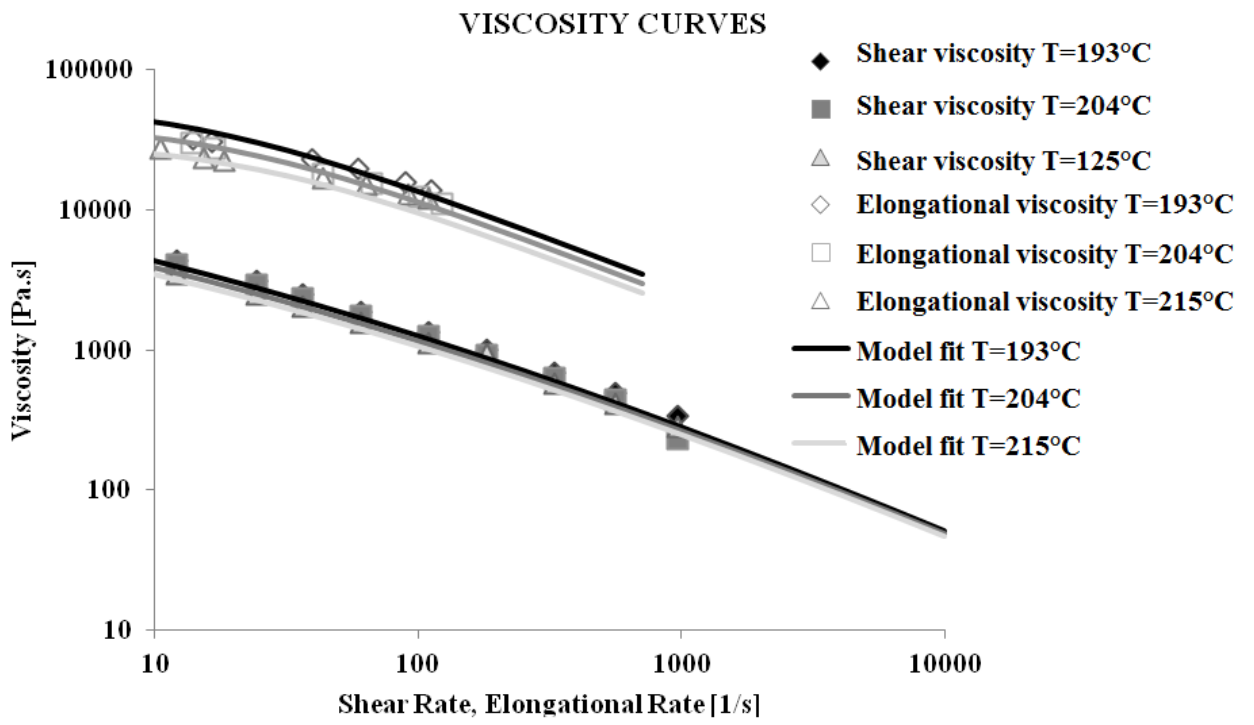
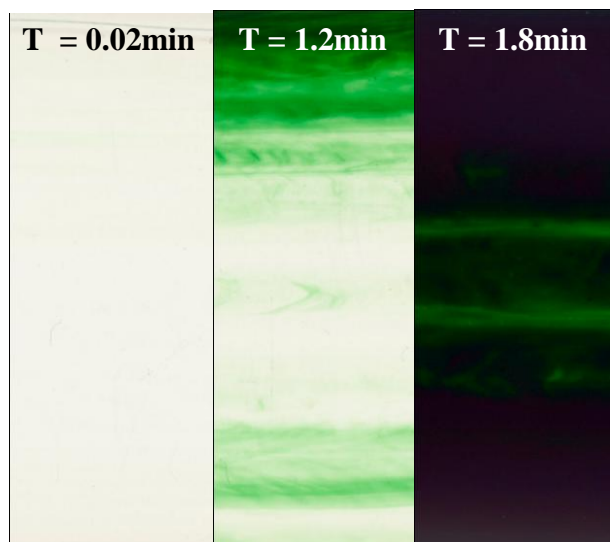FIGURE 4. Barrel sketch

FIGURE 5. Viscosity curves of HDPE

FIGURE 6. Film samples in different extrusion times by using the "Open" mixer

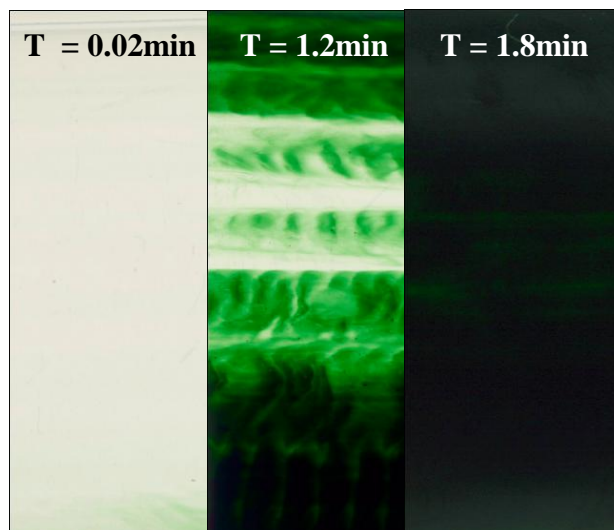FIGURE 7. Film samples in different extrusion times by using the "Closed" mixer
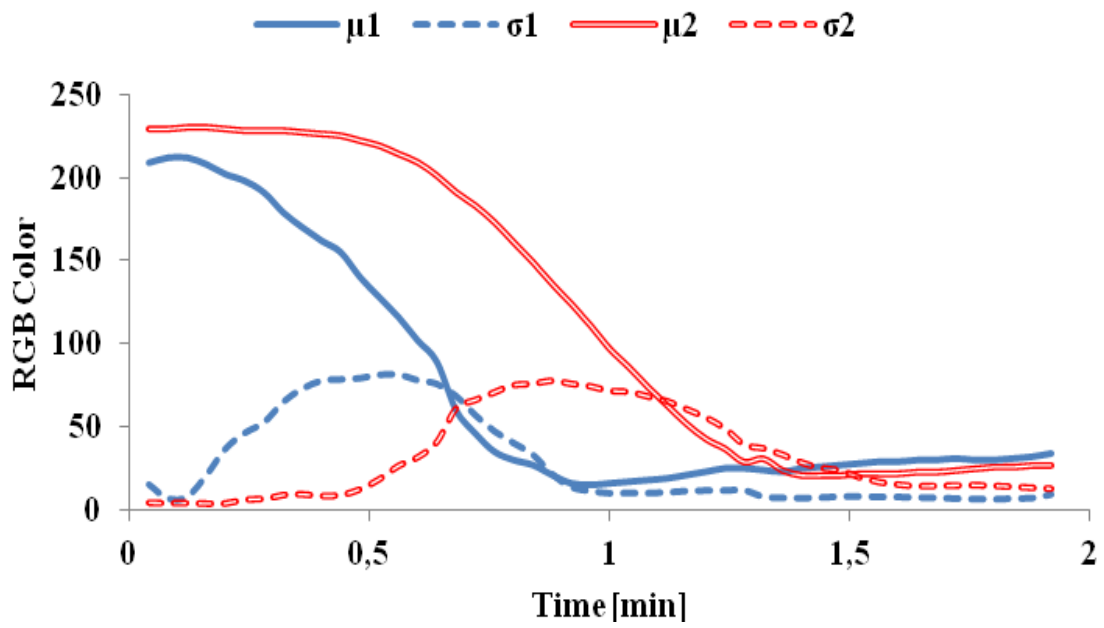
FIGURE 8. RGB analysis of the mixing performance, 1 = "Closed" mixer, 2 = "Open" mixer

FIGURE 9. Residence time RGB analysis, 1 = "Closed" mixer, 2 = "Open" mixer

FIGURE 10. Screen captures from the video, comparing the color change in between the "Open" mixer (Video 1) and "Closed" mixer (Video 2)

FIGURE 11. 3D FEM grid

FIGURE 12. 3D FEM convergence

FIGURE 13. Typical Pathline in the "Closed" mixer

FIGURE 14. Typical pathlines in the "Open" mixer

FIGURE 15. Detail view of mixing element cross section

FIGURE 16. Normalized angle direction velocity profiles for Carreau-Yasuda model in wiping gap (left and bottom) and shearing gap (right and top)

FIGURE 17. Normalized angle direction velocity profiles for modified White-Metzner model in wiping gap (left and bottom) and shearing gap (right and top)

FIGURE 18. Predicted normalized angle direction velocity profiles in wiping gap (left and bottom) and shearing gap (right and top) of the Open Maddock mixer for viscoelastic modified White-Metzner model and purely viscous Carreau-Yasuda model.

74

FIGURE 1. Visualization of the shearing and wiping flights in Maddock mixer
(dimensions are in mm)

FIGURE 2. Cross section view of "Closed" Maddock mixer (dimensions are in mm) where the gap between the barrel and the wiping flight (section with 2.5mm width) is 0 mm

FIGURE 3. Cross section view of "Open" Maddock mixer (dimensions are in mm) where the gap between the barrel and the wiping flight (section with 2.5mm width) is 0.4 mm

FIGURE 4. Barrel sketch

FIGURE 5. Viscosity curves of HDPE

FIGURE 6. Film samples in different extrusion times by using the "Open" mixer

FIGURE 7. Film samples in different extrusion times by using the "Closed" mixer

FIGURE 8. RGB analysis of the mixing performance
1 = "Closed" mixer, 2 = "Open" mixer

FIGURE 9. Residence time RGB analysis
1 = "Closed" mixer, 2 = "Open" mixer

FIGURE 10. Screen captures from the video, comparing the color change in between the "Open" mixer (Video 1) and "Closed" mixer (Video 2)
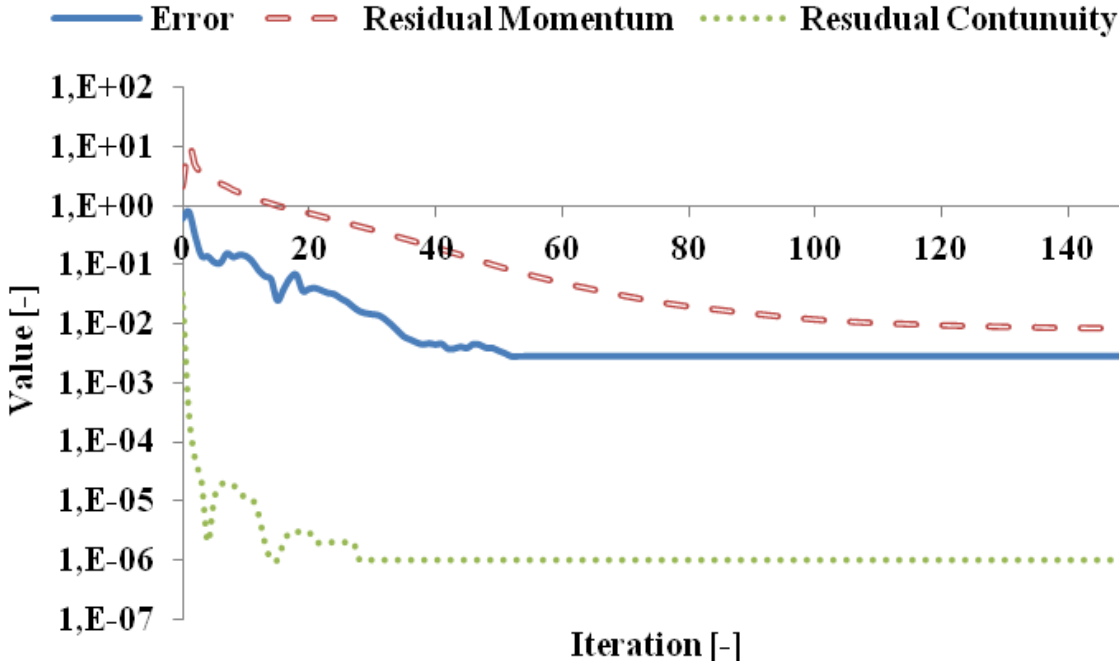
FIGURE 11. 3D FEM grid
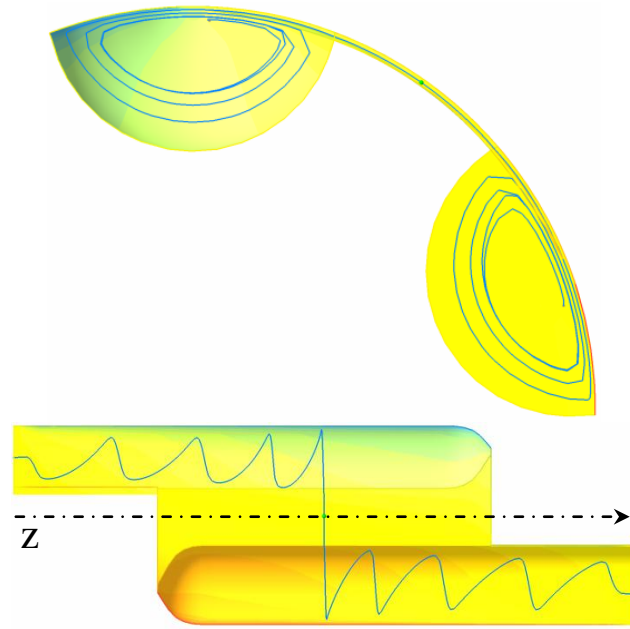
FIGURE 12. 3D FEM convergence

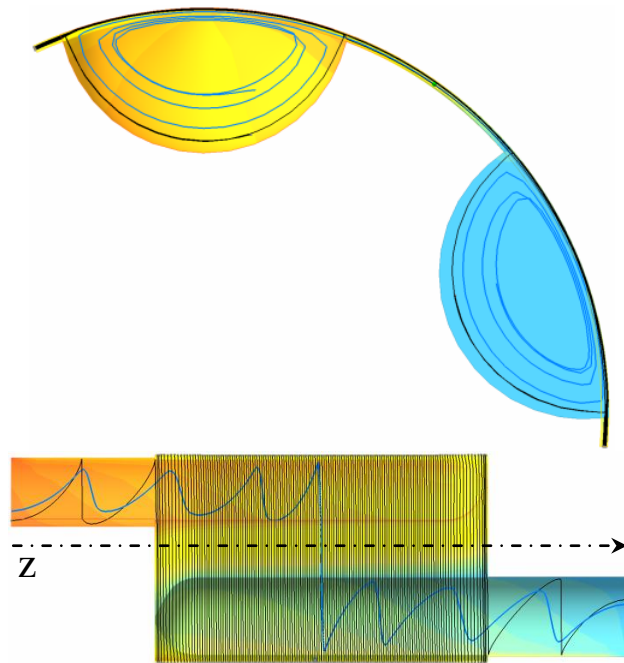FIGURE 13. Typical Pathline in the "Closed" mixer

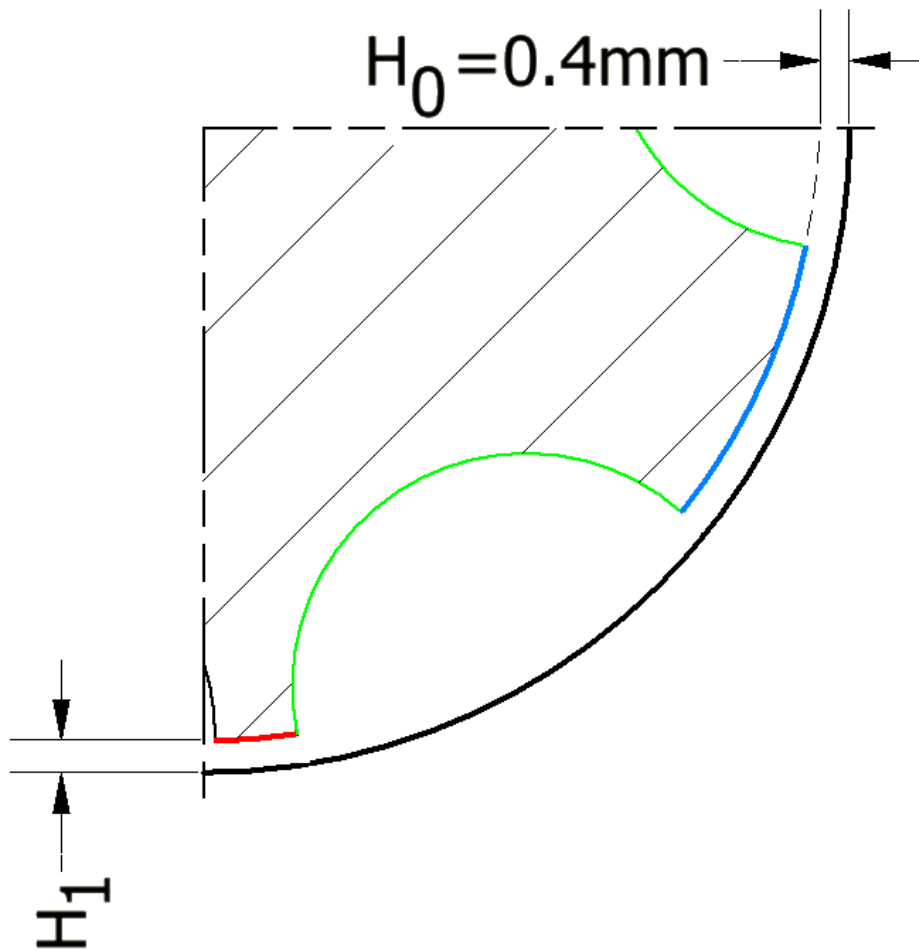FIGURE 14. Typical pathlines in the "Open" mixer

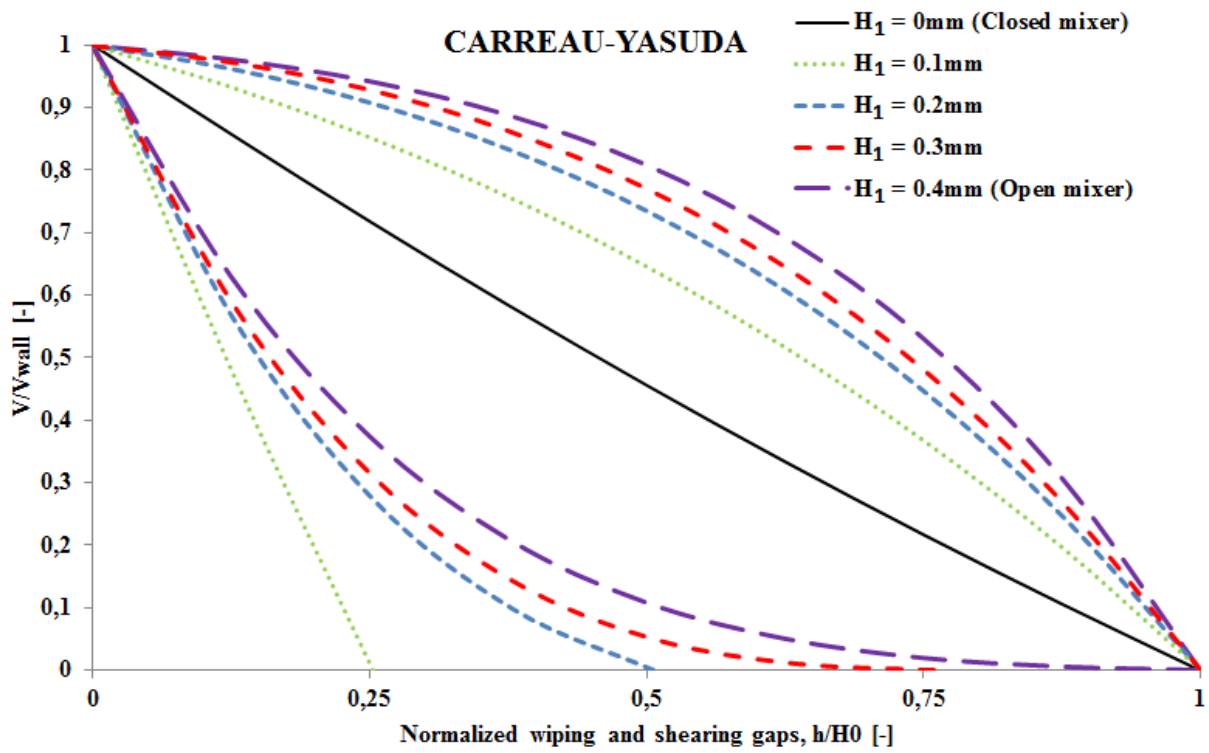FIGURE 15. Detail view of mixing element cross section

FIGURE 16. Normalized angle direction velocity profiles for Carreau-Yasuda model in wiping gap (left and bottom) and shearing gap (right and top)
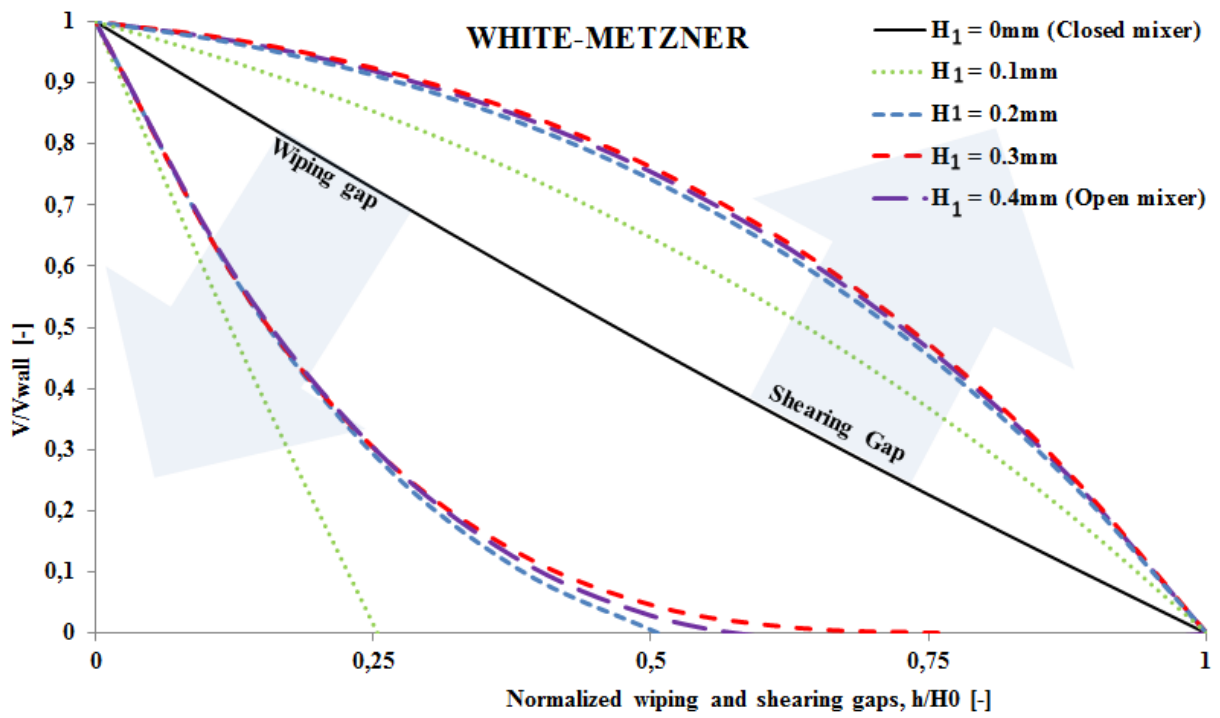
FIGURE 17. Normalized angle direction velocity profiles for modified White-Metzner model in wiping gap (left and bottom) and shearing gap (right and top)
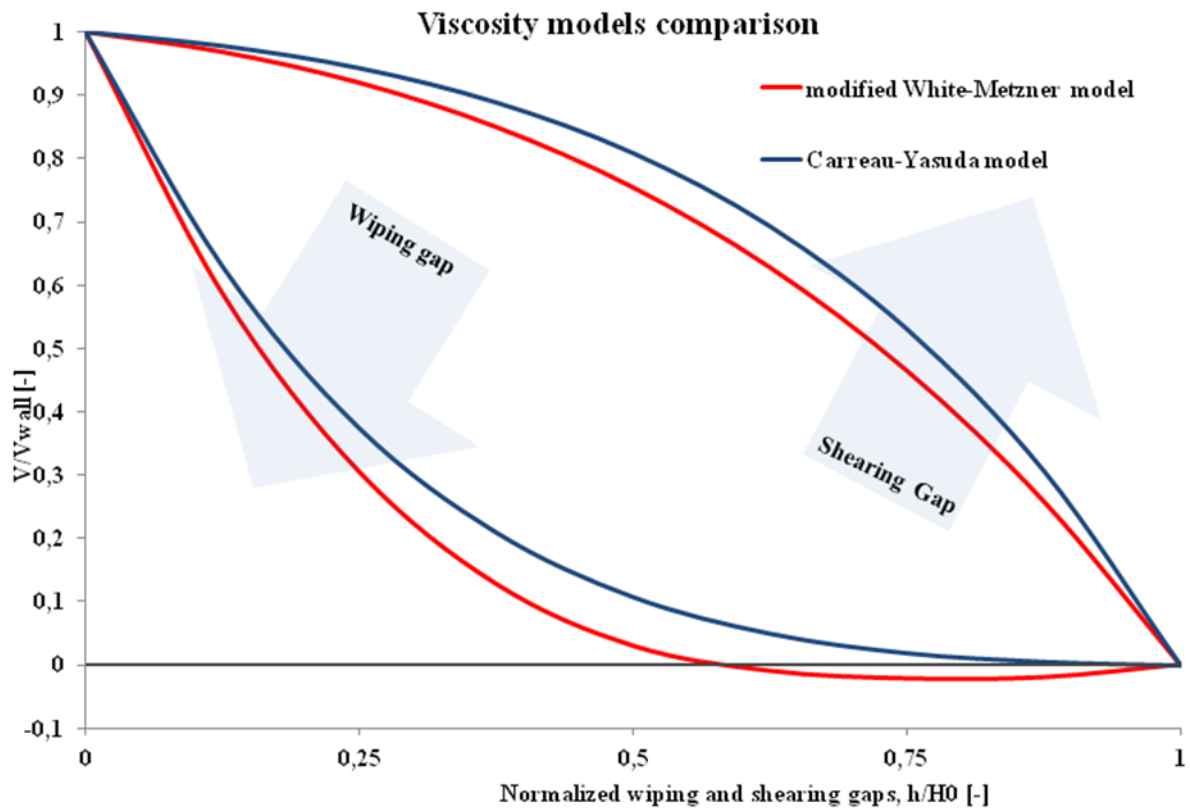
FIGURE 18. Predicted normalized angle direction velocity profiles in wiping gap (left and bottom) and shearing gap (right and top) of the Open Maddock mixer for viscoelastic modified White-Metzner model and purely viscous Carreau-Yasuda model.

THREE-DIMENSIONAL FINITE ELEMENT METHOD SIMULATION STUDY OF THE FUSION SCREW GEOMETRY

Pavel Kubik [1], Martin Zatloukal [2], Jiri Vlcek [3], Tim Womer [4]

1 Tomas Bata University in Zlín, Faculty of Technology, Department of Polymer Engineering, Namesti T.G. Masaryka 275, 762 72 Zlín, Czech Republic

2 Polymer Centre, Faculty of Technology, Tomas Bata University in Zlin, TGM 275, 762 72 Zlin, Czech Republic and Centre of Polymer Systems, University Institute, Tomas Bata University in Zlin, Nad Ovcirnou 3685, 760 01 Zlin, Czech Republic

3 Compuplast International Inc., Svat Cecha 293, 760 01, Zlín, Czech Republic

4 TWWomer & Associates, LLC, 262 East River Road, Edinburg, Pennsylvania 16116, USA

ABSTRACT

In this paper, a detail 3D FEM study of the mixing performance of the Fusion screw geometry by using two different rheological models is presented. Special criteria characterizing the mixing performance in dependence of the barrier undercut separating the waving channels are developed. A great mixing performance is achieved when a right balance in both dispersive and distributive part of the mixing process is found. An optimal undercut of the barrier was found to be about 2mm. Both rheological models were successfully used to validate data of the real experiment with an error less than 15%.

INTRODUCTION

Mixing is very important in many plastics processing industries. So, it is not surprising that considerable effort is spent to study mixing and different types of mixing elements[1-12]. In principle, there are two main mixing mechanisms. The first one, so-called dispersive mixing, is based on lowering of the size of mixture components. The process has a cohesive complexion due to van der Waals forces between particles. The second one is distributive mixing, which redistributes the particles through the volume[1].

Distributive mixing is very useful for blending of polymers with similar viscosities. Distributive mixing is typically caused by any change or interruption of velocity in the screw channel. A lot of different distributive mixing elements[13-16] was invented to increase mixing behavior of single-screw extruders. Probably the most advanced distributive mixing element is a cavity transfer mixer[17,18] which greatly combines the effect of reorientation and shearing.

On the other hand, dispersive mixing is needed when some agglomerates had to be broken down. It can be applied in extrusion of thin films or fiber spinning. The Maddock mixer[19-21] is one of the most widely used mixing elements ever invented. The Maddock mixer had several pairs of fluted channels separated with a shearing gap in between. The shearing gap was undercut and provided intense dispersive mixing. Channels of the mixer were oriented in an axial direction of the screw and a construction of the mixer allowed the material only one pass over the shearing gap. The Maddock mixer was mainly situated in the metering zone of the extruder and strongly influenced the overall quality of the mixing process. Similar devices based on the Maddock mixer concept were patented later[22-25].

A significant invention of the wave screw[26] by George Kruger brought a new look to a problem of mixing. The Double Wave screw[27] could well combine both dispersive and also distributive mixing. The metering section of the conventional single-screw extruder was replaced with Double Wave section. The secondary flight was undercut to support dispersive mixing. The undercut allowed the material to flow over the secondary dispersive flight from one channel to another one. Both screw channels alternately changed their depth every 90° or 180° that forced the material to flow over the secondary flight. Barr and Chung[28] improved the Double Wave concept where not only the secondary flight was undercut but the main flight was undercut, as well. Probably the latest Double Wave screw concept extensions were provided by Tim Womer et. All[29-31]. Their concepts were based on coupling the Wave section with the upstream barrier section and the material reorientation section.

In this article, a quantitative comparison of a mixing performance of the Double Wave Fusion™ screw geometry is presented. A main objective of the study is an

understanding of a mixing performance of the Fusion™ screw geometry. It is believed that the balance between dispersive and distributive mixing should be a key variable of an overall mixing process. Some criteria are needed for the quantification of a mixing quality of the Fusion™ screw geometry, as well. An undercut of the barrier separating waving channels is chosen to be a key parameter of the study. All numerical results are obtained by using a three dimensional Finite Element Method (3D FEM) simulation.

MATERIAL

The material used for the experiment was Hi-Zex 6300M HDPE. Rheological properties were measured on a Kayeness laboratory capillary rheometer, model D6052M where a diameter of a capillary was 1mm and its length was 20 mm. For a purpose of later 3D FEM simulations, rheological data was fitted by two different models. The first one was well known Carreau-Yasuda (C-Y) model in which the viscosity dependence is described by a following equation:

$$\eta(II_D, T) = \frac{\eta_0 \, f(T)}{\left[1 + \left(\lambda \sqrt{II_D} \, f(T)\right)^a\right]^{\frac{1-n}{a}}} \tag{1}$$

Where η_0 is the zero shear viscosity, a is a constant, n stands for a non-newtonian index, λ represents a relaxation time, T is temperature and II_D stands for the second invariant of the deformation rate tensor. The material temperature dependence $f(T)$ is exponential and is given by an equation:

$$f(T) = e^{-b(T - T_r)} \tag{2}$$

The parameter b represents the temperature sensitivity and T_r is the reference temperature.

For a purpose of more detailed understanding of the Fusion™ screw geometry, elongational viscosity data was added to the calculation model, as well. Uniaxial elongational viscosity was determined on a laboratory grade twin-bore capillary rheometer Imatek R6000[32] with ϕ1x16mm long die and ϕ1×0.25mm short die utilizing Cogswell model[33]. In order to take steady shear as well as steady uniaxial elongational viscosity into account, the following modified White-Metzner model[34] was used.

$$\tau_{i,j} + \lambda\left(II_D\right)\frac{\delta\tau_{i.j}}{\delta t} = 2\eta\left(II_D\right)D_{i,j} \tag{3}$$

Where $\tau_{i,j}$ is the stress tensor, λ (II_D) stands for the relaxation time, η (II_D) means the viscosity defined by Eq. 1, $\delta\tau_{i.j}/\delta t$ is the upper-convected time derivative of the stress tensor, $D_{i,j}$ is the deformation rate tensor and II_D represents its second invariant.. The relaxation time has a form:

$$\lambda\left(II_D\right) = \frac{L_0 f(T)}{1 + K_0 f(T) II_D} \tag{4}$$

Where L_0 and K_0 are constants and II_D again stand as the second invariant of deformation rate tensor. Rheological model parameters are presented in Table 1 and fitted viscosity curves of both models are shown in Figure 1.

EXPERIMENTAL

The experiment was done in a laboratory of Xaloy Inc., New Castle, Pennsylvania, USA. The main objectives of the test were to obtain run information such as mass flow rates, amps, melt temperature and pressure profiles at different screw speeds. A Fusion[TM] screw device was used for the test. The Fusion[TM] screw is an advanced type of a barrier screw with a Fusion[TM] mixing section. The Fusion[TM] mixing section is characterized by double waving channels separated by a barrier in between. An optimal undercut of the barrier is based on the experience from previous testing done on the optimization of the barrier flight clearance[35]. The undercut of the barrier is 2.3 mm. Waves continuously change their depth in both channels. Thus, one channel wave reaches its maximum when the opposite wave is on its minimum. The maximal depth of the wave is 5.5 mm and the minimal depth was designed to be 11 mm. Both depths are measured from a barrel surface. The material do not has to flow only through the channel but it can also cross flow over the barrier. Therefore, this design allows chaotic mixing where both, dispersive and distributed, parts have a significant role.

An experimental extrusion line was equipped with fifteen pressure transducers along the barrel and twelve heat zones were used to control temperature profile of

the polymer melt, as well. A power of the extrusion line motor was 112 kW, 243 Amps and its maximum screw speed should be 125 RPM. A diameter of the barrel was 90 mm and an overall length of the screw was manufactured to 33D. All main screw parameters are summarized in Table 2 and the off-scale screw geometry is visualized in Figure 2.

The extrusion line was also equipped with a melt restrictor valve and ended with a 711 mm wide sheet die. The first five zones of the extrusion line allowed water cooling. Specific experimental processing conditions are presented in Table 3. Rate checks and melt temperature were taken every 15 RPM up to 90 RPM. Melt restrictor valve was used to obtain real life head pressure.

EXPERIMENTAL RESULTS

All experimental data of pressure transducers was taken every second during more than five minute intervals at each RPM. Thus, each set of data had about four hundred points to study. This data was averaged and final pressure profiles along the whole screw are shown in Figure 3.

As can be seen, pressure development along the whole screw was observed at each screw speed. Pressure transducers 1 – 3 shows pressure generation in the solids conveying zone caused by a cooling of the barrel under a hopper. Next, a small decrease of pressure was observed around the transducer 4 because of a pitch change at the beginning of the barrier section. Then, pressure still grew up in the barrier section. A closing depth of a primary channel and ending of the barrier section together with another pitch change caused pressure fluctuation between transducers 9 - 12. Finally, the Fusion^{TM} mixing section, visualized by dash lines, again helped to pressure development. Melt temperature was measured by using a melt probe. Melt temperature increased according to used RPMs. Measured pressure rise of the Fusion^{TM} mixing section and overall melt temperature is presented in Table 4.

VALIDATION OF MODELS

A 3D FEM simulation was later used to check and verify a rightness of using the chosen Carreau-Yasuda and White-Metzner models. For this purpose, a 3D FEM module of Virtual Extrusion Laboratory^{TM} software[36] created by Compuplast International, Inc. was chosen. A 3D FEM grid was created completely manually from 920,349 points and 105,600 twenty-seven nodes brick hexahedral elements. The grid is displayed in Figure 4. The grid was created in unwrap state and then transformed by using internal routines of the VEL^{TM} software.

All simulations were run on a personal computer (PC) equipped with 64-bit Windows Vista^{TM} Bussiness edition operating system with Service Pack 2. PC was powered by FPS Group Blue Storm II 400W power source. Intel(R) Core(TM)2

Quad Q9300 @2.5GHz CPU with a passive cooler was used as a processor. Display adapter was ATI Radeon HD 4800 series and four Transcend 2GB DDR2 800DIMM memories were also installed. One calculation by using this PC configuration took about 50 hours to reach a chosen maximum of 300 iterations with an overall tolerance set to 10^{-6}. Temperature was calculated once per iteration and a value of upwinding was set to 0.5. Solver settings for main calculating variables are given in Table 5.

A 3D FEM solver calculates convection-diffusion Navier-Stokes equations, mass and energy balance equations together with particular constitutive equation. In more detail, the system is solved in a segregated manner, where velocities are calculated at first. Then, pressure is found. Next, velocities are corrected to satisfy a continuity equation. Finally, temperature is found by solving segregated energy balance equation by using latest stress data. All these subsystems are solved by fast iterative solvers.

A solution of a system Ax=b is considered to be converged when some error or residual is below a required threshold. The error is usually defined as some ratio between two subsequent iteration results:

$$Error = \frac{\sum \frac{|v^n - v^o|}{\max(v^n, v^o)}}{n}$$

(5)

The error is easy to be found after the each iteration. However, the error might be close to zero, even though, the solution has not reached correct results.

Another method of measuring the convergence is a residual. The residual is some norm of suitable |Ax-b|. The Galerkin FEM is based on minimizing the residuals. Once residuals are zero the solution is finished. Results of pressure and temperature values calculated by 3D FEM simulations are summarized in Figures 5 and 6.

As can be seen, all pressure and temperature calculated data was close to experimentally obtained data. The highest calculations error was below 15%. It can be clearly concluded that simulation results are in good agreement with experimentally obtained data and the chosen Carreau-Yasuda and White-Metzner models can be further used for a parametrical simulation study describing a mixing performance of the Fusion^{TM} mixing section.

PARAMETRICAL STUDY

The undercut of the barrier separating double wave channels of the Fusion[TM] mixing section was taken as a main parameter for the study. The study was done at 90RPM between two geometrical extremes of the barrier undercut. The first chosen undercut of the barrier was 0 mm. Thus, the barrier was completely closed and the material could flow only through two fully separated waving channels. Then, the barrier undercut was opened by 1 mm in each step until the top of the wave was reached. The biggest undercut could be therefore set to 5.5 mm. A sketch of the undercut opening is presented in Figure 7. The more the barrier undercut was opened the more material could obviously travel from one channel to another one. 3D FEM grids were similar as the grid created for validating simulations. All calculations were also performed by using the same PC configuration and calculation time was again close to 50 hours.

The most significant variables characterizing mainly dispersive mixing behavior were surely shear and elongational stress. About fifty pathlines were created for each 3D FEM grid to quantify a stress behavior. A pathline is a FEM feature of the VEL[TM] simulation software used for a tracing of particles inside of a flow domain.

The polymer melt experience a stress history and only a fraction of the melt passes through high stress regions. Therefore, the maximum level of shear stress reached by the polymer melt cannot be used as a main parameter to quantify the mixing performance. An average stress value[2], calculated according to Eq. 6, can be taken to characterize the dispersive mixing performance.

$$\bar{\tau} = \frac{1}{t_{max}} \int_{0}^{t_{max}} |\tau(t)| dt$$

(6)

Where t_{max} is the residence time of the pathline and $\tau(t)$ represents stress (shear or elongational) along the chosen pathline. Calculated shear and elongational average stress are provided in Table 6.

As shown in the Table, values of average shear stress were in range from 80kPa to 85kPa for simulations by using the Carreau-Yasuda model, while using of the White-Metzner model showed about 5kPa higher values for each undercut. Maximal average shear stress was found for the original Fusion[TM] screw geometry. However, the maximum was not strong enough so it is not certain that Fusion[TM] screw could be considered as an option providing the best mixing performance. Average elongational stress went down with increasing of the barrier undercut for both viscosity describing models. Maximal average elongational stress was reached

for 0 mm undercut. The material in such a case could not cross flow in between the channels and had to flow only through the waving section. The material therefore could not avoid elongational stress caused by waves. The more the undercut was opened the less elongational stress was reached because the resistance of the opening undercut was not so high and the material would rather cross flow over the barrier than be stretched by the wave. The too narrow opening of the undercut creates area of high shear and mainly elongational stress. The material typically flows in a way of a minimal flow resistance so it prefers to stay in the waving channel for smaller undercuts. However, bigger undercut showed stronger cross flow of the material especially at places where one of waves was close to its maximum. The original Fusion^{TM} screw geometry showed a nicely balanced flow where a half of pathlines represented cross flows over the undercut, while the second half of pathlines preferred to stay in the middle of the waving channel. The modeling situation of the most characteristic flow field pathlines is visualized in Figure 8 and Figure 9. As can be seen, figure 8 shows some pathlines belonging to 0 mm undercut of the barrier. Pathlines clearly had to travel through waving channels without a possibility of any cross flow over the undercut. On the other hand, Figure 9 gives a detail view of the most opened undercut of the barrier. The material preferred chaotic movement between channels because a resistance of the undercut was negligible. The same trend was observed for the White-Metzner model, as well.

Next, proper optimizing criteria had to be implemented for a purpose of dispersive and distributive mixing quantification. Criteria were also developed to find a balance in between dispersive and distributive mixing with consideration of the changing undercut of the barrier. Thus, the first one, a dispersive function, was calculated by a following equation:

$$Dispersive = \frac{\int \tau_{barrier}}{\bar{\tau} + \int \tau_{barrier}}$$

(7)

Where $\tau_{barrier}$ is total stress along the whole length of the barrier and $\bar{\tau}$ stands as overall average total stress . The second one, a distributive function, was given by an equation:

$$Distributive = \frac{\dot{m}_{barrier}}{\dot{m}_{input} + \dot{m}_{barrier}}$$

(8)

Where $m_{barrier}$ represents mass flow rate over the undercut and m_{input} is mass flow rate from the input. Both criteria were intentionally adjusted to acquire variability from 0 to 1 for better comparison. Calculated values are summarized in Table 7 and graphic visualization is displayed in Figure 10.

As can be seen, dispersive functions slowly decreased from 1 mm undercut, while distributive functions permanently increased. The more the undercut was opened the more material could travel in between the channels. The movement of the material over the undercut therefore supported an influence of distributive mixing over dispersive mixing. Profiles of distributive and dispersive curve by using the White-Metzner model were below values of mixing characteristics by the Carreau-Yasuda model calculation. Added elongational properties of the material actually strongly affected the amount of the material that flew over the undercut. Mass flow rate of cross flows with elongational properties was about 25% smaller (see Table 8) than mass flow rate of cross flows given by the Carreau-Yasuda model. Smaller mass flow rate of cross flows influenced also overall total stress over the undercut, thus, the dispersive function. The optimal mixing performance of the Fusion™ screw was considered to be achieved when dispersive and distributive functions are both high enough to maximize a mixing efficiency. A reasonable compromise assumes that dispersive and distributive functions, thus dispersive and distributive mixing, are even. Both functions are even only in an intersection point. The optimal mixing performance of the Fusion™ screw is then found to be about 2 mm undercut of the barrier by using both viscosity describing models. Such the optimized undercut was very close to the original Fusion™ screw undercut which was 2.3 mm. It can be supposed that the well known great mixing performance of the Fusion™ screw geometry is given mainly by achieving a good balance between dispersive and distributive mixing. Both criteria can be used as a designing parameter, as well.

CONCLUSIONS

The 3D FEM parametrical study of the Fusion™ screw geometry clearly shows that 2 mm undercut of the barrier separating screw channels appears to be the optimal parameter for the most efficient mixing performance. A solution where dispersive and distributive parts of the mixing process are even is considered to

provide the most efficient mixing performance. The solution is achieved by two criteria developed just for the purpose of dispersive and distributive mixing quantification of the Fusion^{TM} screw geometry. These two criteria give also a helpful tool in designing of the Fusion^{TM} screw geometry. Another mixing quantification is presented by the average stress criterion where original Fusion^{TM} screw geometry reaches the highest value of shear stress. A key variable for the great mixing performance of the Fusion^{TM} screw geometry is the right balance in between dispersive and distributive mixing. 3D FEM simulation is also firstly successfully used to check results of experimentally taken data of the Fusion^{TM} screw geometry and verify the rightness of using the Carreau-Yasuda and White-Metzner model. It is presented that all temperature and pressure data are in good agreement with calculated values. The error is always below 15%. However, it is still necessary to spend an effort to find some general quantitative criteria judging the mixing process.

ACKNOWLEDGEMENT

REFERENCES

1. Olbrich, M., Zitzenbacher, G., Hochenauer, C., Kneidinger, C., Lawlor, V. Analytical and numerical methods for the design of Maddock mixers in single screw plasticizing technology,(2012) *Macromolecular Symposia*, 311 (1), pp. 83-91.

2. Kubik, P., Vlcek, J., Tzoganakis, C., Miller, L., Method of analyzing and quantifying the performance of mixing sections, (2012) *Polymer Engineering and Science*, 52 (6), pp. 1232-1240.

3. Darvishi, R., Computational study of velocity field in Maddock kneader with CFD method (2011), *Society of Plastics Engineers - EUROTEC 2011 Conference Proceedings*, 5 p.

4. Zitzenbacher, G., Karlbauer, R., Thiel, H., A new calculation model and optimization method for maddock mixers in single screw plasticising technology, (2007) *International Polymer Processing*, 22 (1), pp. 73-81.

5. Tokihisa, M., Yakemoto, K., Sakai, T., Utracki, L.A., Sepehr, M., Li, J., Simard, Y. Extensional flow mixer for polymer nanocomposites, (2006) *Polymer Engineering and Science*, 46 (8), pp. 1040-1050.

6. Galaktionov, O.S., Anderson, P.D., Peters, G.W.M., Meijer, H.E.H., Analysis and optimization of Kenics static mixers, (2003) *International Polymer Processing*, 18 (2), pp. 138-150.

7. Rwei, S.-P., Distributive mixing in a single-screw extruder - Evaluation in the flow direction, (2001) *Polymer Engineering and Science*, 41 (10), pp. 1665-1673.

8. Klason, C., Jinescu, V.V., Poştoacă, I., A Network Analysis of a Screw Mixing Zone (2000) *International Polymer Processing*, 15 (1), pp. 3-11.

9. Klason, C., Jinescu, V.V., Postoaca, I., Pressure variation by dispersive mixers in plasticating extrusion, (1999) *KGK-Kautschuk und Gummi kunststoffe*, 52 (7), pp. 501-509.

10. Rauwendaal, C., Osswald, T., Gramann, P., Davis, B., Design of Dispersive Mixing Devices, (1999) *International Polymer Processing*, 14 (1), pp. 28-34.

11. Esseghir, M., Gogos, C.G., Yu, D.-W., Todd, D.B., David, B., A comparative study on the performance of three single-screw elements in melt-melt mixing of immiscible blends, (1998) *Advances in Polymer Technology*, 17 (1), pp. 1-17.

12. Wang, Y., Tsay, C.C., Non-newtonian flow modeling in the mixing section of a single-screw extruder with flow analysis network method, *(1996) Polymer Engineering and Science, 36 (5), pp. 643-650.*

13. C. Rauwendall: '*Polymer Extrusion'*, Munich: Carl Hanser Verlag, 1990.

14. F. E. Dulmage: U. S. Patent 2,753,595.

15. R. L. Saxton: U. S. Patent 3,006,029.

16. German Patent 2,026,834.

17. English Patent 930,339.

18. M. H. Pah: '*Dispersive Mischern mit dynamischen Mischern*', VDI-Verlag, Duesseldorf, 177-196 (1978).

19. B.H. Maddock: US Patent 3,730,492 (1973).

20. B.H. Maddock: US Patent 3,756,574 (1973).

21. B. H. Maddock: SPE Journal, July, 23-29 (1967).

22. G. LeRoy: US Patent 3,486,192 (December 30, 1969).

23. R.F. Dray, US Patent 3,788,612 (1974).

24. R.B. Gregory: US Patent 3,788,614 (1974).

25. R. B. Gregory and L. F. Street: U. S. Patent 3,411,179.

26. G.A. Kruder: US Patent 3,870,284 (March 11, 1975).

27. G.A. Kruder: US Patent 4,173,417 (1979).

28. C.I. Chung and R.A. Barr: US Patent 4,405,239 (1983).

29. T.W. Womer, E.J. Buck, and B.J. Hudak Jr.: US Patent 6,672,753 (2004).

30. T.W. Womer, E.J. Buck, and B.J. Hudak Jr.: US Patent 7,014,353 (2006).

31. T.W. Womer and W. Smith: US Patent 7,156,550 (2007).

32. http://www.imatek.co.uk/product-r6000.php

33. F.N. Cogswell, Polym. Eng. Sci., 12 (1972), pp. 64p.

34. H.A. Barnes, G.P. Roberts, J. Non-Newtonial Fluid Mech., 44 (1992), p. 113-126

35. T. Womer, G. Garrah: '*SPE-ANTEC Tech. paper*', **44**, 81 (1998).

36. *Compuplast International, Inc.* [online]. ©2006 [viewed 2014-02-08]. Available from: http://www.compuplast.com/

TABLE 1. HDPE rheological model parameters

HDPE – Rheological model parameters			
Rheology		**Thermal Properties**	
η_0 [Pa.s]	48684	ρ kg/m^3]	768
n [-]	0.1		
λ [s]	0.1171	Cp[J/(kg.^{o}C)]	2250
a [-]	0.2542		
T_r [°C]	204	K [W/(m.K)]	0.25
b [1/°C]	0.0191		
L_0 [s]	0.3829	H_0 [J/kg]	180000
K_0 [s]	0.3050		

TABLE 2. Main screw parameters

	Total length	33D	Channel depth [mm]		Lead [mm]	
			Beginning	End	Main	Aux
A)	Solids conveying zone	7D	20	20	101.6	-
B)	Barrier melting zone	14D	20	8	122.2	122.2
C)	Metering zone	3D	8	8	101.6	-
D)	Mixing section	6D	FUSION SECTION		101.6	101.6
E)	Metering zone	3D	8	8	101.6	-

TABLE 3. Processing condition

Extrusion Line Heat Zones Temperature [°C]											
Zone 1	Zone 2	Zone 3	Zone 4	Zone 5	Zone 6	Zone 7	Melt Valve	Zone 9	Die 1	Die 2	Die 3
176.7	221.1	218.3	215.6	212.8	210.0	204.4	204.4	204.4	204.4	204.4	204.4

Screw speed [RPM]		**15**	**30**	**45**	**60**	**75**	**90**
Amps		70.27	99.15	123.03	142.18	155.31	165.27
kW required		3.93	10.94	20.18	30.80	41.99	53.52
Mass Flow Rate [kg/hr]		39	83.7	127.5	168.3	213	254.7

TABLE 4. Experimental results

RPM	15	30	45	60	75	90
Pressure drop [MPa]	7.5	7.9	8.5	9.8	9.9	10.6
Temperature [°C]	211.9	216	219.4	222.4	224.7	227

TABLE 5. Solver settings

Variable	Relaxation Residuum [min to max]	Relaxation [min to max]
Velocity	0.01 ÷ 0.3	0.1 ÷ 0.5
Pressure	0.001 ÷ 0.5	0.15 ÷ 0.8
Temperature	0.1 ÷ 0.4	0.000001 ÷ 0.1

TABLE 6. Average stress criterion results

Undercut [mm]	Carreau-Yasuda		White-Metzner	
	Shear stress [kPa]	Elongational stress [kPa]	Shear stress [kPa]	Elongational stress [kPa]
0	82.75	6.34	88.02	7.01
1	84.16	6.12	88.46	6.25
2.3	85.40	5.38	90.84	6.64
3	84.93	5.20	89.29	6.01
4	84.18	4.91	88.40	6.05
5	82.68	4.79	88.62	5.84
5.5	82.30	4.65	87.00	5.80

TABLE 7. Mixing criteria results

Undercut [mm]	Carreau-Yasuda		White-Metzner	
	Dispersive Function [-]	Distributive Function [-]	Dispersive Function [-]	Distributive Function [-]
0	0.00	0.00	0.00	0.00
1	0.70	0.48	0.63	0.43
2.3	0.63	0.70	0.59	0.62
3	0.61	0.73	0.56	0.64
4	0.58	0.78	0.54	0.72
5	0.56	0.80	0.52	0.76
5.5	0.55	0.83	0.52	0.78

TABLE 8. Mass flow rate of cross flows

Undercut [mm]	Carreau-Yasuda	White-Metzner	1 - (W-M / C-Y)
	Cross Flow MFR [kg/hr]		[%]
0	0.00	0.00	0.00
1	233.20	194.19	16.73
2.3	595.47	419.44	29.56
3	633.40	458.77	27.57
4	900.25	620.61	31.06
5	1113.72	808.36	27.42
5.5	1220.60	916.03	24.95

LIST OF FIGURES

Figure 1. Viscosity curves
Figure 2. Fusion screw geometry off-scale sketch
Figure 3. Pressure profiles
Figure 4. 3D FEM grid
Figure 5. Temperature comparison
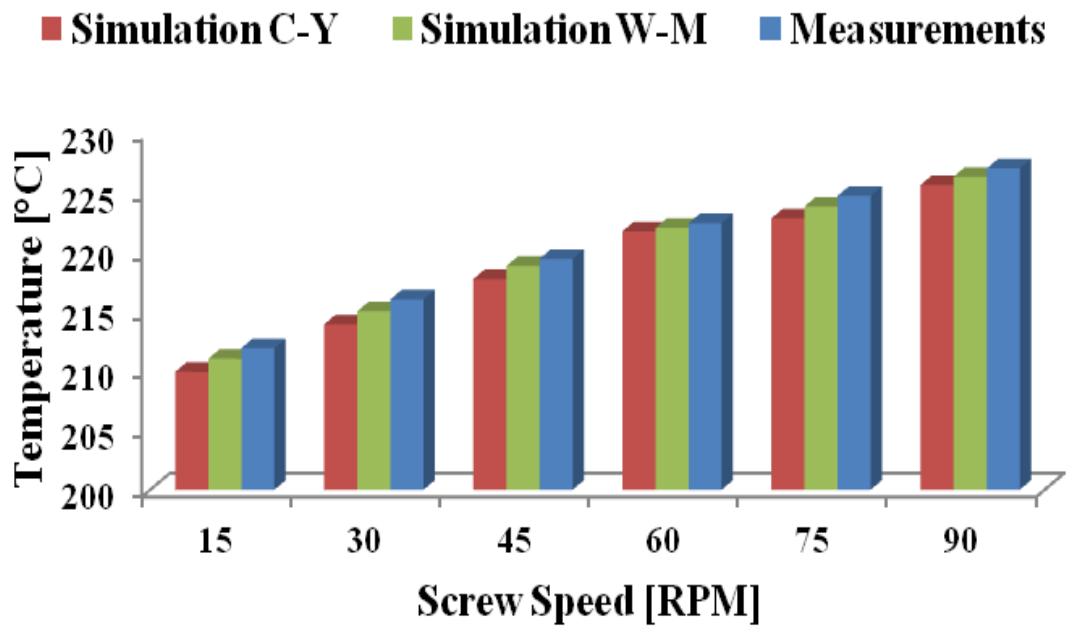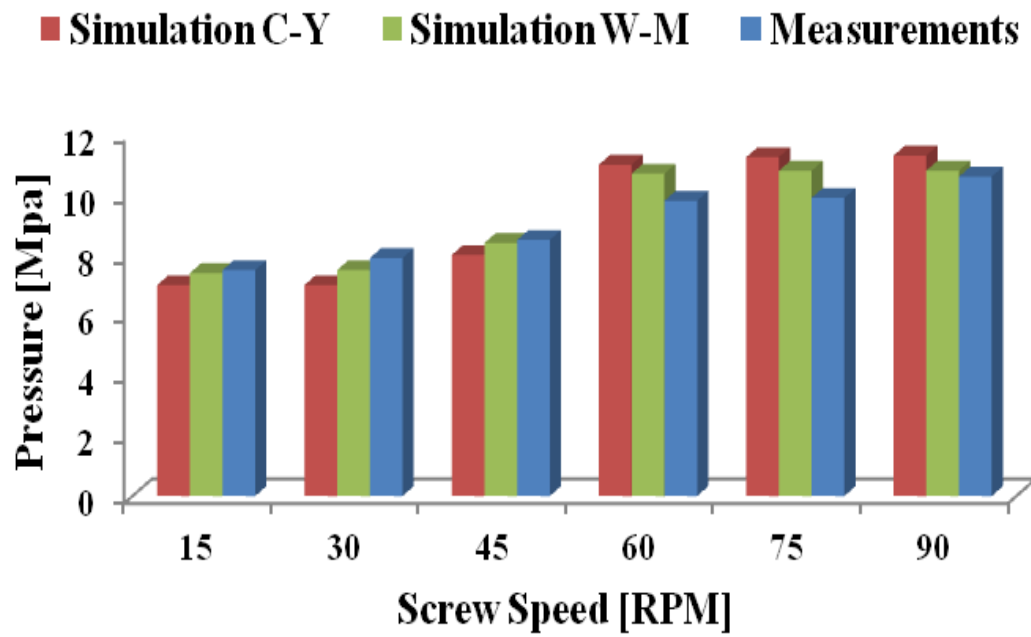Figure 6. Pressure comparison
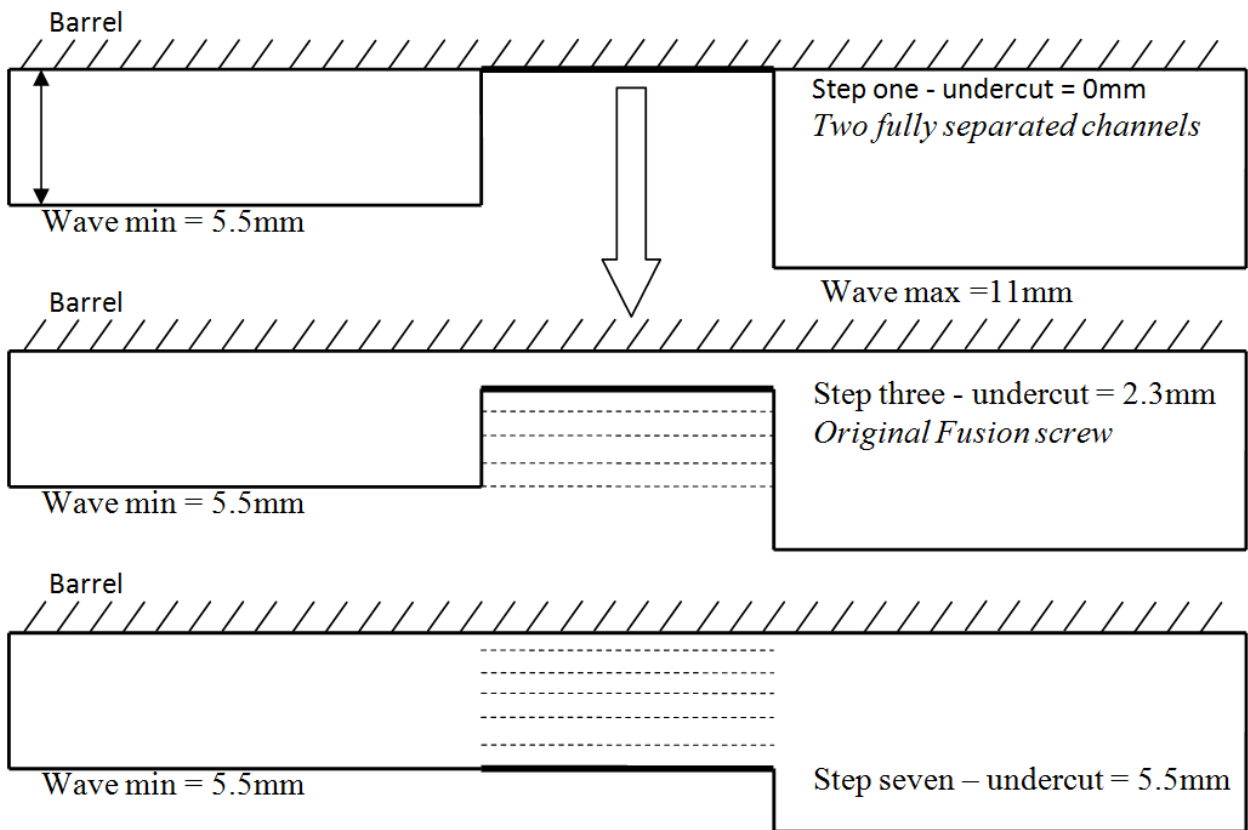Figure 7. Scheme of the undercut development
Figure 8. Pathline examples of 0 mm undercut
Figure 9. Pathline examples of 5.5 mm undercut
Figure 10. Dispersive/distributive mixing criteria curves
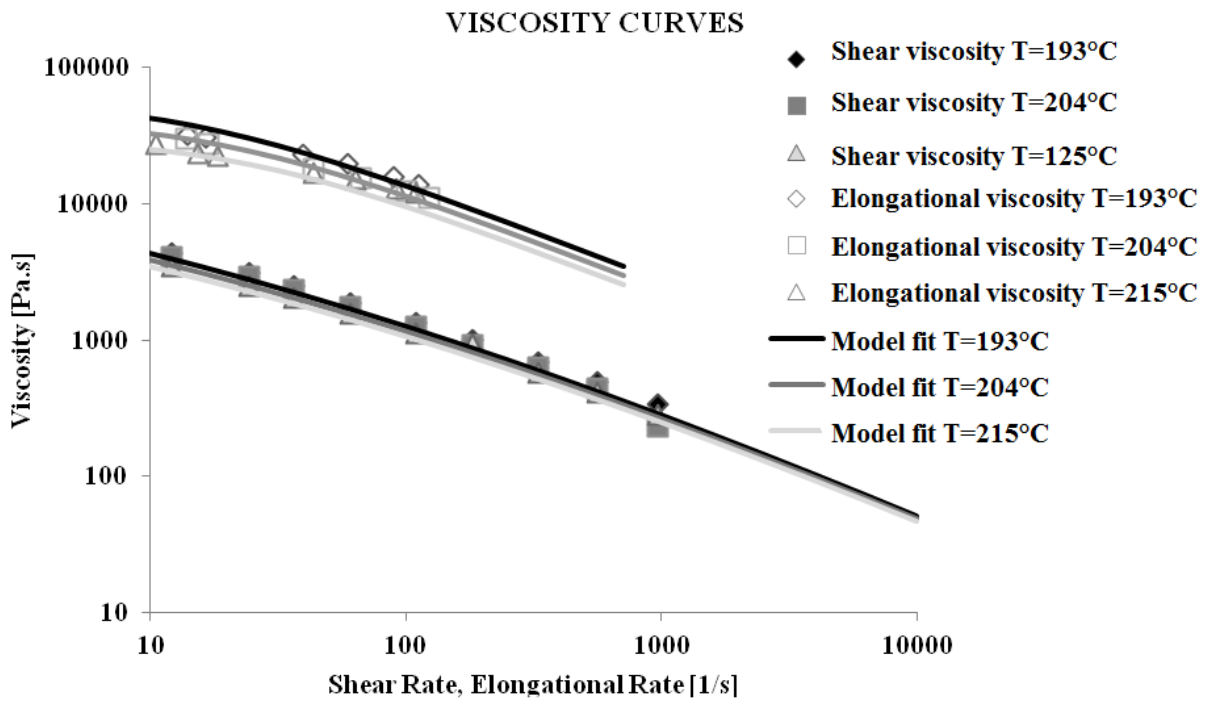
Figure 1. Viscosity curves
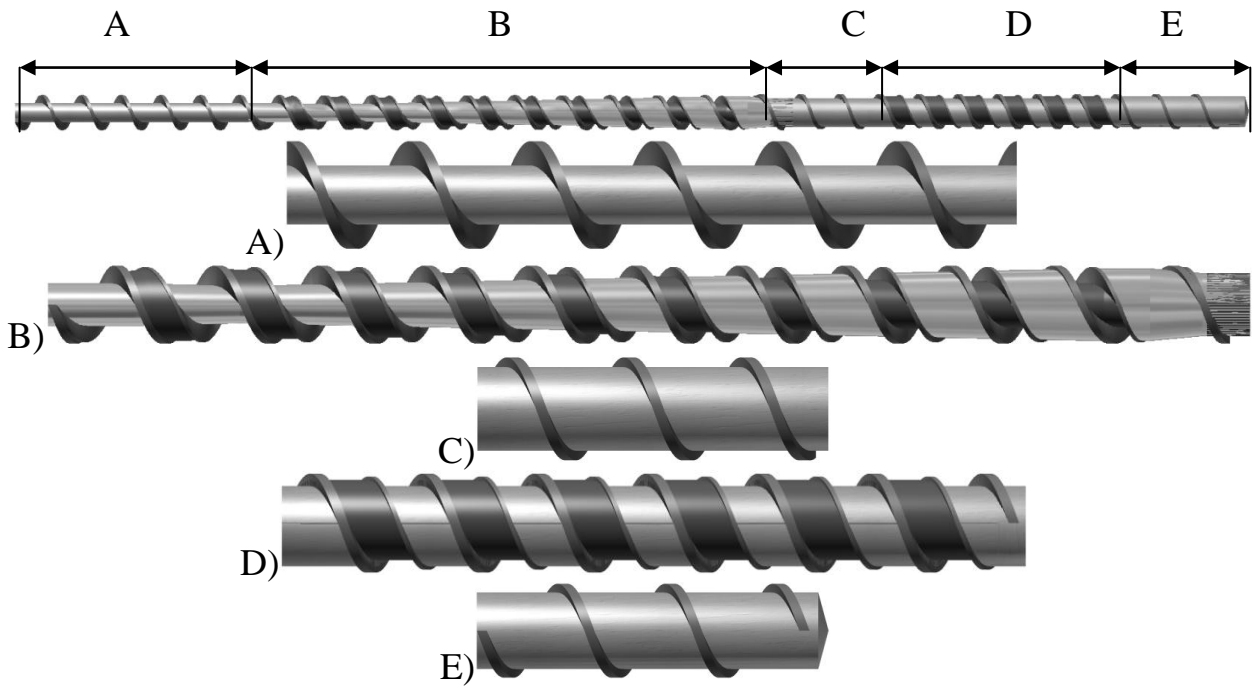
Figure 2. Fusion screw geometry off-scale sketch
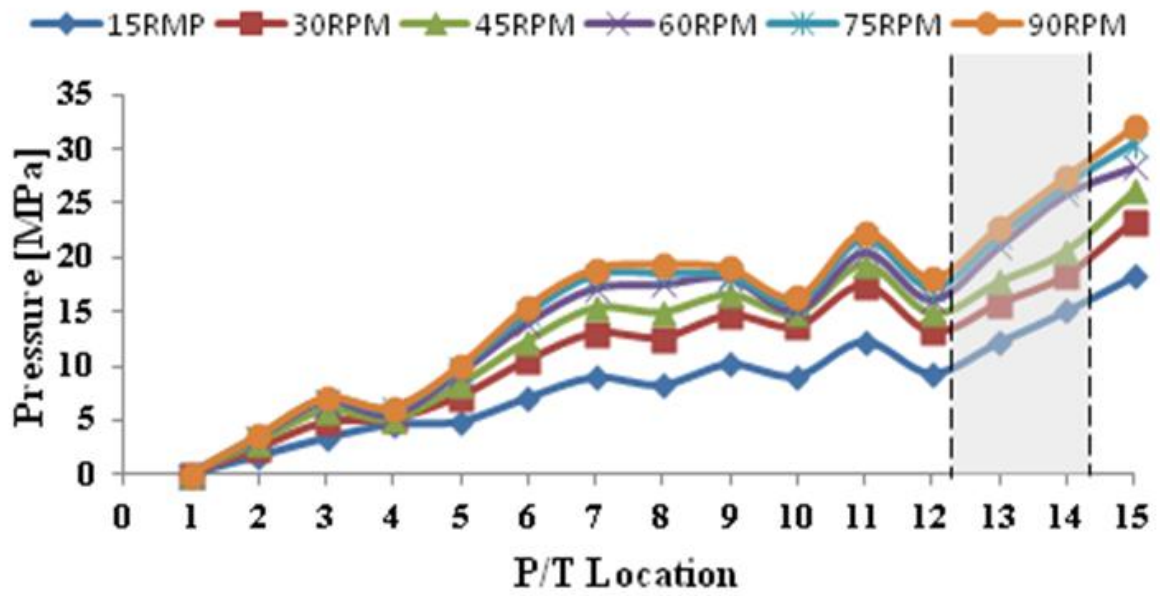
Figure 3. Pressure profiles
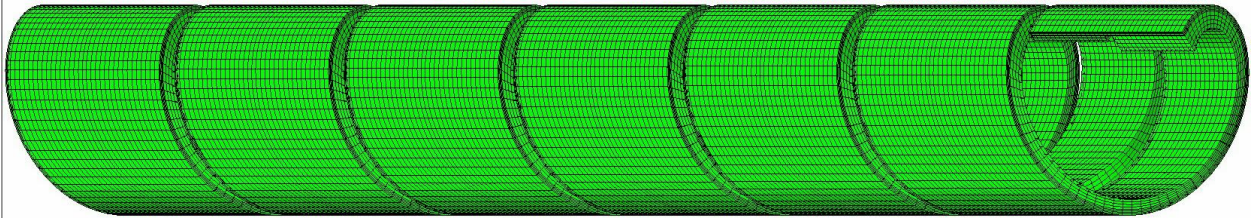
Figure 4. 3D FEM grid

Figure 5. Temperature comparison

PRESSURE COMPARISON

■ Simulation C-Y   ■ Simulation W-M   ■ Measurements

Figure 6. Pressure comparison

Barrel

Wave min = 5.5mm

Step one - undercut = 0mm
Two fully separated channels

Wave max =11mm

Barrel

Wave min = 5.5mm

Step three - undercut = 2.3mm
Original Fusion screw

Barrel

Wave min = 5.5mm

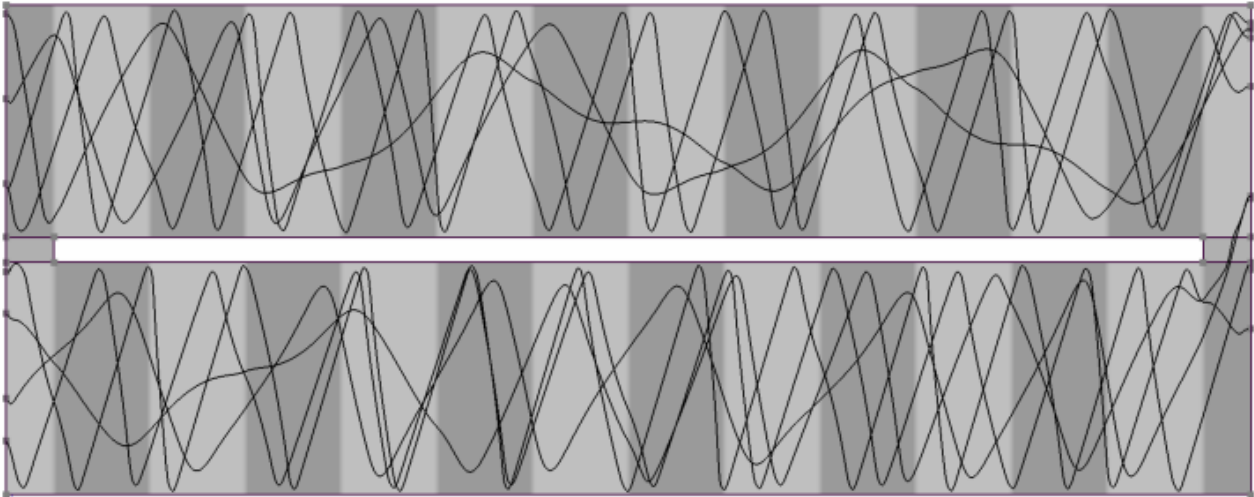Step seven – undercut = 5.5mm

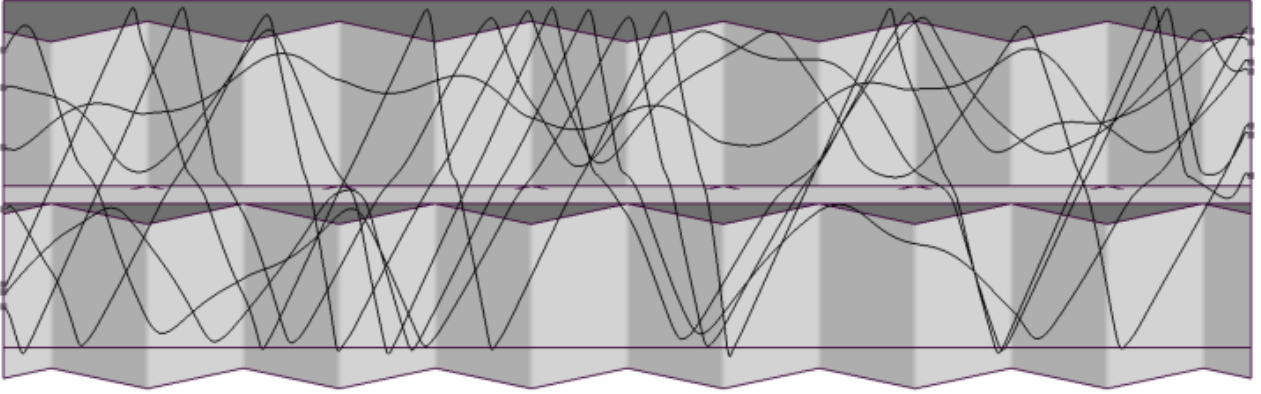Figure 7. Scheme of the undercut development

Figure 8. Pathline examples of 0 mm undercut

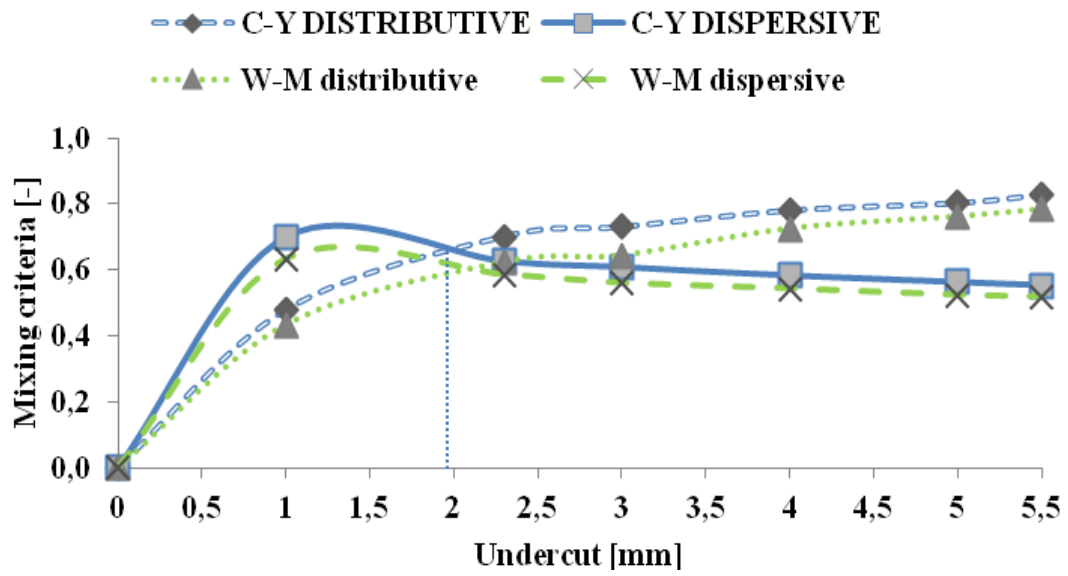Figure 9. Pathline examples of 5.5 mm undercut

Figure 10. Mixing Criteria

LIST OF PUBLICATIONS

Impact factor journal publications (Jimp)

1. Kubik, P., Vlcek, J., Tzoganakis, C., Miller, L.: Method of analyzing and quantifying the performance of mixing sections. *Polymer Engineering and Science*, 52 (6), 1232-1240 (2012). ISSN: 00323888

2. P. Kubik, M. Zatloukal, J. Vlcek, T. Womer: Three-dimensional finite element method simulation study of the fusion screw geometry. Accepted in July 2014 (with only minor revision requested) in *Plastics, Rubber and Composites*. ISSN 1465-8011.

Conference proceedings papers abstracted in SCOPUS (D)

1. P. Kubik, M. Zatloukal, Y. Asai, R. Haruna, Y. Iwasaki, J. Vlcek, I. Paseka: The Influence of Design and Processing Parameters on the Mixing Performance of a Fluted Mixer. *Annual Technical Conference - ANTEC, Conference Proceedings,* 2, 1481-1488 (2013). ISBN: 978-163266530-0.

2. Kubik, P., Vlcek, J., Tzoganakis, C., Miller, L.: An evalution of mixing quality of three different types of mixing elements. *Annual Technical Conference - ANTEC, Conference Proceedings*, 2, 1229-1236 (2011). ISBN: 978-161782960-4

3. Kubik, P., Vlcek, J., Svabik, J., Zatloukal, M.: 3D simulation of the fluted mixer element behavior. *Annual Technical Conference - ANTEC, Conference Proceedings*, 1, 773-778 (2010). ISBN: 978-161738660-2

4. Kubik, P., Vlcek, J., Svabik, J., Paseka, I., Zatloukal, M.: 3D simulation of the fluted mixer element behavior. *AIP Conference Proceedings*, 1152, 293-301 (2009). ISSN: 0094243X, ISBN: 978-073540689-6.

CURRICULUM VITAE

Pavel Kubík

_____

Address: Podlesi II / 4936

76005 Zlín, Czech Republic

Phone Number: +420737735143

Email: p.avel.kubik@seznam.cz

Date of Birth: 25. 10. 1983

Birthplace: Gottwaldov, Czech Republic

Nationality: Czech Republic

_____

Areas of Specialization

Polymers, engineering, extrusion, mixing, mixing elements, screws, rheology, polymers processing, computer flow simulations

Employment history

SPUR a.s. – Technological engineer	**[2014 – nowadays]**
Boco Pardubice Machines – Screw design specialist	**[2013 – 2014]**
Compuplast International, Inc. – Part-time employee	**[2012 – 2013]**

Academic Positions

Ph.D. **[2008 – nowadays]**

- Investigation of Melt Flow Through Waving Screw Channels and Other Mixing Elements Using Extensional Flows
- Tomas Bata University in Zlín / Faculty of Technology / Department of polymer engineering

Master Degree **[2006 – 2008]**

- A Comparison of Results from 2D and 3D Approaches for Spiral Mandrel Die Flow Simulation
- Tomas Bata University in Zlín / Faculty of Technology / Department of Production Engineering

Bachelor Degree [2003 – 2006]

- A Study of Mechanical Behavior of Thermoformed Thin-wall Plastic Elements in Stress Due to Bending
- Tomas Bata University in Zlín / Faculty of Technology / Department of Production Engineering

Technical Skills

- Cooperation with Compuplast International, Inc., Zlín, Czech Republic, 2007 – nowadays

- Stay at University of Waterloo, Waterloo, Ontario, Canada, May 12th – November 10th, 2010
- Stay in Xaloy, New Castle, Pennsylvania, USA, October 25th – November 13th, 2009

Work on projects

Grant UTB IGA/3/FT/10/D Modeling of the Vortex Development during Polymer Extrusion Process

Member of research team

Personal Skills

Languages: Czech (native speaker), English

CAD systems: Solid Works 2013, Autodesk Inventor, Autodesk Moldflow, Catia V5, Rhinoceros 4

Other PC Programs: Virtual Extrusion Laboratory^{TM}, Moldex Mesher R11, Adobe Photoshop, MS Windows, MS Office – Word, Excel, Power Point

Sport: Former representative of the Czech Republic in Skeleton

31st place World Championship 2008 Altenberg (GER)

24th place in European Championship 2007 Köenigssee (GER)

Active: Body building

Fun: football, athletics, basketball, cycling, swimming …

Others: Gun license – group B, C, E, Driving license – group B

Awards

SPE / Extrusion Division – Paper of the Month – *The Influence of Design and Processing Parameters on the Mixing Performance of a Fluted Mixer, March 2014*
http://s3.amazonaws.com/rdcms-spe/files/production/public/Microsites/MicrositeContent/Extrusion/2014-03-POTM.pdf

SPE / Extrusion Division – Paper of the Month – *3D simulation of the Fluted Mixer Element Behavior, April 2011*
http://www.exdiv-spe.com/files/POTMapr2011.pdf

Pavel Kubik

Investigations of polymer melt flow through different mixing elements and waving screw channels

Studium toku polymerních tavenin uvnitř různých typů míchacích elementů a vlnových šneků

Doctoral thesis